CNWRA 2002-05
Revision 1

SYSTEM-LEVEL PERFORMANCE ASSESSMENT OF THE PROPOSED REPOSITORY AT YUCCA MOUNTAIN USING THE TPA VERSION 4.1 CODE

Prepared for

U.S. Nuclear Regulatory Commission
Contract NRC–02–02–012

Prepared by

Sitakanta Mohanty (CNWRA)
Richard Codell (NRC)
Jose M. Menchaca (SwRI)
Ronald Janetzke (CNWRA)
Michael Smith (CNWRA)
Patrick LaPlante (CNWRA)
Meraj Rahimi (NRC)
Albert Lozano (SwRI)

Center for Nuclear Waste Regulatory Analyses
San Antonio, Texas

September 2002
Revised December 2002

ABSTRACT

The U.S. Nuclear Regulatory Commission (NRC), with the technical assistance from the Center for Nuclear Waste Regulatory Analyses, developed the Total System Performance Assessment (TPA) code. This code was developed as a tool to assist NRC in its evaluation of performance assessments in any potential license application by the U.S. Department of Energy (DOE) for a repository at Yucca Mountain, Nevada. This report describes a series of computations performed using the TPA Version 4.1 code to calculate long-term repository performance estimates in light of uncertainty in conceptual models and associated input parameters. This report includes (i) system-level and process-level modeling results (e.g., intermediate results) to understand the influence of trends and variabilities in outputs; (ii) system-level sensitivity and uncertainty analysis results based on a variety of analysis techniques to understand the influence of parameters, alternative conceptual models, and subsystems (especially repository components) on repository performance; (iii) capability of barriers to reduce the flow of water and delay transport of radionuclides; (iv) consequence of human intrusion; and (v) synthesis of results to apply risk insights to assess the relative importance of the integrated subissues used by NRC to review the DOE total system performance assessment.

An influential parameter, alternative conceptual model, or subsystem is one that either produces significant uncertainty in performance estimates or one to which performance measures (e.g., regulatory compliance limits) are sensitive. Sensitivity and uncertainty analyses were conducted using numerous TPA Version 4.1 code runs for each sensitivity analysis technique. Results of system-level analyses are based on the peak dose from any realization and the peak expected dose to a receptor group 20 km [12.4 mi][1] from the repository during the 10,000-year compliance period. Limited results are presented for a 100,000-year time period to understand system characteristics that may not become apparent in the 10,000-year modeling results because of the calculated long life of the waste package.

For the basecase modeling scenario, which includes the seismic and climatic activity, peak risks of 0.21 μSv/yr [0.021 mrem/yr] and 90 μSv/yr [9 mrem/yr] were obtained for the 10,000- and 100,000-year simulation periods, respectively. The faulting scenario changed the peak expected dose negligibly. The igneous activity scenario increased the peak expected risk in 10,000 years to 3.5 μSv/yr [0.35 mrem/yr]. For the stylized human intrusion scenario, a peak risk of 1μSv/yr [0.1 mrem/yr] was obtained for the 10,000-year period. Only initially defective waste package failures contribute to the basecase risk because the performance calculations show that no waste packages in the repository fail from corrosion within 10,000 years. The geologic properties of the unsaturated and saturated zones limit releases to the accessible environment to only a few, long-lived, nonsorbing radionuclides. Np-237 is the only sorbing radionuclide contributing to dose estimates in this time period. Only a fraction of the precipitating water (0.002 percent of the precipitation or 0.0037 percent of the infiltration) was estimated to contact the waste form, which reflects diversion processes of the unsaturated zone, drip shield, and waste package.

Sensitivity analyses show that conceptual models of colloidal transport, spent nuclear fuel dissolution, spent nuclear fuel wetting, and wetted fuel surface area may substantially influence

[1]The analyses presented in this report were completed before the location of the receptor group was defined to be 18 km [11.2 mi] in 10 CFR Part 63.

estimated risk from the basecase scenario. The direct release of radioactivity to the surface of the earth for extrusive basaltic volcanism uses a geometry-based model, which estimates the number of waste packages affected directly from the width of the volcanic conduit intersecting the repository. Alternative, explicit models for the interaction of magma with waste packages, based on physics of magma flow, can show an increased risk of an order of magnitude.

Limited distributional sensitivity analyses conducted in this report with the most influential parameters suggest a 10 percent change to the mean of a parameter's distribution can increase risk by as much as 150 percent. Performance results show comparable sensitivity to both the engineered and the natural repository component groups. The influential parameters, alternative conceptual models, and repository components were then compared to the current integrated subissues, which are used by the NRC to focus work on items important to repository performance. Five of 14 integrated subissues did not show up as significant.

Parametric sensitivity analysis serves an important purpose in identifying the effect of input parameter uncertainty on system performance to obtain risk insights. Repository component and alternative conceptual model sensitivity analyses provide additional key information about the importance of integrated subissues that can be used as a starting point by the analyst to determine why certain parameters or models do or do not show up as important.

The analyses and results are limited by simplifications in models and assumptions regarding parameter values. As a consequence, these results are for illustration and are not indicative of repository safety. However, the estimates resulting from this study will assist the staff to focus its attention on phenomena that may be most important relative to repository performance. The manner in which these analyses were conducted or the assumptions and approaches used should not be construed to express the views, preferences, or positions of the NRC staff regarding implementation of regulations for Yucca Mountain or the ability of a potential Yucca Mountain repository to comply with those regulations.

CONTENTS

CONTENTS (continued)

CONTENTS (continued)

Section | Page

CONTENTS (continued)

CONTENTS (continued)

CONTENTS (continued)

FIGURES

FIGURES (continued)

FIGURES (continued)

Figure Page

FIGURES (continued)

TABLES

TABLES (continued)

Table Page

EXECUTIVE SUMMARY

The U.S. Nuclear Regulatory Commission (NRC), with the technical assistance from the Center for Nuclear Waste Regulatory Analyses, developed the Total System Performance Assessment (TPA) code. This code was developed as a tool to assist NRC in its evaluation of performance assessments in any potential license application by the U.S. Department of Energy (DOE) for a repository at Yucca Mountain, Nevada. To date, four reports have been written by the NRC staff about performance assessment for the proposed Yucca Mountain repository. The first, referred to as Iterative Performance Assessment Phase 1 (Codell, et al., 1992), assembled and demonstrated the NRC assessment methodology. The second, NRC total system performance assessment, Iterative Performance Assessment Phase 2 (Wescott, et al., 1995), used the TPA Version 2.0 code to investigate the features, events, and processes influencing performance of the proposed Yucca Mountain repository. Information obtained in these iterative performance assessment analyses was used in NRC reviews of early DOE total system performance assessments of Yucca Mountain. The third NRC total system performance assessment (Mohanty, et al., 1999) used the TPA Version 3.1 code (Mohanty and McCartin, 1998) to assist the NRC to evaluate the DOE viability assessment. The fourth NRC Total System Performance Assessment (Mohanty, et al., 1999) used the TPA Version 3.2 code (Mohanty and McCartin, 1998), which implemented the Total System Performance Assessment–Viability Assessment design changes. This allowed an independent, in-depth analysis at the system and subsystem levels to attribute risk significance to integrated subissues. Revisions were made to the TPA Version 3.2 code to implement the DOE Enhanced Design Alternative II, new and revised NRC conceptual models and risk assessment methods leading to the development of the TPA Version 4.1 code (Mohanty, et al., 2002). The revised code was a tool used by the staff in evaluating the Total System Performance Assessment–Site Recommendation. This report documents the most recent overall system- and process-level sensitivity and uncertainty analyses performed by NRC and CNWRA using models and conditions similar to the Total System Performance Assessment–Site Recommendation. This report presents

- A brief description of the conceptual models implemented in the TPA Version 4.1 code and a formal presentation of the method for combining the disruptive event scenario results with the basecase scenario (Chapters 2 and 3)

- An indepth discussion of deterministic and stochastic results for the basecase and disruptive scenario cases based on peak risk and capability of barriers to reduce flow of water and to prevent or delay radionuclide transport (Chapters 3 and 7)

- The results of system-level parametric sensitivity and uncertainty analyses using statistical and nonstatistical techniques to determine the parameters and barrier components that most influence repository performance (Chapters 4, 5, and 6)

- The results from the alternative conceptual model sensitivity analysis using either models explicitly incorporated in the TPA Version 4.1 code or models that can be mimicked through adjustment of input parameters to determine model and parameter uncertainties (Chapters 2, 3, and 4)

- An estimation of the relative importance of the integrated subissues to focus staff efforts (Chapter 7)

- A documentation of improvements in NRC staff capabilities in performance assessment based on the insights gained from process- and system-level results and sensitivity analyses (Chapter 8)

System-level performance was evaluated using the basecase data set in which 330 of 950 parameters were sampled to represent data uncertainty and variability. The chosen parameters were screened from the larger list on the basis of staff experience with the models, to include those parameters most likely to have a significant impact on the results. To develop a better understanding of the trends of the outputs at a process level, results from a single realization (using the mean value data set) were also analyzed. Calculations to date using the basecase data set (the basecase is defined as the undisturbed scenario along with the effects of rockfall due to seismicity) indicate peak expected doses of 2.1×10^{-4} mSv/yr [0.021 mrem/yr] in 10,000 years the compliance period. For a simulation period, three radionuclides (I-129, Tc-99, and Np-237) consistently are the primary contributors to the peak expected dose. The gap fraction does not substantially influence peak expected dose. Igneous activity is the primary disruptive scenario contributing to the peak expected dose, estimated to be 3.5×10^{-3} mSv/yr [0.35 mrem/yr]. The faulting disruptive event is a negligible contributor to the peak expected dose (Chapter 3).

The consequences of human intrusion were evaluated using a stylized, bounding analysis. One waste package was assumed to fail non-mechanistically, resulting in a peak dose of 0.001 mSv/yr [0.1 mrem/yr] during the compliance period.

Barrier capabilities for reducing the water flow rate and preventing or delaying radionuclide transport were derived from the total system performance assessment results. The analyses showed that only a fraction of the precipitating water contacts the drip shield and the waste package (0.02 percent of the precipitation) and enters the failed waste packages in the basecase (0.002 percent of the precipitation) showing the capability of the unsaturated zone above the repository (Chapters 3 and 7).

The sensitivity and uncertainty analyses were conducted using numerous (several thousand for each analysis method) TPA Version 4.1 code runs. The sensitivity and uncertainty of repository performance to specific parameters were evaluated using different statistical and nonstatistical tests. These tests examined the sensitivity of repository performance to individual parameters to identify those most important to repository performance. Although the report identifies and presents influential parameters for both 10,000- and 100,000-year simulation periods, risk insights are summarized for only the 10,000-year compliance period. Limited results are presented for a 100,000-year time period to understand system characteristics that may not become apparent in the 10,000-year modeling results because of the calculated long life of the waste packages. An influential parameter, alternative conceptual model, or repository component is one that either drives uncertainty in repository performance, or one to which the estimated performance is sensitive. Several parameters were found most influential for the basecase (in order of influence on the peak dose for each realization): (I) mean annual infiltration at start, (ii) drip shield failure time, (iii) the preexponential term for the spent nuclear fuel dissolution rate calculation, (iv) areal fraction of the repository wetted by water infiltrating into the repository, (v) the focusing factor that modifies the flow reaching a wetted waste package, (vi) the well pumping rate at the 20-km [12.4-mi][1] receptor group location, (vii) alluvium sorption properties for Np-237, (viii) length of the alluvium pathway in the saturated zone, (ix) fraction of the condensate from thermal reflux moving toward the repository, and (x) fraction of waste packages that are initially defective (Chapters 4 and 7).

The significantly high risk (i.e., probability-weighted dose) from the igneous activity case compared to the basecase implies that the igneous activity model parameters play a dominant overall role in the performance assessment. The influential parameters include (I) airborne mass load above the fresh ash blanket, (ii) wind speed, (iii) diameter of volcanic conduit, (iv) volcanic event power, (v) volcanic event duration, (vi) time of next volcanic event in the region of interest, and (vii) ash mean particle diameter (Chapters 4 and 7).

Distributional sensitivity analyses were conducted to investigate the impact of distribution function shape on the dose responses. Using the 10 most influential parameters identified by the parametric sensitivity analysis, the distributional sensitivities showed that the choice of distribution function plays an important role in the performance assessment estimation. For example, a 10 percent change to the mean of the distribution function representing the uncertainty in the flow multiplication factor that modifies the flow reaching a wetted waste package results in a 150 percent change in the peak expected dose. Performance calculations also showed high sensitivity to the choice of the distribution function for the drip shield failure time parameter. The types of errors in constructing a distribution function that could lead to the improper choice of a distribution function have been highlighted (Chapter 5 and 7).

Alternative conceptual model sensitivity studies were conducted on a case-by-case basis with appropriate consideration of uncertainty in the model parameters. Analyses used peak expected dose as the performance measure. Alternative conceptual model sensitivity analyses showed that colloidal transport (if plausible, in the Yucca Mountain environment) and the spent nuclear fuel dissolution rate, in combination with the spent nuclear fuel wetting mode and the surface area over which water contacts spent nuclear fuel, could substantially influence basecase scenario risk. The process-based model for determining the number of waste packages contributing to direct release (magma-tunnel interaction model) increased risk by one order of magnitude (Chapters 2, 3, 4, and 7).

Repository component sensitivity analyses were performed for two reasons: (I) obtaining sensitivity at an easily understood subsystem level such as a physical repository component and (ii) estimating the importance of the subsystem when parametric sensitivity analysis did not lead to failure (e.g., waste package) during the compliance period or the conservativeness in the conceptual model prevented noticeable dose response to the data range. Analyses showed that repository performance is very sensitive to the waste package repository component. Also, the group of natural repository components (i.e., unsaturated zone and saturated zone together) showed approximately the same level of sensitivity as the waste package repository component. This suggests that analyses should focus on determining if any undesirable constraints in parameters and models for waste package life prediction are responsible for the long waste package life. The repository component sensitivity analysis described in this report is not intended to provide either guidance to DOE or to describe a preferred approach for

---

[1]The analyses presented in this report were completed before the location of the receptor group was defined to be 18 km [11.2 mi] in 10 CFR Part 63.

demonstrating the capability of a barrier. These analyses were performed to further the staff efforts to understand the TPA Version 4.1 code and to explore where to improve understanding of the repository system (Chapter 6 and 7).

The influential parameters were traced back to the integrated subissues used by NRC to focus its high-level waste program on aspects important to repository performance (NRC, 1998). Nine out of 14 integrated subissues have at least 1 influential parameter (including the integrated subissues related to disruptive scenarios), based on the results of the TPA Version 4.1 code. The integrated subissues that showed up as important to performance are (I) volcanic disruption of waste packages (DIRECT1), (ii) airborne transport of radionuclides (DIRECT2), (iii) radionuclide transport in the saturated zone (SZ2), (iv) degradation of engineered barriers (ENG1), (v) flow paths in the unsaturated zone (UZ2), (vi) quantity and chemistry of water contacting waste packages and waste forms (ENG3), (vii) radionuclide release rates and solubility limits (ENG4), (viii) climate and infiltration (UZ1), and (ix) mechanical disruption of engineered barriers (ENG2). The integrated subissues that did not show up as important are (I) radionuclide transport in the unsaturated zone (UZ3), (ii) flow rates in the saturated zone (SZ1), (iii) representative volume (DOSE1), (iv) redistribution of radionuclides in soil (DOSE2), and (v) biosphere characteristics (DOSE3). DOSE1 has a one-to-one linear effect on estimated dose, however, this integrated subissue is moot because the pumping rate is now specified in the regulation. Note that DOSE2 and DOSE3 integrated subissues were determined to be unimportant only on the basis of parametric sensitivity. Alternative conceptual models may alter this finding (Chapter 7).

This total system performance assessment aids the NRC staff by focusing their review of DOE total system performance assessments on those models and parameters that most affect estimated system performance. It should be noted that the results presented in the following chapters are based on numerous simplifying assumptions and use only limited site-specific data. Parametric sensitivity analysis sometimes fails to show the importance of processes or parameters, especially those associated with radionuclides that never arrive at the pumping well within the regulatory period. Therefore, several analyses in this report were conducted using data outside the range (e.g., alternative conceptual model and repository component sensitivity) to identify areas where the analyst should focus.

Conclusions drawn from the analyses presented in this report may change as the models and assumptions are updated based on revised design, ongoing site characterization, recommendations from reviewers and experts, changes in regulatory requirements, and improved model conceptualization and data interpretation by staff. The analysis also contains uncertainties regarding conceptual models for consequences and scenarios. Finally, this report should be considered as an interim demonstration of some of the methods the NRC staff developed to review a performance assessment submitted by DOE as part of any potential license application. Neither the manner in which these analyses were conducted nor the assumptions and approaches used should be construed to express the views, preferences, or positions of the NRC staff regarding implementation of regulation for Yucca Mountain.

This report was prepared to document work performed by the CNWRA for NRC under Contract No. NRC–02–02–012. The activities reported here were performed on behalf of the NRC Office of Nuclear Material Safety and Safeguards, Division of Waste Management. The report is an independent product of the CNWRA and does not necessarily reflect the views or regulatory position of the NRC.

References

Codell, R.B, N. Eisenberg, D. Fehringer, W. Ford, T. Margulies, T. McCartin, J. Park, and J. Randall. NUREG–1327, "Initial Demonstration of the NRC's Capability to Conduct a Performance Assessment for a High-Level Waste Repository." Washington, DC: NRC. 1992.

Mohanty, S., T.J. McCartin, and D.W. Esh. "Total-system Performance Assessment (TPA) Version 4.0 Code: Module Descriptions and User's Guide." San Antonio, Texas: CNWRA. 2002.

Mohanty, S., R. Codell, R.W. Rice, J. Weldy, Y. Lu, R.M. Byrne, T.J. McCartin, M.S. Jarzemba, and G.W. Wittmeyer. "System-Level Repository Sensitivity Analyses Using TPA Version 3.2 Code." CNWRA 99-002. San Antonio, Texas: CNWRA. 1999.

Mohanty, S. and T.J. McCartin. "Total-system Performance Assessment (TPA) Version 3.2 Code: Module Description and User's Guide." San Antonio, Texas: CNWRA. 1998.

———. "Issue Resolution Status Report Key Technical Issues: Total-system Performance Assessment and Integration." Revision 1.0. Washington, DC: NRC. 1998.

Wescott, R.G., M.P. Lee, N.A. Eisenberg, T.J. McCartin, and R.G. Baca, eds. NUREG–1464, "NRC Iterative Performance Assessment Phase 2." Washington, DC: NRC. 1995.

ACKNOWLEDGMENTS

This report was prepared to document work performed by the Center for Nuclear Waste Regulatory Analyses (CNWRA) for the U.S. Nuclear Regulatory Commission (NRC) under Contract No. NRC–02–02–012. The activities reported here were performed on behalf of the NRC Office of Nuclear Material Safety and Safeguards, Division of Waste Management. The report is an independent product of the CNWRA and does not necessarily reflect the views or regulatory position of the NRC.

The authors wish to thank G. Wittmeyer, T. McCartin (NRC), and J. Firth (NRC) for their technical reviews and B. Sagar for his programmatic review. The authors also wish to thank G. Wittmeyer, T. McCartin (NRC), J. Peckenpaugh (NRC) and I. Chichkov for their informal review of chapters of the document prior to the finalization of the report. Technical support provided by J.M. Menchaca [Southwest Research Institute (SwRI)] at all stages of this report is gratefully acknowledged. The assistance J. Wu (consultant) provided in extending the cumulative distribution function sensitivity analysis method, along with the sensitivity measures (that complement NRC regulatory criteria) originally developed as a SwRI internal research and development project, to the NRC and CNWRA sensitivity analysis effort is gratefully acknowledged. Thanks to R. Janetzke and J.M. Menchaca (SwRI) for code quality assurance and debugging the code when needed, to D. Esh (NRC) and O. Pensado for their indirect comments that have enriched some of the analyses presented in this report. This report has benefitted from the efforts of B. Sagar, W. Patrick, T. McCartin (NRC), G. Wittmeyer, S. Wastler (NRC), and D. Esh (NRC) toward making a clear distinction between the analyses required by regulation and the analyses NRC and CNWRA may perform to improve understanding of the repository system. Thanks are also expressed to M. Muller and G. Adams (SwRI) and R. Rice (consultant) for assistance in performing several complicated TPA Version 4.1 code executions and to V. Troshanov and J. Reynolds (student assistants) for help in generating some of the outputs and plotting results at the early stage of the report development. Thanks are also expressed to C. Cudd, B. Long, J. Pryor, and A. Woods for editorial reviews and to C. Weaver for secretarial support.

This report has used several templates of the previous sensitivity analysis report, System-Level Repository Sensitivity Analyses Using TPA Version 3.2 code. We acknowledge all those who contributed to this TPA Version 3.2 sensitivity analysis report, including C. Lui (NRC), G. Wittmeyer, T. McCartin (NRC), R.W. Rice (consultant), M. Byrne (NRC), Y. Lu, and J. Weldy.

QUALITY OF DATA, ANALYSES, AND CODE DEVELOPMENT

DATA: CNWRA–generated data contained in this report meet quality assurance requirements described in the CNWRA Quality Assurance Manual. Data from other sources are freely used. The respective sources of non-CNWRA data should be consulted for determining levels of quality assurance.

ANALYSES AND CODES: The TPA Version 4.1k code and variations have been developed following the procedures described in the CNWRA Technical Operating Procedure (TOP–018), which implements the quality assurance requirements contained in the CNWRA Quality Assurance Manual. The TPA Version 4.1.1 code reflects a minor modification to the

Version 4.1k code to produce additional information for Chapter 7. Codes used in conducting sensitivity analyses have also been developed following procedures described in TOP–018.

1 INTRODUCTION

In accordance with the provisions of the Nuclear Waste Policy Act of 1982, (U.S. Congress, 1982), the U.S. Nuclear Regulatory Commission (NRC) is responsible for evaluating any license application for a proposed geologic repository constructed for emplacement of high-level radioactive waste [i.e., commercial spent nuclear fuel, several types of U.S. Department of Energy (DOE)-owned high-level radioactive waste from the production of nuclear weapons, spent nuclear fuel from weapon production reactors, research reactors, and U.S. Navy reactors] at Yucca Mountain, Nevada. In support and preparation of the regulatory review activities outlined in the Nuclear Waste Policy Act of 1982, the NRC staff is conducting detailed technical performance assessments to understand the potentially important isolation characteristics and capabilities of the proposed repository system at Yucca Mountain.

The performance assessment activity is a part of an ongoing iterative process at the NRC to prepare for the review of a potential DOE license application. As part of these iterative performance assessment activities, NRC and its support contractor, the Center for Nuclear Waste Regulatory Analyses (CNWRA), are using the TPA code. The TPA code is not meant to demonstrate compliance (that is the responsibility of the DOE), but is a tool to allow NRC to perform an independent analysis of a license application for the proposed repository and to support review capability. The TPA code, which evolves with each iterative performance assessment phase, is designed to simulate the behavior of the repository system, taking into account the essential characteristics of the natural and engineered barrier subsystems and changes in knowledge about the geologic setting and design. To support identification of features, events, and processes of the repository important to safety, this document presents a variety of estimates of the sensitivity of repository performance to uncertainty in the repository system using the latest version of the TPA code, Version 4.1.[1] For this report, sensitivity is defined as the relative change in model response (i.e., output) for a unit change of input, and uncertainty is defined as the comparative change in overall output range because of input value uncertainty.

NRC previously conducted analyses of repository performance (Codell, et al., 1992; Wescott, et al., 1995; Mohanty, et al., 1999). For the latest iteration, Version 4.1 of the TPA code was developed to accommodate changes to the design of the proposed repository and incorporate the latest understanding of features, events, and processes at Yucca Mountain. This latest version includes (i) a much finer spatial discretization capability for the repository and geologic system; (ii) incorporation of the DOE Enhanced[2] Design Alternative II, including the drip shield barrier; (iii) an alternative waste package failure mode that accounts for complex igneous processes; (iv) variable length flow paths in the alluvium to account for uncertainties in site saturated zone hydrology; and (v) enhanced biosphere dose modeling capabilities that incorporate biosphere parameter uncertainties.

---

[1]TPA Version 4.0 code is the last iteration of the user's guide, however, Version 4.1, more specifically, Version 4.1j was used for calculations in this report. Despite several changes to the code in moving from Version 4.0 to 4.1j, the documentation in the user's guide for Version 4.0 remains applicable. Most revisions pertain to replacing old with new data as these were made available through the course of developing this report.

[2]DOE has modified the Enhanced Design Alternative II several times. The particular modified design used in this report is the one that was available at the early stage of the development of this report.

1.1 Background

Performance assessments for geologic repositories are based on conceptual models of physical processes and parameters derived from field and laboratory data or expert elicitation. Because of measured data being sparse and spatially variable and the inherent uncertainty involved in simulating physical processes for many thousands of years, the results of performance assessment are uncertain. Therefore, an important aspect of conducting a performance assessment is quantifying the sensitivity of the results to the uncertainty associated with the input parameters and alternative conceptual models. Such an analysis will provide information delineating those input parameters, alternative conceptual models, and subsystems that most affect the model results. Knowing which parameters, models, and subsystems most influence model results allows the analyst to improve the conceptualization of the repository system and improve confidence in the numerical results. Likewise, identification of the parameters, models, and subsystems that produce the most uncertainty in results provides a means of comparing and evaluating different performance assessment models and indicates where future design, site characterization, and analysis activities should be focused.

Staff developed a systematic, hierarchical approach to reviewing the DOE total system performance assessments, illustrated in Figure 1-1. The focal point is the overall repository system where the performance measure is the expected annual dose to the reasonably maximally exposed individual during the 10,000-year time period of interest. Analysis of overall repository system performance results using a variety of techniques provides useful insights to the contribution of subsystems and components to overall performance. To facilitate review of the DOE total system performance assessments, staff will examine the contribution to performance from each of three repository subsystems—engineered, geosphere, and biosphere—as shown in the second tier of Figure 1-1. Each of these subsystems is further subdivided into discrete components that include the engineered barriers that make up the engineered system, unsaturated zone flow and transport, saturated zone flow and transport, direct release to the biosphere, and dose calculation for the biosphere. Recognizing there are many different ways of dividing the overall system into smaller, analyzable components, this particular division is primarily based on the natural progress of radionuclide release and transport to a receptor group at the Yucca Mountain site and takes advantage of the results of past NRC total system performance assessments and reviews of the DOE total system performance assessments. At the base of the hierarchy are the key elements of the repository system (integrated subissues) that need to be abstracted into a total system performance assessment.

1.1.1 Previous Iterative Performance Assessment Analyses

To date, four reports have been written by the NRC staff on performance assessment for the proposed Yucca Mountain repository. The first, referred to as Iterative Performance Assessment Phase 1 (Codell, et al., 1992), developed and demonstrated the NRC assessment methodology. Iterative Performance Assessment Phase 1 examined the sensitivity and uncertainty in radionuclide releases to the accessible environment for a geologic repository in unsaturated tuff. The second NRC total system performance assessment, Iterative Performance Assessment Phase 2 (Wescott, et al., 1995), was performed using the TPA Version 2.0 code to investigate the features, events, and processes influencing isolation performance of the proposed Yucca Mountain repository.

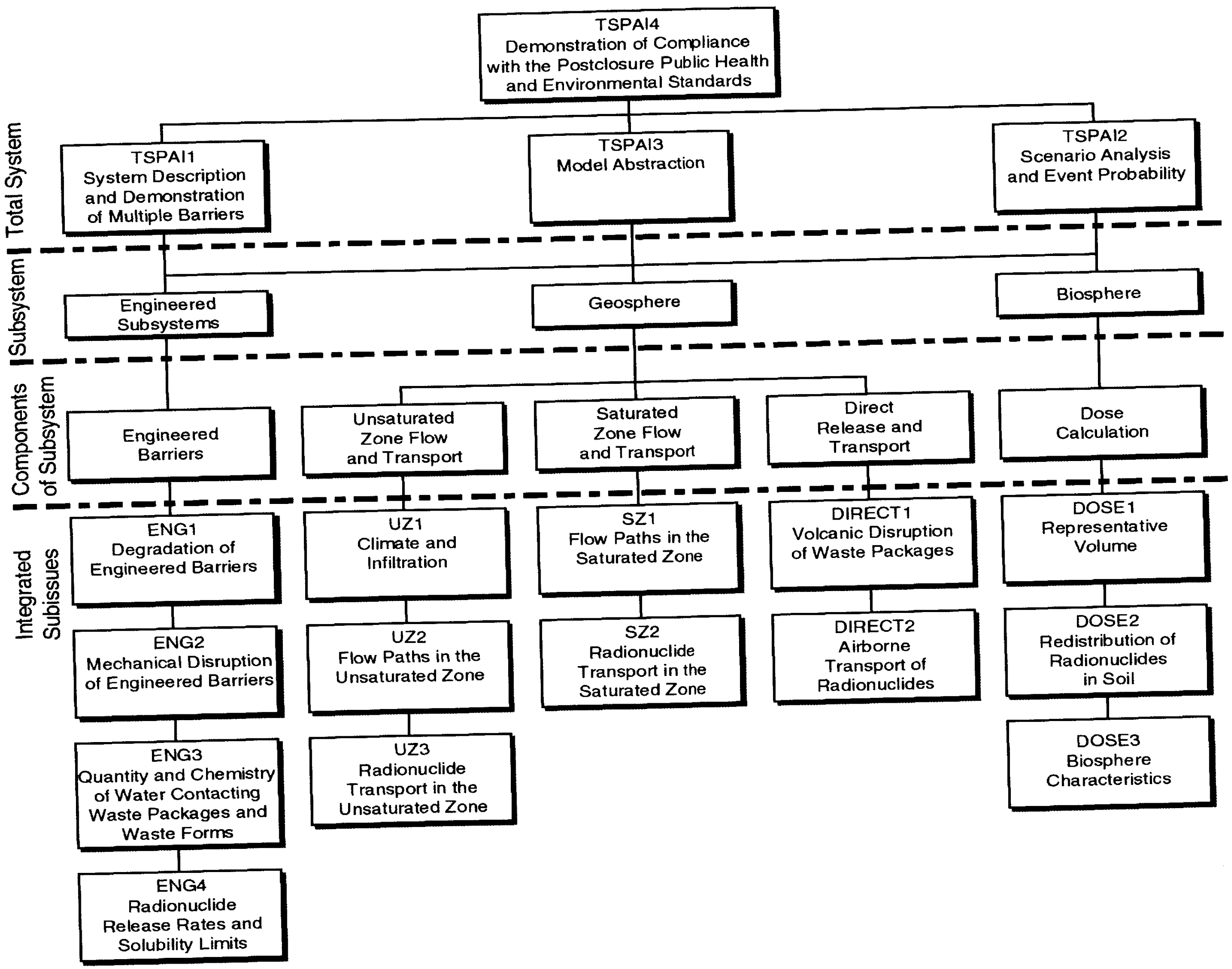

Figure 1-1. Flowdown Diagram Showing the Subsystems and the Integrated Subissues

Information obtained in these iterative performance assessment analyses was used in NRC reviews of early DOE total system performance assessments for Yucca Mountain. At the time Phase 2 analyses were completed in 1993, the overall performance measures for the geologic repository used in the iterative performance assessment were cumulative total releases of radionuclides (normalized release) to the accessible environment and radiation dose (effective dose equivalent) to the exposed population. These performance measures were consistent with regulations in 40 CFR Part 191 and 10 CFR Part 60, in effect at the time. The third NRC total system performance assessment (NRC, 1999b) was performed a few years later using the TPA Version 3.1 code to determine whether or not the NRC would be able to quantitatively evaluate the conclusions reached by DOE in its viability assessment. During this period, the focus of performance estimates emphasized radiation dose as a primary performance measure in anticipation of forthcoming U. S. Environmental Protection Agency standards for Yucca Mountain in 40 CFR Part 197 (Code Federal Regulations, 2001). Subsequent to developing and testing the TPA Version 3.1 code, detailed sensitivity and uncertainty analyses were undertaken (NRC, 1999b) that indicated the need for further refinement of the TPA code prior to its use to evaluate the DOE Total System Performance Assessment–Viability Assessment [Civilian Radioactive Waste Management System Management and Operating Contractor (CRWMS M&O), 1998]. Revisions made to the TPA code led to the TPA Version 3.2 code (Mohanty and McCartin, 1998), which was used to evaluate the Total System Performance Assessment–Viability Assessment (CRWMS M&O, 1998). This version of the TPA code was used to conduct additional sensitivity analyses documented in the fourth of the aforementioned performance assessment reports (Mohanty, et al., 1999). Analyses using the TPA Version 3.1 code and above were based on the new regulation [10 CFR Part 63 (Code Federal Regulations, 2002), which was based on the risk-informed, performance-based approach. The new regulation provides site-specific criteria (including design criteria) and eliminates detailed requirements such as quantitative subsystem performance objectives.

In addition, the total system performance assessment analyses are used to focus NRC activities on factors of greatest importance to repository performance. The site-specific regulations developed by NRC for the Yucca Mountain repository are risk informed and performance based. Therefore, the NRC review of a potential license application to build and operate a deep geologic repository at Yucca Mountain will focus on those physical aspects of the repository system of greatest importance to radiological safety. The results from this study, in part, will be used to assist development of the review strategy outlined by the NRC in its Yucca Mountain Review Plan (NRC, 2002).

1.1.2 Iterative Performance Assessment Phase 1 Sensitivity and Uncertainty Analyses

Four sensitivity or uncertainty analyses were performed for Iterative Performance Assessment Phase 1 (Codell, et al., 1992): (i) demonstration of the effect of individual parameters on the resultant complementary cumulative distribution function of cumulative release to the accessible environment, (ii) use of stepwise linear regression to estimate sensitivity of key parameters in the consequence models, (iii) determination of relative importance of individual radionuclides in the waste, and (iv) sensitivity of complementary cumulative distribution functions to the performance of the natural and engineered barriers. The sensitivity and uncertainty analyses considered only groundwater pathway releases. Gaseous release of radionuclides was not part of the Iterative Performance Assessment Phase 1 total system performance assessment results but was included as an auxiliary analysis.

Although Iterative Performance Assessment Phase 1 conducted full sensitivity and uncertainty analyses for the groundwater pathway, only complementary cumulative distribution functions for cumulative release (as required by 40 CFR Part191 and 10 CFR 60) were generated for the scenario cases (basecase, basecase with human intrusion, and basecase with pluvial conditions with and without human intrusion). Cumulative release refers to the sum of releases to the accessible environment of all radionuclides during the time period of interest. Cumulative distribution functions reflected the uncertainty in the sampled parameters propagated through the analysis. Peak dose was not calculated as a performance measure for the Iterative Performance Assessment Phase 1 study.

1.1.3 Iterative Performance Assessment Phase 2 Sensitivity and Uncertainty Analyses

In Iterative Performance Assessment Phase 2 (Wescott, et al., 1995), model results were evaluated to develop regression equations describing total-system performance assessment model output and to analyze input parameter sensitivity. Techniques used to develop a regression equation that emulated the total-system performance assessment model included transformation of data (Iman and Conover, 1979; Seitz, et al., 1991); test for heteroscedasticity (residual variation—Draper and Smith, 1981; Bowen and Bennett, 1988; Sen and Srivastava, 1990); and Mallows' C_p statistic (Sen and Srivastava, 1990). In addition to techniques used in previous performance assessments (e.g., the stepwise linear regression), several techniques were evaluated to determine parameter importance and sensitivity, including Kolmogorov-Smirnov and Signs tests (Bowen and Bennett, 1988) and differential analysis (Helton, et al., 1991).

Phase 2 Iterative Performance Assessment also included igneous activity, seismicity, faulting, climate change, and exploratory drilling. Sensitivity and uncertainty analyses were conducted for the undisturbed case as well as for the aforementioned disruptive scenarios. These analyses were conducted with radionuclide release to the accessible environment and integrated population dose as the output variables.

1.1.4 TPA Version 3.1 Code Sensitivity and Uncertainty Analyses

For the TPA Version 3.1 code (NRC, 1999b), a variety of analytical procedures were implemented to assess sensitivity of the estimated peak dose because of variations in the values of model parameters as well as changes resulting from use of alternative conceptual models. Scaled sensitivity coefficients were obtained by univariate and stepwise, multiple linear regression, and by standard differential analysis. To make linear regression models as accurate as possible, the dependent (peak dose) and independent (sampled inputs) variables were transformed using four methods: (i) normalization, in which the variable is divided by its mean; (ii) standardization, in which the difference between the variable and its mean is divided by the standard deviation of the variable; (iii) rank transformation, in which the value of the variable is replaced by its numerical rank; and (iv) logarithmic transformation, in which a multiplicative model is converted to an additive model. The statistical significance of the scaled sensitivity coefficients obtained by stepwise regression was determined using student t-statistic. The importance or influence of each parameter was ranked by the order in which the stepwise procedure selected the parameter for inclusion as an explanatory variable in the regression equation and by the use of Kolmogorov-Smirnov and Sign tests (Boron and Bennett, 1998).

Sensitivity coefficients were calculated for both 10,000- and 50,000-year time periods and for waste canisters constructed with an inner corrosion-resistant layer of either Alloy 625 or Alloy 22 leading to the identification of four distinct sets of important parameters. The effects of employing alternative conceptual models were also investigated for a variety of repository subsystems. Descriptions of alternative conceptual models considered include (i) backfilling of the repository, (ii) diffusion in the rock matrix, (iii) credit for protection of the fuel provided by zircalloy cladding, (iv) focusing the flow of water to a smaller number of waste packages, (v) use of the flow through model for spent nuclear fuel dissolution and transport, (vi) radionuclide release rates based on natural analogs for spent nuclear fuel, (vii) no credit for sorption of radionuclides, and (viii) instantaneous failure of all waste packages.

Based on the results of the sensitivity and uncertainty analyses, preliminary conclusions were drawn about the relative importance of the integrated subissues. For the 10,000-year simulation period, the most important integrated subissues are those for waste package corrosion and the quantity and chemistry of water contacting the waste packages. When Alloy 22 is used, corrosion of the waste packages is minimal during the 10,000-year simulation period, and mechanical disruption of the waste packages is the most important integrated subissue. For the 50,000-year time period, the integrated subissues related to dilution of radionuclides in groundwater through well pumping and retardation in water production zones and alluvium are most important.

1.1.5 TPA Version 3.2 Code Sensitivity and Uncertainty Analyses

The TPA Version 3.2 code sensitivity and uncertainty analyses (Mohanty, et al., 1999) emphasized step-by-step evaluation of total system performance using intermediate code results that reflected the behavior of individual processes and subsystems. Analyses of results were based on TPA Version 3.2 code runs involving (i) a single realization with all sampled parameters fixed at mean values and (ii) multiple realizations where uncertain parameters were sampled from assigned data ranges. Effects of parametric uncertainty on performance results were analyzed using scatterplot and stepwise multiple linear regression techniques (as previously done), however, the application of additional techniques such as the Morris method, Fourier Amplitude Sensitivity test, and Parameter Tree method diversified the suite of methods used to gain insight to parameter sensitivities. The sensitivity and uncertainty analyses were conducted using numerous TPA Version 3.2 code runs (several thousand realizations) for each sensitivity analysis technique. Results of system-level analyses were based on peak dose and peak expected dose to a receptor group 20 km [12.4 mi] from the repository during the 10,000-year compliance period at 50,000 or 100,000 years after closure (a longer period was used for investigating any significant effects that may not be evident because of the calculated long life of the waste package).

System-level results indicated the igneous activity scenario presented a greater risk than the basecase scenario representing undisturbed repository performance. Influential parameters for the 10,000-year and 50,000-year time periods were mapped to the integrated subissues, and seven of the integrated subissues were identified as not significant for the 10,000-year period. The most sensitive integrated subissues identified for 10,000 years included (i) waste package degradation, (ii) quantity and chemistry of water contacting waste packages and waste forms,

(iii) spatial and temporal distribution of water flow, (iv) retardation in the water production zone and alluvium, (v) dilution of radionuclides in groundwater because of well pumping, (vi) volcanic disruption of waste packages, and (vii) airborne transport of radionuclides. Staff working on various key technical issues used this information to improve models and data supporting parameter uncertainty distributions.

1.2 Purpose of Current Analysis

The current sensitivity and uncertainty analyses involve a variety of techniques used in the aforementioned previous iterations. The objectives of the analyses described in this report build on the goals of previous iterations and include

- Inform staff reviews of the DOE TPA on those factors most significant to total system performance.

- Within the framework of the total system performance assessment model, determine the extent repository barriers reduce water flow and prevent or delay radionuclide transport to the receptor location.

- Explain the performance of the repository system based on modeled repository behavior at the process, subprocess, and subsystem levels.

- Estimate the risk and associated uncertainty to an average individual at the receptor location from the basecase scenario (a scenario where the deterioration of the engineered system takes place through a naturally slow process) and from disruptive event scenarios (where rare acute natural events can impact repository performance).

- Determine the input parameters (range and type of distribution), alternative conceptual models, and subsystems in the TPA Version 4.1 code that have the greatest effect on the estimated peak dose for the time period of interest at the receptor location by using a variety of techniques. This report summarizes analyses conducted to determine the parameters, alternative conceptual models, and subsystems that have the greatest influence on total system performance.

- Estimate the relative importance of the integrated subissues or key elements of subsystem abstraction.

- Continue improving staff capabilities, including the TPA code, for independent evaluation of future DOE total system performance assessments for the site recommendation and license application for the proposed Yucca Mountain repository.

Since the release of the TPA Version 3.2 code, which was used in the last published sensitivity analysis report (Mohanty, et al., 1999), several major improvements were incorporated into the TPA code and associated input data sets that affect sensitivity analysis results. Although most changes were based on new information provided by DOE after completion of the TPA Version 3.2 code, major modifications made to the TPA Version 4.1 code include

- Incorporation of the DOE Enhanced Design Alternative II and drip shield barrier into performance calculations

- Addition of waste package failure modes resulting from complex igneous process calculations performed outside the TPA Version 4.1 code

- Improvements of the matrix diffusion model for saturated zone hydrologic transport calculations

- Variation of length for the tuff and alluvium groundwater flow paths to incorporate current uncertainties in site hydrology

- Addition of time dependency to the calculation of resuspension of ash deposits for the inhalation dose calculations following a postulated igneous event

- Enhancement of biosphere dose modeling capabilities to improve integration with total system calculations, propagate input uncertainties to dose results, and provide greater flexibility in parameter input and output

- Inclusion of much finer discretization capability for the repository and geologic setting

A detailed list of modifications made for the TPA Version 4.1 code is provided in Mohanty, et al. (2002).

1.3 Report Organization

This report documents the most recent system-level analyses performed by NRC and CNWRA that were conducted using the TPA Version 4.1 code. Chapter 2 provides a brief description of the conceptual models in the TPA Version 4.1 code. Chapter 3 presents an analysis of total system behavior. Analyses using the mean value data set to explain the trend in the intermediate and final outputs are presented in this chapter for the basecase and for the disruptive events cases. Results from multiple realizations using basecase data and data associated with disruptive events are explored in this chapter to highlight how variability in sampled parameters leads to variability in dose. These results have been used to analyze the extent to which the barriers in the repository reduce flow of water and delay transport of radionuclides.

Chapter 4 describes the system-level sensitivity studies, which were conducted in two parts. The sensitivity and uncertainty of repository performance to specific parameters were evaluated using a variety of statistical tests because no single test is comprehensive. The use of numerous methods (described in this chapter and Appendixes A–D) to examine the sensitivity of repository performance to individual parameters is intended to identify, as comprehensively as possible, those parameters most important for understanding repository performance. The parameters identified as important are also verified to provide additional confidence in the results. Alternative conceptual models and disruptive scenario cases were compared to evaluate the relative importance of specific components and assumptions used in the model. Analyzing the influence of individual components of the model using the full set of parameter values and a comprehensive model of repository behavior allows the relative importance of the components to be investigated.

Chapter 5 describes distributional sensitivity analysis methods and results. This chapter investigates if the repository performance is sensitive to the selected distribution type for a parameter. The choice of distribution function, which is greatly influenced by the lack of sufficient data, can affect significantly the dose responses. Chapter 6 presents the subsystem sensitivity analysis approach and results used to understand the influence of the subsystems on performance assessment results. Chapter 7 provides a synthesis of all results, including risk insights, gained from the analyses. Risk insights are presented through (i) the description of barrier capabilities in reducing flow of water and preventing or delaying movement of radionuclides, (ii) the identification of parameters that are important based on parametric and distributional sensitivity analyses, (iii) subsystems that are influential based on repository component sensitivity analyses, (iv) conceptual models that are important based on alternative conceptual model studies, and (v) results that are mapped to the integrated subissues. Chapter 8 presents the summary and conclusions. Appendix E describes the abbreviated parameter names used throughout the report, and Appendixes F and G provide additional details supporting performance calculations of human intrusion and in-package criticality.

1.4 Caveats

Because it is not practical to model a system as complex as a geologic repository in a complete and exhaustive manner, numerous assumptions and simplifications are used directly, or are implicit. Consequently, there are limitations associated with any models that makes assumptions and simplification. Even if it includes assumptions and simplifications, the objective of a performance assessment model is to provide a reasonable representation of repository performance. These assumptions and limitations for the analyses presented in this report are listed next.

- Any underlying assumptions, limitations, and bases used to construct the models in the TPA Version 4.1 code also apply to these analyses. These models are described in Chapter 2 and discussed in greater detail in the TPA Version 4.0 code user's guide (Mohanty, et al., 2002).

- The results are limited by the use of simplifying assumptions and models, and parameters based on limited data. As a consequence, these results are for illustration only. Moreover, the manner in which these analyses were conducted or the assumptions and approaches used should not be construed to express the views, preferences, or positions of the NRC staff regarding implementation of regulations at Yucca Mountain.

2 OVERVIEW OF THE TOTAL SYSTEM PERFORMANCE ASSESSMENT CONCEPTUAL MODELS IN THE TPA VERSION 4.1 CODE

The TPA Version 4.1 code focuses on the postclosure performance of the proposed high-level waste repository at Yucca Mountain for long time periods (e.g., 10,000 years). To quantify the uncertainty in estimating repository performance during long time periods, the total-system performance assessment analysis is conducted in a probabilistic manner in which many realizations are simulated using input parameter sets sampled from probability distributions. Detailed simulation models that include all the process couplings, heterogeneities, and complexities are not incorporated into the code to maintain reasonable computer execution times with modest hardware resources.

The TPA Version 4.1 code is used in this analysis to obtain deterministic and probabilistic estimates of dose for specified time periods (e.g., regulatory compliance simulation period and beyond) at designated receptor locations {e.g., 20 km [12.4 mi] downgradient of Yucca Mountain}. The TPA Version 4.1 code, which is specifically tailored for evaluation of performance of the proposed repository at Yucca Mountain, is an update of the code used in the review of the U.S. Department of Energy (DOE) Total System Performance Assessment–Viability Assessment Phase 2 study (Mohanty, et al., 1999). Conceptual models used in the previous version of the TPA code have been documented in Mohanty and McCartin (1998) and for the 4.0 version in Mohanty, et al. (2002).

The TPA Version 4.1 code user's guide contains additional detailed information on the conceptual and mathematical models and the code structure. A simplified flowchart illustrating the structure of the TPA Version 4.1 code is presented in Figure 2-1. The total-system performance assessment input parameter values and the bases for their selection are presented in Appendix A of the same user's guide.

2.1 Conceptualizations of the Repository and its Geologic Setting

For ease of use and computational efficiency, the TPA Version 4.1 code replaces the intricate repository layout and the complex geologic setting with relatively simple conceptual representations. The repository layout, for example, is represented by an idealized planar feature discretized into a set of subareas, while the geology is replaced by a sequence of laterally homogeneous layers. Properties and environmental conditions for each subarea are assumed uniform. Except for the influence of the climatic conditions (e.g., precipitation) and thermal load, flow and transport processes in and below a given subarea are independent of processes in other subareas. Thus, flow is entirely vertical with no lateral diversion in the unsaturated zone.

As illustrated in Figure 2-2, quadrilateral subareas of uniform thickness are used to represent individual subregions of the repository. In the current application, the repository is divided into 10 subareas; however, the TPA Version 4.1 code has the capability to use much finer discretizations of both the repository and the geologic setting beneath it. The number of waste packages in each subarea is assumed proportional to the fraction of the total repository area represented. Radionuclide releases from the engineered barrier subsystem are calculated by modeling a single prototypical waste package for each subarea and for each failure type. Performance characteristics of the waste package and subsequent release in each subarea are

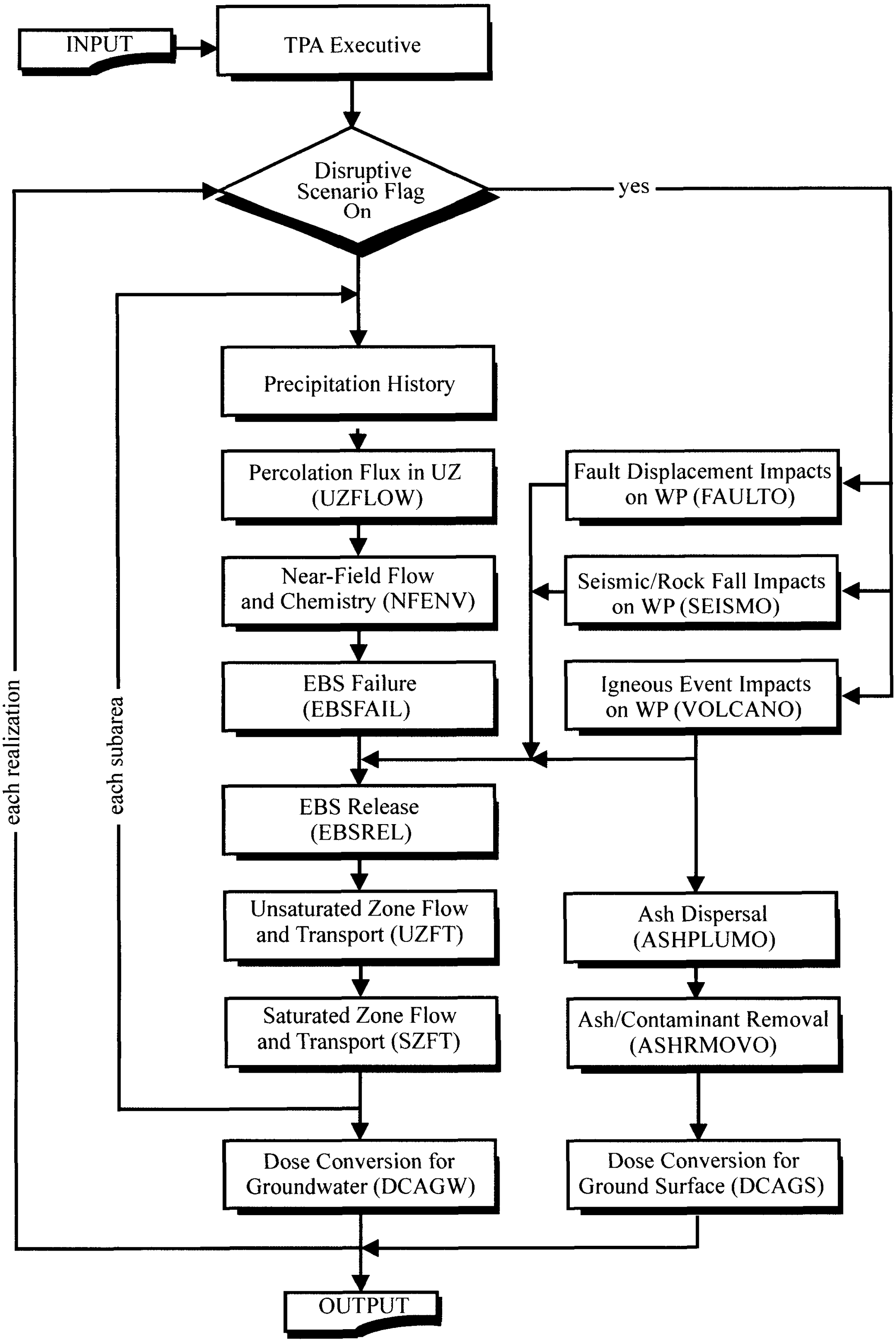

Figure 2-1. Flow Diagram for TPA Version 4.1 Code

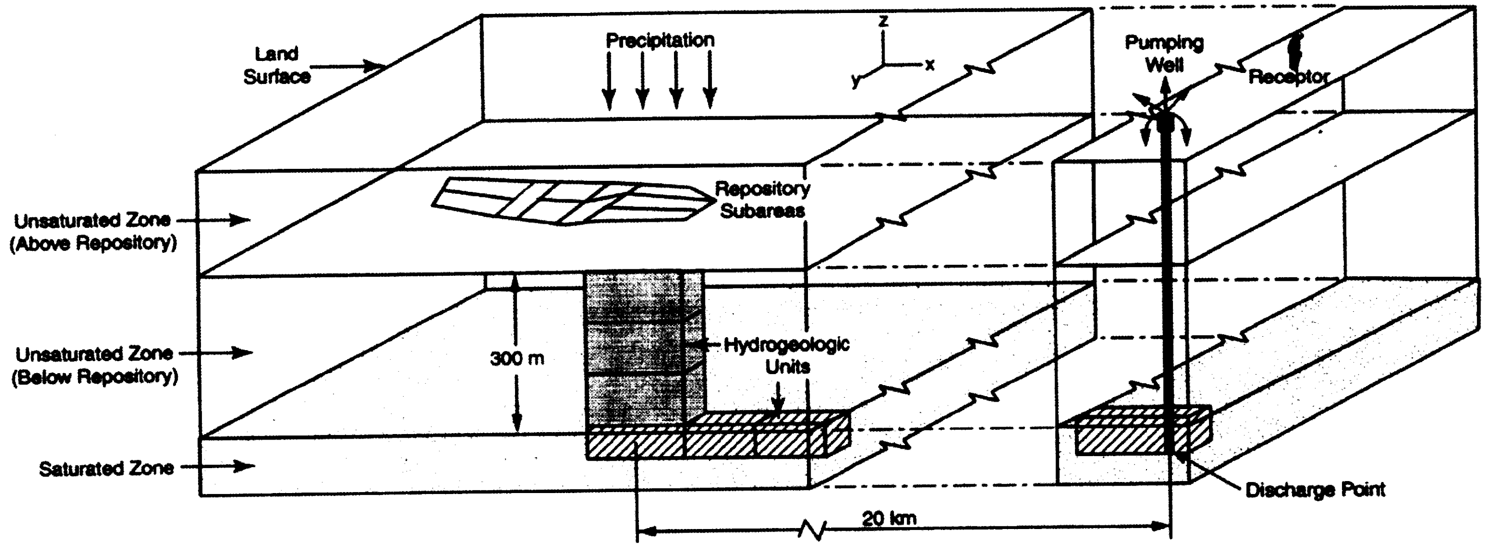

Figure 2-2. Conceptualization of the Repository System

calculated by considering the evolution of such characteristics as climatic conditions, water flux, thermal and chemical conditions, and geologic processes (e.g., seismicity, fault displacement, and igneous activity). Breaching of the waste package by human intrusion and the associated release are considered separately.

The geologic setting is composed of the unsaturated zone (i.e., geologic media between the ground surface and the water table) and the saturated zone (i.e., groundwater aquifer beneath the repository, extending to the location of the receptor group). For simplicity, the stratigraphy is assumed laterally continuous and uniform within a subarea, but differing from subarea to subarea. This simplification implies that, in general, flow in the unsaturated zone is primarily vertical with little or no lateral diversion of flow along hydrostratigraphic units. This simplification is based on the assumptions that the shallow infiltration does not vary substantially among subareas and the near-field thermohydrologic processes do not show substantial subarea-scale variation. The geologic setting also includes features, events, and processes, such as seismicity, tectonism (faulting), and igneous activity (intrusive and extrusive) that may adversely affect the performance of the repository. Seismicity, tectonism, and intrusive igneous activity affect the performance characteristics of the waste package and contribute to groundwater releases.

To model flow and transport in the saturated zone, the total-system performance assessment conceptual model consists of three distinct streamtubes over the width of the repository footprint normal to unsaturated zone flow. Each of the 10 subareas in the unsaturated zone is connected to 1 of the 3 streamtubes in the saturated zone, based on proximity. Radionuclide releases from each of the unsaturated zone streamtubes provide the source term to the saturated zone streamtubes. The saturated zone streamtubes are treated as separate conduits and have flow velocities that vary along the individual flow paths. The mass flowrate of radionuclides exiting all saturated zone streamtubes at the well head is used to calculate annual dose to the average member of the receptor group. The annual dose computation accounts for all releases in the groundwater pathway at the location of the receptor group, the spatial extent of the releases in the saturated zone at the location of the receptor group, the extent of the production zone containing the radionuclides (all radionuclides are assumed released in one production zone), and the influence of the pumping rate attributed to water use by the receptor group.

Direct release of radionuclides to the accessible environment because of an extrusive igneous event is also modeled in the TPA Version 4.1 code. The physical characteristics of the extrusion and the assumption of a uniform distribution of waste packages in the repository are used to determine the number of waste packages affected by the event. Alternative modeling is also used to capture the complex magma-repository interaction in determining the waste packages affected by the extrusive event. Radionuclides are transported to the receptor location, based on characteristics of the eruption and meteorological conditions. The areal density of radionuclides in the soil, resulting from the deposition of volcanic ash containing spent nuclear fuel particles, is then calculated. This soil concentration is used in computing the annual dose to the average member of the receptor group.

2.2 Conceptual Models Implemented in the TPA Version 4.1 Code

In developing the TPA Version 4.1 code, several conceptual models were formulated, integrated, and implemented through abstracted mathematical models. These basic conceptual models, which describe the interactions and couplings of physical and chemical processes believed present in a proposed geologic repository at Yucca Mountain, can be grouped into the following generic categories:

- Infiltration and deep percolation
- Near-field environment
- Radionuclide releases from the engineered barrier subsystem
- Aqueous-phase radionuclide transport through the unsaturated and saturated zones
- Airborne transport from direct radionuclide releases
- Exposure scenario and reference biosphere

The conceptual models are designed to apply to the current DOE repository design and specific site characteristics of the Yucca Mountain area and provide flexibility for examining alternative designs and uncertainties in site and engineered material performance. In some generic categories, alternative conceptual models have also been incorporated into the code.

These conceptual models are used to represent a range of system states including disruptive events. The consequences of disruptive events (e.g., fault displacement and igneous activity) are evaluated with the TPA Version 4.1 code by assessing the effects on engineered barrier failure (producing releases to groundwater), direct releases of radionuclides (airborne releases to the biosphere), or both. Disruptive event consequences are weighted by the probability of the event affecting the repository to calculate a risk versus time curve as explained in Chapter 3.

The following discussion provides a general overview of the key aspects of the major conceptual models implemented in the TPA Version 4.1 code. Detailed descriptions of these models, including the mathematical basis, assumptions, and calculational methodologies, are presented in the TPA Version 4.0 code user's guide (Mohanty, et al., 2002).

2.2.1 Infiltration and Deep Percolation

A one-dimensional modeling approach is used in the TPA Version 4.1 code to describe how meteoric water at the land surface moves vertically downward through the unsaturated zone, to the repository horizon, and ultimately to the water table. In the conceptual model, the deep percolation flux (q_{perc}) is assumed equal to the shallow infiltration rate (q_{infil}). The annual average q_{infil} is estimated based on

- Present-day shallow-infiltration rate
- Change in climate with time
- Elevation, vegetation, evapotranspiration, and soil depth for the repository subarea

Uncertainty in the present-day infiltration rate estimate is accounted for in the TPA Version 4.1 code by treating it as a statistically sampled input parameter. Temporal variations are incorporated by varying the present-day infiltration rate for the 100,000-year period assumed for long-term climatic changes. The effects of site-specific soil cover thickness, vegetation, and elevation are used to reflect the spatial variation for each of the subareas.

The variation of q_{infil} from changes in climate was developed through consideration of paleo-climatic information and results from detailed process-level auxiliary analysis (Stothoff, et al., 1997; Stothoff, 1999). The q_{infil} response function depends on two independent variables, present-day mean annual precipitation and temperature, as well as the present-day infiltration rate. After computing q_{infil}, the water flux at the repository horizon is then partitioned into

- Water flux diverted around the failed waste package
- Water flux entering the failed waste package

Thus, for the purposes of the TPA Version 4.1 code, the net water flux carrying dissolved radionuclides is a fraction of the total water flux arriving at the repository. It is this net water flux that is used in the TPA Version 4.1 code to calculate the radionuclide source term for each subarea.

2.2.2 Near-Field Environment

Physical and chemical processes in the near field of the repository, such as heat transfer, water-rock geochemical interactions, and refluxing of condensate water, are expected to affect waste package performance. In the TPA Version 4.1 code, a range of near-field characteristics is included in the abstracted mathematical models for heat and water flow, while table look-ups are used for chemical parameters. For estimating waste package failure times and radionuclide release rates, the near-field environment is characterized by

- Surface temperatures of the drift wall rock and waste package
- Relative humidity in the region between the waste package and drift wall
- Water chemistry (e.g., pH, chloride concentration, and carbonate ion concentration)
- Water reflux during the thermal phase

The average rock temperature in the repository horizon is calculated using a conduction-only model that considers the time history of temperature for each subarea calculated from the amount of emplaced waste. The waste package surface temperature is calculated using a multimode heat transfer (i.e., conduction, convection, and radiation) model based on thermal output from the waste package and the repository horizon temperature. Temperature calculations account for ventilation during the preclosure period that could potentially reduce peak waste package temperature and the presence of the drip shield. Water vapor pressure is computed using the standard thermodynamic equation relating vapor pressure to temperature.

Estimates of the pH and chloride concentration histories of water films on the waste package surface were developed in a separate analysis using the multicomponent geochemical module of the MULTIFLO code (Lichtner, et al., 2000). Because the chloride concentration in the water film is likely to be higher than that in the rock mass, the chloride history is scaled by a statistically sampled parameter. The TPA Version 4.1 code provides the option of either using a look-up table that uses the temperature-dependent pH (not currently used) and chloride concentration generated with the MULTIFLO code or specifying constant values in the input file.

The amount of water percolating through the drifts varies with time primarily because of the coupled processes of heat transfer and fluid flow (e.g., vaporization, condensation, and refluxing). Water refluxing produced by these thermohydrologic effects is important for the first few thousand years, after which natural percolation wholly determines the rate of water flow into the repository. Three lumped-parameter water reflux models are included in the TPA Version 4.1 code. The first model considers episodic reflux associated with time-dependent perching above the repository. The second model assumes the volume of refluxing water will always be sufficient to depress the boiling isotherm in fractures and reach the waste package during the times the surface temperature exceeds the boiling point of water. In the third model, the degree to which the boiling isotherm is depressed is a function of the temperature, the thickness of the dryout zone, and the volume of reflux water. These functions vary with time. Each reflux model produces estimates of the total water flux into the repository during the thermal period.

2.2.3 Radionuclide Releases from the Engineered Barrier Subsystem

The specific layout of the underground repository facility is based on the DOE new Enhanced Design Alternative II (CRWMS M&O, 1999). The key engineered barriers for Enhanced Design Alternative II include the waste package and drip shield. The waste package design for high-level waste disposal consists of a large cylindrical cask {i.e., approximately 1.8-m [5.9-ft] diameter and 5.6-m [18.4-ft] length} surrounded by a 15-mm [0.59-in] thick Alloy 22 outer overpack around a 50-mm [1.97-in] thick Type 316L inner overpack, designed to prevent mechanical failure as a result of rockfall. The waste package will be emplaced in the drift on a v-shaped Alloy 22 pallette held together by stainless steel supports. The Alloy 22 and stainless steel supports rest on an invert of sand or gravel ballast held in place by a carbon steel frame.

A 1.5- to 2-cm [0.6-to 0.8-in] thick drip shield, made of Titanium Grade 7, covers the top and sides of the waste package and extends the length of the emplacement drift. The drip shield is intended to protect the waste package surface from dripping water, especially during the thermal reflux period when the environmental conditions could be conducive to crevice corrosion of the Alloy 22 outer overpack. Backfill, however, is not present in the Enhanced Design Alternative II used in the TPA Version 4.1 code.

In the TPA Version 4.1 code, the performance of a prototypical waste package (including the presence of a drip shield) is modeled for each repository subarea for each of the eight waste package failure categories and subcategories. When this prototypical waste package fails, all waste packages in that subarea for a specified failure category are assumed to have failed. The estimation of both waste package failure times and liquid releases is dependent on the nature and extent of corrosion, effectiveness of the drip shield, the near-field environment, the percolation flux in the drift, and external processes that may impose static loads or dynamic loads. Waste package failures are grouped into three basic categories: (i) corrosion and mechanical failure, (ii) disruptive event, and (iii) initially defective waste package failure. After determining the waste package failure time, the TPA Version 4.1 code calculates the aqueous-phase radionuclide releases from the waste package by considering the dissolution of radionuclides from the spent nuclear fuel matrix, advective transport from the waste package (based on the amount of water contacting and entering the waste package, which can be influenced by assumptions for the drip shield), and advective and diffusive transport through the invert directly to the unsaturated zone beneath the repository.

Corrosion failure of the waste package is defined to occur at the time when the inner overpack is fully penetrated by a single pit and the waste form is exposed to water. The abstracted corrosion model uses a conceptual framework that assumes the formation of a water film containing a salt solution (concentrations before and after drip shield failure are different) but does not explicitly consider water dripping on the container. The corrosion processes considered in the model abstraction include dry air oxidation, humid air corrosion, and aqueous corrosion.

In the Enhanced Design Alternative II, the dry air oxidation and humid air corrosion modes have much smaller contributions to the failure of the waste packages compared with the aqueous corrosion, especially of the Alloy 22 outer overpack. Nevertheless, the TPA Version 4.1 code has retained the capability to evaluate dry air oxidation and humid air corrosion. Waste package surface temperature and the chloride concentration in the water film influence the mode and, hence, the rate of corrosion. The predominant mode of corrosion depends on environmental factors and the container material. Mechanical failure of the waste package, also included in the TPA Version 4.1 code, is considered the result of fracture of the steel overpack because of thermal embrittlement arising from prolonged exposure at temperatures sufficiently elevated to cause substantial degradation of mechanical properties. To estimate mechanical waste package failure in the TPA Version 4.1 code, it is assumed that both overpacks have the properties of steel and, therefore, fail together. In adopting Enhanced Design Alternative II, the consideration of mechanical failure of both the outer and inner overpacks is still incorporated in the TPA Version 4.1 code even if the average waste package temperature is relatively low compared to the spent nuclear fuel design. Failure of the drip shield is not mechanistically modeled in the TPA Version 4.1 code, instead, the drip shield failure time is specified by an input parameter that is either a constant or is sampled.

Disruptive event waste package failures are caused by seismicity, fault displacement, and igneous activity. In the case of seismicity, waste package failures are caused by rockfalls that mechanically load and deform the waste package (drip shield assumed not present for seismic rockfall failure of waste package). Movements along undetected faults or new faults that exceed a preestablished displacement threshold are assumed to fail waste packages within the fault zone. For igneous activity, all waste packages contacted by magma are assumed to fail. Waste packages within a drift penetrated by a dike, but outside the volcanic conduit, are assumed to fail and expose the spent nuclear fuel to water while those within the conduit are assumed entrained in the magma and released directly to the biosphere. Alternatively, a range of waste package failures from entrainment by magma can be specified and determined as external to the TPA code using a one-dimensional hydrodynamic model for magma movement in the drifts. For fault displacement, failures are modeled by superimposing the physical dimensions of the perturbation (i.e., length, width, and orientation of the fault) on the repository footprint to determine the total number of waste packages potentially affected in each repository subarea. Separate failure times are calculated for seismicity, fault displacement, and igneous activity. Multiple seismic events occur during the compliance simulation periods; however, seismic failure occurrences are collected into four distinct failure times.

For most applications of the TPA Version 4.1 code, it is assumed that a small number of waste packages have failed by the time of repository closure. These initially failed waste packages are attributed to fabrication defects or damage to the waste package as a result of improper emplacement. The number of initially defective waste packages is typically assumed to be 0.01 to 1.0 percent of the total number of containers.

Radionuclide releases from the waste package are calculated by considering the alteration rate of spent nuclear fuel (i.e., rate at which radionuclides in fuel become available for release), radionuclide solubility limits, and transport mechanisms out of the waste package. The

TPA Version 4.1 code incorporates numerous parameters, such as the fraction of spent nuclear fuel that is wet, particle size of the spent nuclear fuel, alteration rate of UO_{2+x}, and credit for cladding, that control the release of radionuclides from the spent nuclear fuel matrix. The effects of the formation of secondary minerals such as schoepite on spent nuclear fuel dissolution are treated separately. After radionuclides are leached from the spent nuclear fuel waste form, the calculated releases are adjusted to ensure consistency with the radioelement solubility limits. The gap fraction inventory of radionuclides is available for instantaneous release and, therefore, may be a major contributor to early dose.

A parameter value in the input file is used to specify the fraction of failed waste packages in the subarea that is wetted and available to contribute to the source term. To compute the time-dependent source term, the TPA Version 4.1 code provides two conceptual models: (i) a bathtub model—the waste package must fill with water before the radionuclides are released and (ii) a flow-through model—radionuclides are released by water dripping on the waste form. For the bathtub model, the waste package is treated as a stirred tank, with the tank capacity dependent on the statistically sampled water outlet height. Water will fill the waste package until the capacity (height) is reached and, thereafter, the amount of water entering the waste package will equal the amount of water flowing out. The water capacity of the bathtub is assumed to be unique to the failure modes and to subareas (except for faulting and igneous activity failures). Releases from waste packages will travel through the invert before exiting the engineered barrier subsystem and entering the unsaturated zone below the repository. If the physical properties of the invert are conducive, the radionuclide species could be sorbed, thus providing an additional barrier to radionuclide release. The flow-through model is a variant of the bathtub model except water does not have to first fill the bathtub before release, and the fraction of fuel wetted is independent of the water level. The user has the option of selecting the mode of water retention in the waste package (bathtub or flow-through) for each failure type.

2.2.4 Treatment of Transport in the Unsaturated and Saturated Zones

Movement of aqueous-phase radionuclides from the repository horizon through the unsaturated and saturated zones to the receptor group is modeled in the TPA Version 4.1 code using the streamtube approach. Each streamtube encompasses one or more repository subareas and is composed of a vertical section from the repository to the water table and horizontal sections in the saturated zone. The transport module NEFTRAN II (Olague, et al., 1991) simulates the spectrum of processes (e.g., advection, dispersion, matrix diffusion, sorption, and decay) occurring within individual streamtubes. Currently, 20 radionuclides, including the most important contributors to dose, are specified for groundwater transport; however, the TPA Version 4.1 code has the capability to model up to 43 radionuclides, if necessary.

Time-dependent flow velocities in the unsaturated zone are calculated using the hydraulic properties of each major hydrostratigraphic unit. The transport module simulates the transport of radionuclides through either the porous rock matrix or fractures.[1] Radionuclide retardation by chemical sorption in the rock matrix can significantly reduce the transport rates and is,

[1]Transport though rock matrix takes place if the percolation rate, q_{perc}, is less than the hydraulic conductivity of the rock matrix, K_{matrix}, or through fractures when q_{perc} exceeds K_{matrix}.

therefore, included in the model. Retardation on fracture surfaces, however, is neglected because the significance of this mechanism has yet to be demonstrated.

Although groundwater flow in the saturated zone is assumed at steady state, radionuclide transport within individual streamtubes is time dependent because the source term varies with time. Streamtubes in the saturated zone exhibit variable cross sections along the flow path; this variable streamtube geometry was based on a separate two-dimensional modeling study of the subregional flow. The conceptual model of the saturated zone assumes that flow in the tuff aquifer is in localized conductive zones (i.e., permeable fracture zones) while flow in the alluvium is presumed uniformly distributed in the alluvial aquifer. Although the streamtube approach neglects dilution effects arising from lateral dispersion, credit is taken for sorption in the alluvium, which is likely to retard aqueous phase transport of many radionuclides. The length of the flow path for the alluvium can have a significant effect on radionuclide retardation in the alluvium. The TPA Version 4.1 code uses a variable distance for the length of the alluvium flow path because the location of the transition from the tuff aquifer to the valley-fill aquifer is not well defined. Additionally, matrix diffusion from flowing pores and fractures into the more-or-less stagnant matrix pore water within the rock is included in the saturated zone transport model.

2.2.5 Airborne Transport for Direct Releases

Radiologic risks associated with the volcanic component of igneous activity are calculated in the TPA Version 4.1 code by modeling airborne releases of radionuclides for simulated volcanic eruptions. The volcanism modules assume that the magma intercepts waste packages, moves upward to the land surface, and then ejects the tephra and spent nuclear fuel mixture into the atmosphere. The physical characteristics of each simulated eruption (e.g., vent size and event power and duration) and atmospheric conditions are treated as statistical parameters in calculations of tephra dispersal and deposition patterns, tephra deposit thickness, and radionuclide soil concentrations. Three primary factors determining the tephra plume geometry and transport rates include

- Power and duration of the eruption
- Wind speed and direction
- Spent nuclear fuel particle sizes

The ash transport model developed by Suzuki (1983) was modified by Jarzemba, et al. (1997) and incorporated into the TPA Version 4.1 code to calculate the distribution of the released radionuclides. The time-dependent radionuclide areal densities are calculated taking into account the thickness of the tephra deposit leaching and erosion rates and radionuclide decay rates. The calculated doses attributed to direct releases are strongly influenced by the time of the event (early events result in larger doses, partly caused by the contribution to the estimated doses from short-lived fission and activation products present in the spent nuclear fuel).

2.2.6 Exposure Pathways and Reference Biosphere

Dose calculations are performed in the TPA Version 4.1 code for exposure pathways applicable to a dose receptor approximating the reasonably maximally exposed individual defined in 10 CFR 63.312. Considering local characteristics of the Amargosa Valley, Nevada, area, the dose receptor is represented as a member of a farming community located 20 km [12.4 mi] south of the repository location (note that changes to the TPA code to use an 18-km [11.2-mi] receptor location consistent with the final 10 CFR Part 63 rulemaking were not implemented prior to conducting calculations for this report). The dose receptor is assumed exposed to radionuclides transported through the groundwater pathway, air pathway, or both as a result of direct releases arising from the volcanic component of igneous activity. Results of these calculations are expressed by the total effective dose equivalent.

Geographic location and lifestyle characteristics assigned to the dose receptor are primary aspects defining the dose receptor specified in the TPA Version 4.1 code. The farming community is assumed to include persons that use contaminated water for

- Drinking {i.e., 2 L/day [0.528 gal/day]}
- Agriculture typical of Amargosa Valley area practices (e.g., growing alfalfa and gardening)

The farming community is assumed exposed to surface contamination through

- Consumption of contaminated farm products (i.e., ingestion)
- Breathing air with ash-spent nuclear fuel particles (i.e., inhalation)
- Direct contact

Site-specific dose conversion factors for each radionuclide and pathway are used to convert radionuclide concentrations in the groundwater and soil to total effective dose equivalent values. The individual dose conversion factors are generated through separate pathway calculations using the GENTPA code. A variety of parameters (e.g., irrigation rates and diet) are used to provide flexibility in defining biosphere and exposure scenario. Two separate sets of parameters are included to represent two distinct reference biospheres associated with the present arid climate and the projected future pluvial climate. In addition to computing the annual dose history for each stochastic simulation, the TPA Version 4.1 code scans these dose calculations to identify the magnitude and timing of the peak dose.

2.3 Basecase Definition and Alternative Conceptual Models

The conceptual models available in the TPA Version 4.1 code are briefly presented in the previous sections. The option to evaluate alternatives to the basecase conceptual models is included in the TPA Version 4.1 code. The following sections list the set of conceptual models selected for the basecase studies and also describe the alternatives to the basecase models analyzed at a process level in Chapter 3. The effects of these models on the total system are discussed in Chapter 4.

2.3.1 Basecase

The basecase input data set reflects current repository design features and likely parameter-range estimates for evaluation of processes affecting repository performance. The set of conceptual models that constitute the basecase against which alternative conceptual models are evaluated in the sensitivity/uncertainty analyses include

- No cladding protection

- Dissolution of spent nuclear fuel based on J–13 Well water chemistry

- Bathtub model (i.e., pooling of water in the waste package after failure) to determine water mass balance and fuel wetting of the failed waste package

- Matrix diffusion of contaminants in the unsaturated zone

A complete list of the input parameters used for the basecase can be found in Appendix A in the TPA Version 4.0 code user's guide (Mohanty, et al., 2002). Climate change and seismicity are considered as integral components of the basecase and, therefore, alternative conceptual models to the components are not considered in the analyses.

2.3.2 Alternative Conceptual Models

Various alternative conceptual models are investigated to determine the sensitivity of repository performance to changes in waste package design, radionuclide release mechanisms, and radionuclide transport models. These alternative model runs are conducted with the TPA Version 4.1 code and do not include disruptive events. The alternative models used in this analysis are grouped according to fuel wetting assumptions, fuel-dissolution models, and transport assumptions. For the analyses presented in this report, the repository performance is defined as peak of the expected dose from the multiple-realization calculation.

2.3.2.1 Fuel-Dissolution Models

The TPA Version 4.1 code contains four models (Model 1–Model 4) for the dissolution rate of the spent nuclear fuel that has contacted water. The basecase model uses Model 2 (Mohanty and McCartin, 1998), which is based on the dissolution rate of spent nuclear fuel in J–13 Well water containing silica and calcium ions. The alternative dissolution models—some of which are combined with fuel wetting alternatives—are listed next.

2.3.2.1.1 Fuel-Dissolution Model 1

The first alternative fuel-dissolution model (Model 1) has an increased spent nuclear fuel dissolution rate at high carbonate concentrations (Mohanty, et al., 2002) and reduced silicate and calcium concentrations in the water entering the waste package.

2.3.2.1.2 Fuel-Dissolution Model 3 (Natural Analog)

In this alternative conceptual model, fuel dissolution and contaminant release rates are based on maximum likely rates inferred from measurements at the Peña Blanca, Mexico, natural analog site (Murphy and Codell, 1999). For this alternative, the uranium dissolution rate for fully exposed fuel is 24 kg/yr [53 lb/yr] from the entire repository but is further limited by the fraction of wetted waste packages and the fuel wetting factors, which range from 0 to 1. This alternative conceptual model is invoked by setting Model 3.

2.3.2.1.3 Fuel-Dissolution Model 4 (Schoepite Dissolution)

The schoepite-alternative conceptual model assumes that all radionuclides released from the spent nuclear fuel matrix are captured in the secondary uranium mineral schoepite (Murphy and Codell, 1999) and are subsequently released at a limit controlled by schoepite solubility. This model is specified by setting Model 4. Although there is evidence of incorporation into secondary minerals of some radionuclides (notably Np-237), it is unlikely that other radionuclides important to dose such as I-129 and Tc-99 would be so incorporated. Therefore, this model maybe overly optimistic.

2.3.2.2 Fuel Wetting Assumptions

This grouping includes alternative conceptual models related to the way spent nuclear fuel in the waste package is contacted by water. These five alternative models use combinations of the flow-through and dissolution-rate models and also the TPA Version 4.1 code input parameters for the amount of water and fraction of the subarea wetted by impinging water.

2.3.2.2.1 Flow-Through Model with Fuel-Dissolution Model 2

This alternative conceptual model evaluates the flow-through option in which water enters waste packages through corrosion pits but does not pool in the container. In the bathtub model used in the basecase, the bathtub height is determined by the fraction of fuel wetted (determined by the position of the exit port, which is a corrosion pit), which is sampled and ranges from 0 to 1. In the flow-through model, the fraction of fuel wetted is unrelated to the water level in the waste package. Additionally, the fraction of fuel wetted is likely much smaller than in the bathtub model and depends on poorly understood phenomena such as dripping patterns, surface tension, and vapor-phase wetting. This alternative conceptual model is invoked by setting the appropriate Water Contact Mode flags to 1, which selects flow-through, and by specifying a smaller range for the parameter WastePackageFlowMultiplicationFactor (one-tenth of the normal range for the basecase)[2] to simulate a smaller fraction of wet fuel surface. In this model, solubility limits for the radionuclides might become important because of the limited amount of water in contact with the fuel.

2.3.2.2.2 Flow-Through Model with Fuel-Dissolution Model 1

This alternative conceptual model uses the flow-through model described in the last paragraph but with the Model 1 (carbonate-dissolution model), which assumes that silica and the calcium ion will be depleted from much of the water entering the waste package by reaction with the fuel and metal in their path.

2.3.2.2.3 Focused Flow

The basecase conceptual model assumes that all parts of a repository subarea will receive an equal quantity of infiltrating water. This alternative conceptual model accounts for the possibility

[2]WastePackageFlowMultiplicationFactor is a parameter that controls the fraction of water infiltrating the repository from the unsaturated zone above the repository that will enter the waste package contributing to the release of radionuclides. Water dripping toward the drifts may be diverted around the drift because of capillary action, may be diverted down the side of the drift, or may not enter the waste package for other reasons.

that infiltration reaching the waste packages will be focused or funneled by discrete fractures, which will wet some of the waste packages more heavily than others. This alternative model is invoked by increasing the range of WastePackageFlowMultiplicationFactor parameter by a factor of four (from 3.15×10^{-2} — 1.05×10^{3} to 1.26×10^{-1}— 4.20×10^{3}), while decreasing the fraction of waste packages wetted by a factor of one-fourth (from 0–1 to 0–0.25). This setting has the effect of funneling the same quantity of water for each subarea to one-fourth the number of waste packages.

2.3.2.2.4 Cladding Credit Plus Spent Nuclear Fuel-Dissolution Model 1

The basecase conceptual model assumes that once the inner and outer containers have been breached, spent nuclear fuel is exposed and available for dissolution and transport. This assumption ignores any protection afforded the fuel from intact and only partially failed cladding. In this alternative model, the effect of cladding protection is simulated by setting the cladding credit factor at a constant value of 0.01 for the entire simulation period, which is 1/100th of the cladding credit factor used in the basecase. A factor of one represents no cladding credit.

2.3.2.2.5 Grain-Size Model with Fuel-Dissolution Model 1

This conceptual model uses the grain size from the uranium dioxide fuel instead of the particle size to determine surface area, which leads to a higher dissolution rate because of the increased surface area. This alternative conceptual model combines the fuel-dissolution Model 1 for relatively fast dissolution by carbonate water, with the large surface area of the grain size.

2.3.2.3 Transport Alternatives

The transport assumptions in the basecase unsaturated zone and saturated zone conceptual models are investigated with three alternative models. These assumptions affect the releases and time of release from the engineered barrier subsystem, unsaturated zone, and saturated zone.

2.3.2.3.1 No Retardation of Plutonium, Americium, and Thorium

This alternative conceptual model demonstrates the contribution to repository performance of retardation of plutonium, americium, and thorium in the geosphere and the effect on the groundwater doses if chemical conditions resulted in no sorption. Once released from failed waste packages, plutonium, americium, and thorium are assumed to travel at the same speed as water through the engineered barrier subsystem, unsaturated zone, and saturated zone to the receptor location. This alternative model is invoked by setting partition coefficients (K_d) to zero and retardation coefficients (R_d) to unity for these elements. This model approximates the potential effect of colloids that could move through the geosphere unretarded if filtration processes were not considered radioactive.

2.3.2.3.2 No-Solubility Limit Model

This alternative conceptual model demonstrates the contribution of the solubility limit of each radionuclide and the effect on the groundwater doses if this limit was removed for each radionuclide. Once the spent nuclear fuel is dissolved, the radionuclides are assumed to remain dissolved in the water in the waste package and exit with the water flowing out of the waste package. The model is invoked by setting the solubility limits at high values {100 kg/m^3 [6.24 lb/ft^3]}. This calculation provides an estimate of the capability of the solubility limit in delaying the release of groundwater radionuclides. The effect of the solubility limit in delaying releases has been studied for the bathtub water fuel wetting mode separately from the flow-through fuel wetting mode.

2.3.2.3.3 No Matrix Diffusion

This conceptual model assumes that no matrix diffusion will occur in the tuff saturated zone transport legs where there is fracture flow. No matrix diffusion is specified by setting the parameter DiffusionRateSTFF as a constant value of 0.0 yr^{-1}.

3 ANALYSIS OF TOTAL SYSTEM BEHAVIOR

In this chapter, the relationships between repository performance, key input parameters, and intermediate results for deterministic and probabilistic cases are presented. For the probability case, most techniques rely on the Monte Carlo method for determining system performance. The performance measure of the system in the U.S. Nuclear Regulatory Commission (NRC) Yucca Mountain repository performance assessment exercises is the peak dose in the simulation period to an exposed individual located 20 km [12.4 mi] from the repository. Many of the input parameters are not precisely known and are spatially variable so their values are described by probability distributions. The Monte Carlo technique makes repeated calculations (called realizations) of the possible states for the system, choosing values for the input parameters from their probability distributions. Although 330 input parameters[1] are sampled in the TPA Version 4.1 code, only a few of these parameters contribute significantly to the uncertainty in peak dose because of the great sensitivity of peak dose to the parameters, the large variability of the parameters, or both. The mean values and distributions for the uncertain total-system performance assessment input parameters are summarized in Tables 3-1 to 3-18.

In the single-realization case, mean values for the input parameters are used. The mean-value simulation establishes a quantitative baseline demonstration of the behavior of the total system at the process level and of repository performance as measured by groundwater dose. Additionally, the repository performance is related to the key input parameters and intermediate results in a deterministic mode.

After the discussion of results from the mean-value simulation, a description of the variability in the total-system performance assessment results from multiple realizations is presented. The variability in the behavior of the total system at the components level and the system level are analyzed in multiple realizations using distributions for the input parameters. For example, the variability in dose is related to variability in the release rate from the engineered barrier subsystem. Both the single- and multiple-realization basecase analyses provide background information and form the framework to evaluate the sensitivity of repository performance to input parameters presented in Chapter 4. After the multiple-realization results, the outputs from alternative conceptual models and disruptive events are presented. This chapter concludes with a discussion of a methodology used to calculate risks from the disruptive events. Results are primarily evaluated for the 10,000-year regulatory compliance period. To better understand several processes, results are also evaluated out to 100,000 years.

3.1 Single-Realization Deterministic Analyses

This section examines repository behavior for a single realization to illustrate how a repository component influences both the dose and the behavior of other repository components. For the single realization, all input parameters are specified at their mean values. It should be emphasized that the annual dose obtained from using the mean value data set is not the same as the expected annual dose (which is the performance measure) obtained from multiple realizations because of the nonlinear dependency of dose on input parameters.

---

[1]The actual number of parameters contributing to the variability in peak dose is fewer than 330, depending on which group of conceptual models is used in the calculation. The Latin Hypercube Sampling module in the TPA Version 4.1 code samples all parameters that are not constant, regardless of their use in a specific run.

The following is a description of how the repository is described for the calculations. The waste emplaced at Yucca Mountain is assumed to total 70,040 MTUs[1] in an area of 5,400,000 m^2 [2.1 mi^2] {approximately 5,000 m [3.1 mi] long and 1,000 m [0.6 mi] wide}. Assuming an average of 7.89 MTU per waste package and an equivalence between the spent nuclear fuel and other types of wastes, such as U.S. Department of Energy (DOE) spent nuclear fuel and glass high-level waste, approximately 8,877 waste packages will be needed for waste disposal. The initial inventory activity is approximately 6.65×10^{20} Bq [1.8×10^{10} Ci]. Waste packages with a 5.275-m [17.3-ft] length and a 1.579-m [5.2-ft] diameter are emplaced in drifts 5.5 m [18.0 ft] in diameter, spaced 81.0 m [266 ft] apart. The average age of the spent nuclear fuel is 26 years. The descriptions of the mean values for the key parameters used in various process-level calculations are presented in each of the following sections.

3.1.1 Unsaturated Zone Flow

Detailed modeling (Stothoff, 1999) suggests that climate conditions could significantly affect the flow of water in the unsaturated zone and into the repository. As a consequence, the amount of water contacting a waste package, which affects the release rate of radionuclides from the engineered barrier subsystem and the transport of the radionuclides in the unsaturated zone, may also be significantly influenced.

In the TPA Version 4.1 code,[2] precipitation is assumed to vary from present-day to pluvial conditions for 100,000 years. Although the compliance period is just 10,000 years, simulation up to 100,000 years shows possible wetter conditions for the site, and furthers the understanding of performance of the repository if estimates of infiltration, heat-induced evaporation and diversion are beyond the expected ranges. For the mean value data set, Figure 3-1 shows the mean annual precipitation changes from approximately 160 to 330 mm/yr [6.29 to 12.99 in/yr], whereas the infiltrating water entering the unsaturated zone changes from 7 to 37 mm/yr [0.3 to 1.5 in/yr]. At a user-specified time in the TPA Version 4.1 code, the climatic condition switches from nonpluvial to pluvial and back to pluvial at a later time. The nonpluvial to pluvial transition takes place at 13,000 years (based on the Milankovich cycle), which is outside the regulatory period. In a 100,000-year period, the climatic condition is characterized by pluvial conditions approximately 74 percent of the time and by present-day condition 26 percent of the time. Because the onset of the pluvial period lies beyond 10,000 years, the pluvial climates will not affect the waste package failure and the release of radionuclides in the regulatory period of interest.

For higher flow rates, there are generally larger releases because of the greater amount of water available to dissolve and transport radionuclides out of the waste package. Increasing flow rates in the unsaturated zone are not only expected to transport a larger mass of radionuclides from the engineered barrier subsystem, but also lead to higher doses. The mean values of the parameters used to calculate the time-varying infiltration rates in the unsaturated zone are presented in Table 3-1.

---

[1]The repository design specification uses 70,000 MTUs. The additional 40 MTUs only reflects a numerical artifact associated with the waste specification on a per waste package basis.

[2]The specific version of the TPA code used in developing this chapter is 4.1k.

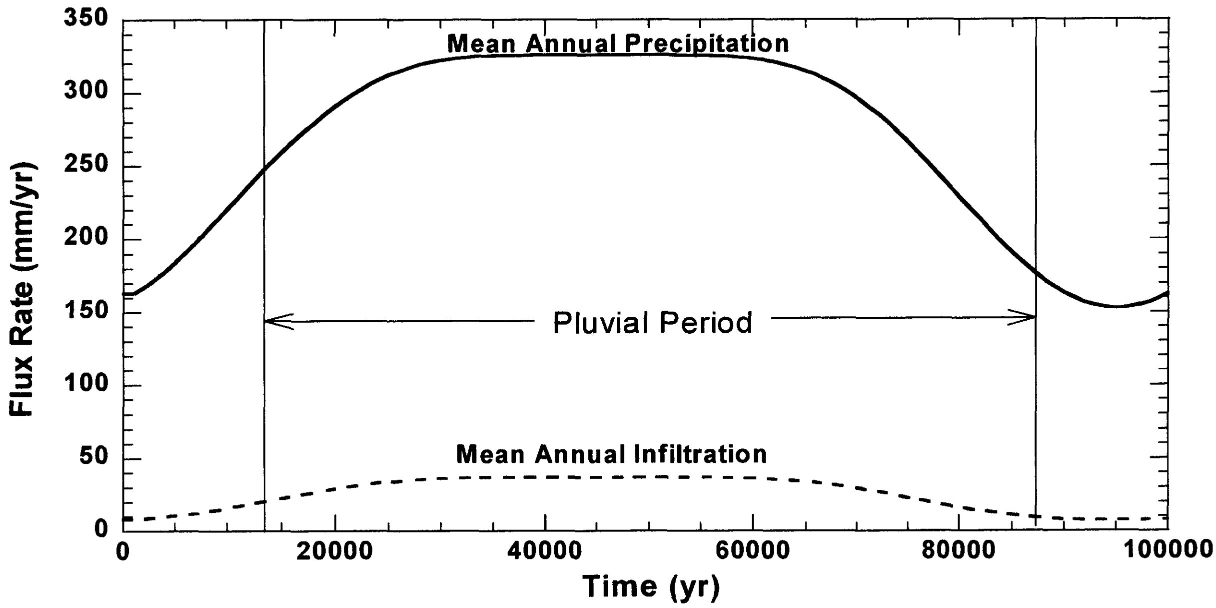

Figure 3-1. Mean Annual Precipitation and Infiltration at the Repository Horizon Averaged Over all Subareas and Encompassing Both the Current and Pluvial Periods for the Mean Value Data Set

Table 3-1. Mean Values and Distributions of Parameters for Infiltration Calculations

Parameter	Mean Value	Distribution
Areally averaged mean annual infiltration for the initial (current) climate	8.5 mm/yr	Uniform; 4.0, 13.0
Mean average precipitation multiplier at glacial maximum	2.00	Uniform; 1.5, 2.5
Mean average temperature increase at glacial maximum	-7.5 °C	Uniform; -10.0, -5.0

3.1.2 Near-Field Environment

Near-field thermal conditions may alter the flow of water into the repository, which influences the quantity of water that contacts, dissolves, and transports the spent nuclear fuel out of the engineered barrier subsystem. The near-field chemical environment, in conjunction with the thermal environment, affects waste package corrosion and determines the quantity and time history of water entering the waste package. These near-field conditions and the flow of water onto the waste packages are discussed in the following sections.

3.1.2.1 Repository-Scale Thermohydrology

Radioactive decay of spent nuclear fuel generates heat that perturbs ambient percolation conditions. The heat evaporates water and creates a dryout zone around the drift. Above the repository horizon, the water vapor condenses and flows back toward the repository by gravity, thus creating a reflux zone. The reflux zone is maintained until the near-field temperature falls below boiling. When the temperature falls below boiling or water from the condensate zone penetrates the dryout zone through fast fracture paths, water flows into the drift. Water entering the drift may impinge on the drip shield and contribute to dripshield corrosion. Water flowing into the drift could change the humidity condition in the drift and, after the drip shield fails, can change the environment at the waste package contributing to waste package corrosion failure, radionuclide release, and transport out of the engineered barrier subsystem into the unsaturated zone.

Of the three reflux models in the TPA Version 4.1 code described in Chapter 2, the third model was used in the basecase. This model estimates the depth of the boiling isotherm (as a function of dryout zone thickness) that water will penetrate and the volume of water flowing from the condensate zone. Table 3-2 presents the mean values of parameters used in the reflux calculations.

Figure 3-2(a) presents subarea-to-subarea variations (see Figure 4-2 in the TPA Version 4.0 code user's guide) in the volume of water contacting waste packages for 100,000 years, which behaves similarly to the infiltration rates in Figure 3-1. Figure 3-2 also shows differences in the seepage flux between subareas and a consistency in the general behavior of the seepage flux for all 10 subareas, with subarea 1 having the largest seepage flow rate, which is attributable to the effects of high elevation and thin soil cover.

The sudden drop in the rate in Figures 3-2(b) and (c) at early times (100–800 years) illustrates a large change in the seepage flux that occurs because of the temperature increase subsequent to the repository closure. Although this thermal perturbation takes place before the corrosion failure of waste packages and drip shields, the modified infiltration rate could affect releases from initially defective failures or seismically induced failures as soon as the drip shield fails. The duration of the thermal perturbation may be significant for the 10,000-year simulation period. The jump in the seepage flux in Figure 3-2(a) at 10,000 years is an artifact of the assumption made in the TPA Version 4.1 code that the thermal perturbation is negligible after 10,000 years, which was made to improve code efficiency. The assumption that the thermal perturbation is negligible beyond 10,000 years, has only a small impact on the peak dose (less than 3 percent), for the 100,000-year simulation. The subarea average infiltration rate in the unsaturated zone is provided in Figure 3-3. Water flowing into the drift and water entering the waste package are also illustrated in this figure. The effects of the thermal perturbation on the flow rate are evident in this figure for approximately 10,000 years. Significant infiltration into the repository is delayed until approximately 900 years and the thermal effects reduce seepage above the repository until just after 10,000 years.

3.1.2.2 Drift-Scale Thermohydrology

Waste package surface temperature, drift wall temperature, and waste package surface relative humidity are computed for each subarea. The mean input parameters used to compute these values are presented in Table 3-2. Figures 3-4(a) and (b) illustrate the subarea-to-subarea differences in the waste package surface temperature, and Figure 3-5 shows waste package

Table 3-2. Mean Values and Distributions of Parameters for Determining Repository Scale and Drift Scale Thermohydrology (Dash in the Last Column Indicates a Constant Value for the Parameter Distribution)		
Parameter	**Mean Value**	**Distribution**
Length of reflux zone*	2.00×10^{1} m	—
Maximum flux in reflux zone*	1.00×10^{-9} m/s	—
Perched bucket volume per subarea-area*	5.00×10^{-1} m^3/m^2	—
Emplacement drift spacing	81 m	—
Waste package spacing along emplacement drift	6.4 m	—
Total waste emplaced in repository	70040 MTU	—
Fraction of condensate removed	0.125/yr	Uniform; 0.0, 0.25
Fraction of condensate toward repository	0.525/yr	Uniform; 0.05, 1.0
Fraction of condensate toward repository removed	0.00	—
Density of water at boiling	9.61×10^{2} kg/m^3	—
Enthalpy of phase change for water	2.40×10^{6} J/kg	—
Temperature gradient in vicinity of boiling isotherm	5.05×10^{1} K/m	Uniform; 1.0, 100.0
Waste package pay load	7.89 MTU	—
Age of waste	26.0 yr	—
Ambient repository temperature	2.00×10^{1} °C	—
Mass density of Yucca Mountain rock	2.58×10^{3} kg/m^3	—
Specific heat of Yucca Mountain rock	8.40×10^{2} J/(kg-K)	—
Thermal conductivity of Yucca Mountain rock	1.56 W/(m-K)	Triangular; 1.34, 1.59, 1.75
Emissivity of drift wall	8.00×10^{-1}	—
Emissivity of drip shield	0.63	—
Emissivity of waste package	8.70×10^{-1}	—
Thermal conductivity of floor	6.00×10^{-1} W/(m-°C)	—
Effective thermal conductivity of unbackfilled drift*	9.00×10^{-1} W/(m-°C)	—
Factor for ventilation heat losses	0.70	—
Time of emplacement of backfill	50.0 yr	—
Effective thermal conductivity of backfill*	0.27 W/(m-°C)	—
Thermal conductivity of inner overpack wall	1.50×10^{1} W/(m-°C)	—
Thermal conductivity of outer overpack	11.1 W/(m-°C)	—
Effective thermal conductivity of basket and spent nuclear fuel in waste package	1.00 W/(m-°C)	—
Elevation of repository horizon	1.07×10^{3} m	—
Elevation of ground surface	1.40×10^{3} m	—
*Not used in Reflux 3 Model		

surface relative humidity. For the mean value data set presented in Table 3-2, the highest temperature of approximately 170 °C [340 °F] is observed at approximately 100 years, after which the temperature drops almost exponentially to 50 °C [122 °F] at 10,000 years. The boiling point, 97 °C [210 °F] at the repository, is reached at 1,500 years, and the temperature drops to ambient temperature, 23 °C [73 °F], at 80,000 years. The sharp rise in the temperature in Figure 3-4(b) from 85 °C [200 °F] at 50 years to 165 °C [329 °F] at 80 years corresponds to the repository closure at 50 years when the ventilation stops. Subareas 1 and 2 are the largest subareas, and subarea 7 is the smallest (located away from the center of the repository and having an elongated shape). Thus, in the largest two subareas (i.e., subareas 1

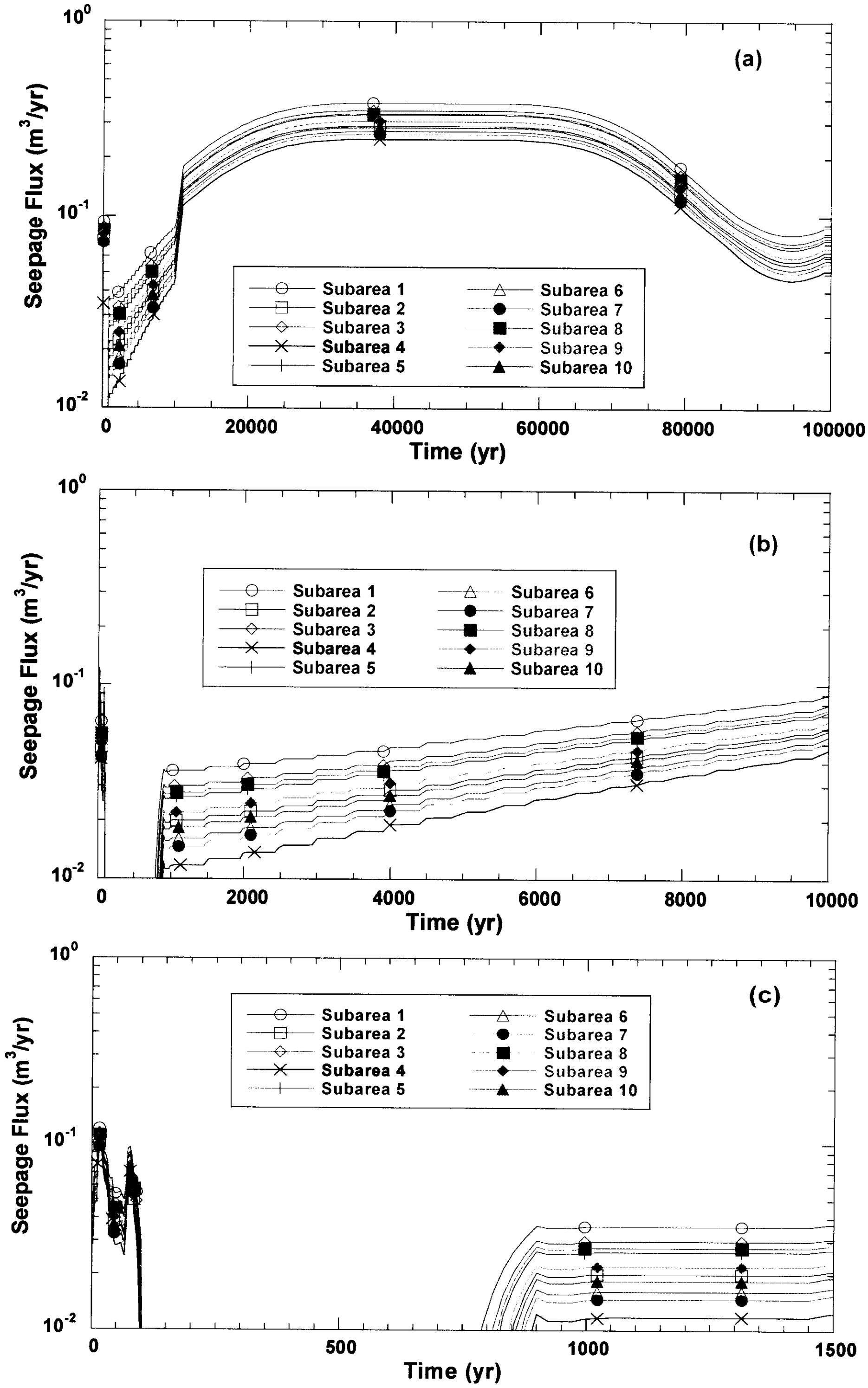

Figure 3-2. Effect of the Thermal Perturbation on the Near-Field Seepage Rate in Each Subarea for the Mean Value Data Set During (a) 100,000-, (b) 10,000-, and (c) 1,500-Year Periods

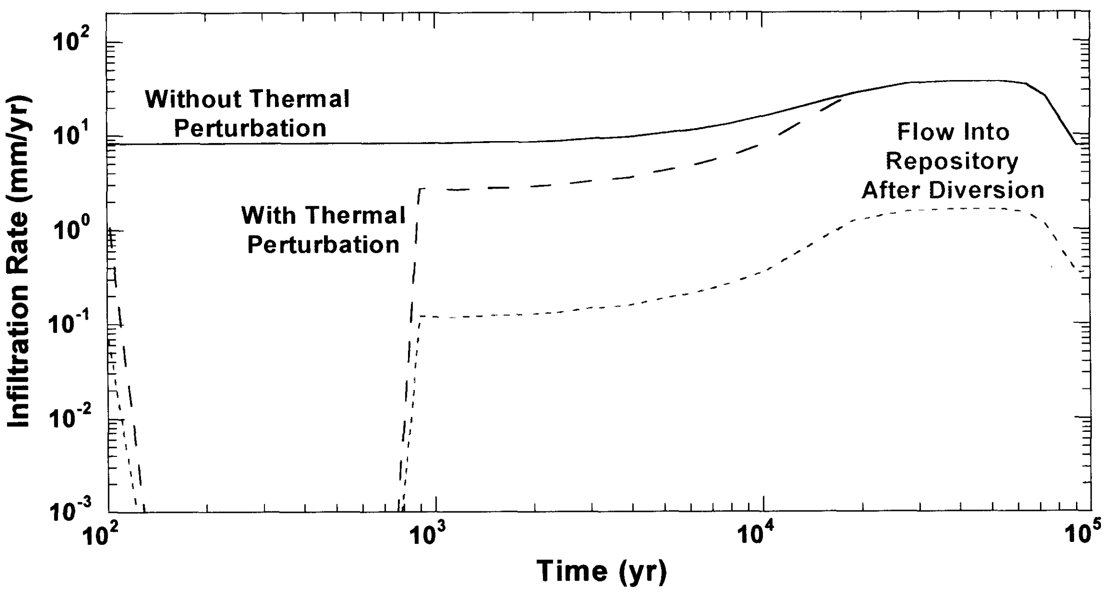

Figure 3-3. Subarea Average Infiltration Rate, Flow into the Drift, and Amount of Water Hitting the Drip Shield (or the Waste Package after the Drip Shield Failure) for the Mean Value Data Set

and 2), waste packages cool slower compared with the smallest subarea (i.e., Subarea 7) because Subarea 7 suffers more from the edge cooling effect than subareas 1 and 2. Cooling is the slowest in Subarea 8 because the exposed surface area for cooling is much smaller than the cooling surface area for Subareas 1 and 2, leading to a much smaller edge cooling effect. At any given time, Subarea 7 exhibits the lowest temperature and Subarea 8 exhibits the highest temperature. Because the temperature for a subarea is determined at its center, the distance of this point from the cooling edge strongly influences predicted temperature in a subarea.

Subarea-dependent temperature and relative humidity values from the near field are also used by the waste package degradation model to determine the waste package failure time. Consequently, the waste package failure time may be different for each subarea. Depending on the selection of the model, spent nuclear fuel dissolution also can be a function of temperature. Therefore, the spent nuclear fuel dissolution rate and, thus, the quantity of radionuclides available for release, can be different for each subarea. For the drift-scale thermohydrology, the climatic conditions were found insignificant in the detailed calculations using equivalent continuum modeling conducted outside the TPA Version 4.1 code.

3.1.2.3 Near-Field Geochemical Environment

The near-field geochemical environment is represented by the time-dependent chloride concentration in water that interacts with the waste package and waste form. The geochemical environment is also characterized by oxygen partial pressure, the solution pH, and the total

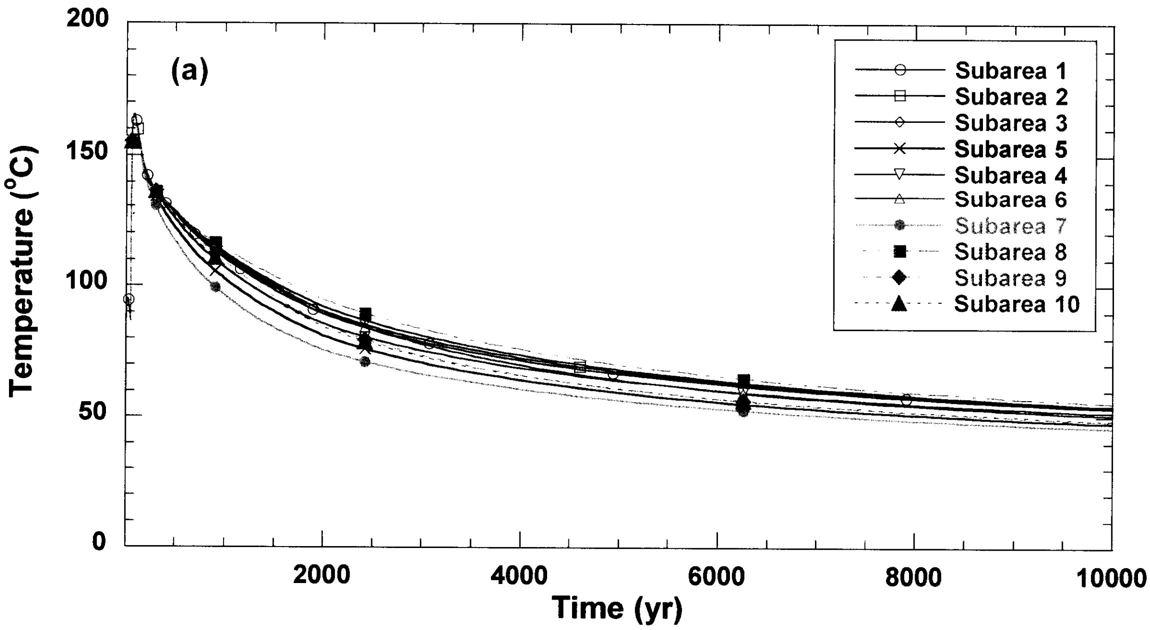

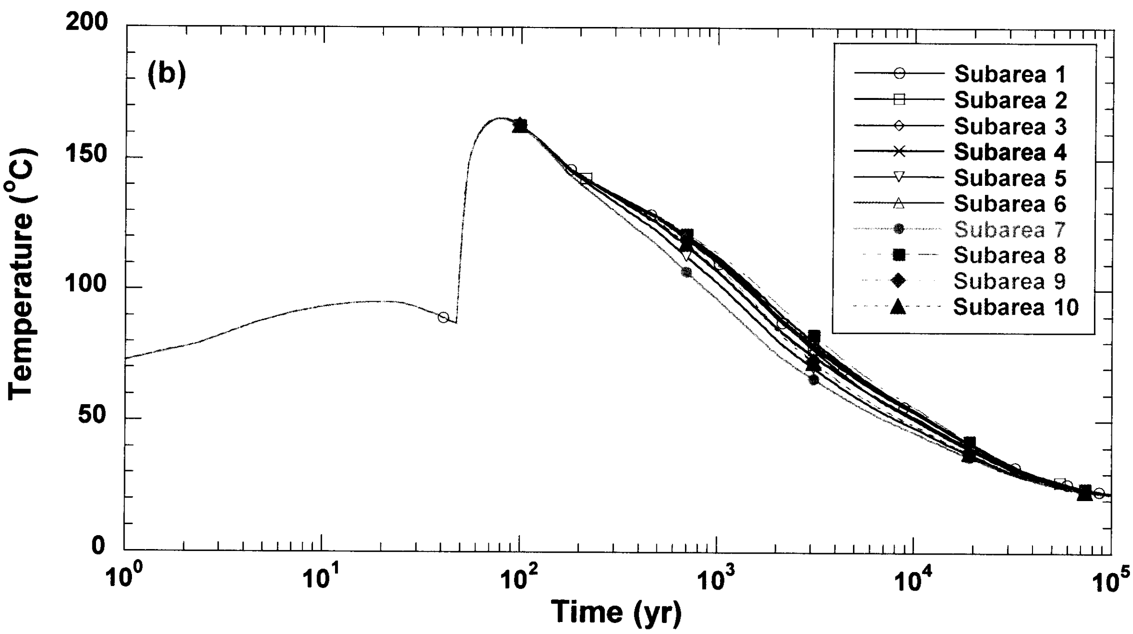

Figure 3-4. Waste Package Surface Temperature in Each Subarea for the Mean Value Data Set in (a) Linear Scale and (b) Log Scale

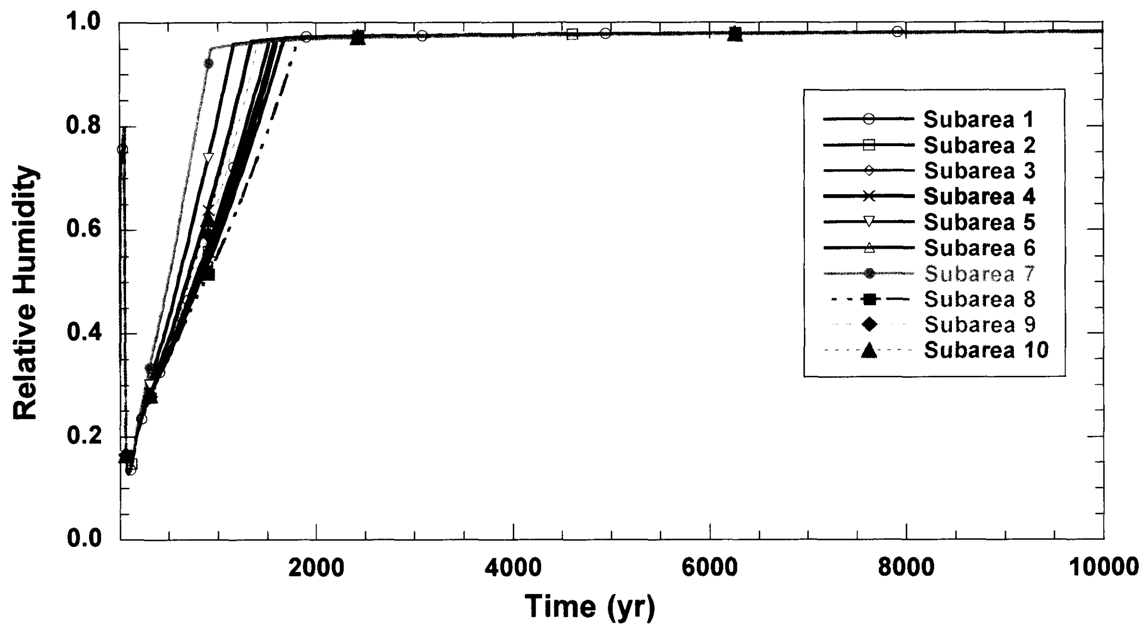

Figure 3-5. Waste Package Surface Relative Humidity in Each Subarea for the Mean Value Data Set

dissolved carbonate, but these characteristics are assumed not to change with time. Figure 3-6 shows the time history of chloride concentration used by the TPA Version 4.1 code, which is calculated with the MULTIFLO (Lichtner, et al., 2000) computer code outside the TPA Version 4.1 code. Uncertainty in the chloride concentration is presented in Table 3-3 along with the other parameters used to calculate waste package corrosion. The chloride concentration is calculated based on an initial fluid composition corresponding to J–13 Well water and represents the time-dependent composition of water available at the drift wall. The fractures dry out quickly and remain dry until approximately 800 years. During this dryout period and within the context of a continuum model, it is not possible to represent the return of liquid water to the waste package and the associated chloride concentration, because this flow would presumably take place along open fractures in the form of gravity-driven flow manifested as dripping. As shown in Figure 3-6, when the fracture system above the drift becomes wet again at approximately 800 years, the chloride concentration at that time has a value that is four orders of magnitude larger than the initial value. The concentration decreases in a nearly exponential fashion to its initial value of 2×10^{-4} mol/L [7.58×10^{-4} mol/gal] beyond 1,500 years after a small rise between 800 and 1,500 years. During the dryout phase, the chloride concentration is assumed in equilibrium with respect to halite. The chloride multiplication factor in Table 3-3 (mean value of 2.3) modifies the time-dependent chloride concentration curve presented in Figure 3-6. The chloride multiplication factor is intended to account for the uncertainty in estimating the water chemistry; the parameter values (chloride concentration) and MULTIFLO results are considered the lower bound for chloride concentration.

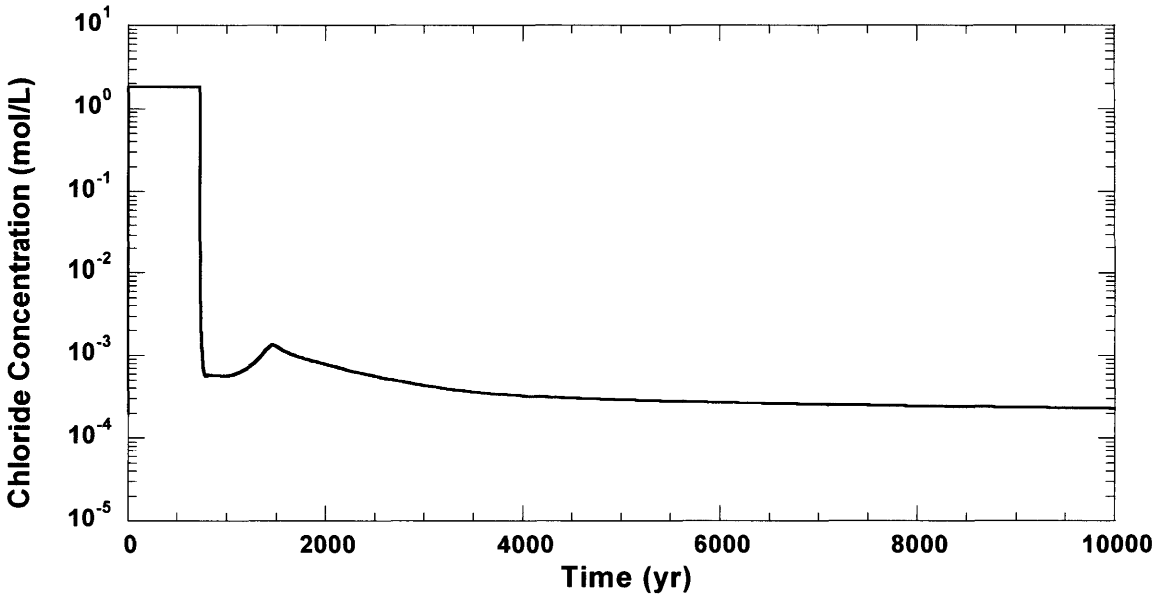

Figure 3-6. Time History of Chloride Concentration Computed by MULTIFLO

3.1.3 Degradation of Engineered Barriers

The engineered barrier subsystem primarily includes two barriers: a drip shield and the waste package. Because the radionuclide release can begin only after waste package failure, the lifetime of a drip shield and a waste package significantly affects repository performance. The failure mechanisms for these two barriers are described in the following sections.

3.1.3.1 Drip Shield Degradation

The 15-mm [0.59-in] thick drip shield is intended to protect the waste package from water dripping on the waste package surface (also protects the waste package from rockfall), especially during the thermal reflux period when environmental conditions could be conducive to crevice corrosion of the waste package outer overpack. The drip shield failure time is estimated outside the TPA Version 4.1 code and is provided to the code as a distribution function. Because of the high level of uncertainty in determining the geometry of failure of the drip shield, it is assumed that the drip shield is completely removed at the time of its failure. The average drip shield failure time is 7,422 years (Table 3-3).

3.1.3.2 Waste Package Degradation

The waste package degradation rate is strongly dependent on the behavior of the inner and outer waste package materials. The outer waste package material is Alloy 22, and the inner material is Type 316L SS. The mean values of the parameters used in computing the waste package failure time are presented in Table 3-3. Figure 3-7 provides a time evolution of the waste package wall thinning and shows waste package wall thinning of less than 4 percent (or 13 percent of the Alloy 22 overpack thickness) by year 10,000. Figure 3-8 shows that, for

Table 3-3. Parameters for Determining the Corrosion Failure of Waste Packages		
Parameter	**Mean Value**	**Distribution**
Outer waste package thickness	0.02 m	—
Inner waste package thickness	0.05 m	—
Metal grain radius	1.38×10^{1} μm	—
Grain boundary thickness	7.00×10^{-4} μm	—
Dry oxidation constant	9999.00	—
Critical relative humidity humid air corrosion	5.50×10^{-1}	—
Critical relative humidity aqueous corrosion	0.625	Normal; 0.6 0.65
Thickness of water film	2.00×10^{-3} m	Uniform; 0.001, 0.003
Boiling point of water	9.70×10^{1} °C	—
Outer overpack E_{rp} intercept	2006.00	—
Temperature coefficient of outer overpack E_{rp} intercept	−15.2	—
Outer overpack E_{rp} slope	−590.7	—
Temperature coefficient of outer pack E_{rp} slope	4.30	—
Inner overpack E_{rp} intercept	−10,000	—
Temperature coefficient of inner overpack E_{rp} intercept	0.00	—
Inner overpack E_{rp} slope	0.00	—
Temperature coefficient of inner overpack E_{rp} slope	0.00	—
Outer waste package beta kinetics parameter for oxygen	7.50×10^{-1}	—
Outer waste package beta kinetics parameter for water	5.00×10^{-1}	—
Inner waste package beta kinetics parameter for oxygen	7.50×10^{1}	—
Inner waste package beta kinetics parameter for water	5.00×10^{1}	—
Outer waste package rate constant for oxygen reduction	3.00×10^{10} C-m/m/yr	—
Outer waste package rate constant for water reduction	3.20 C-m/m^2/yr	—
Outer waste package activation energy for oxygen reduction	40,000 J/mol	—
Outer waste package activation energy for water reduction	2.50×10^{4} J/mol	—
Inner waste package rate constant for oxygen reduction	3.00×10^{10} C-m/mol/yr	—
Inner waste package rate constant for water reduction	3.2 C-m/m^2/yr	—
Inner waste package activation energy for oxygen reduction	4.0×10^{4} J/mol	—
Inner waste package activation energy for water reduction	2.50×10^{4} J/mol	—
Passive current density for waste package outer overpack	9.30×10^{3} C/m^2/yr	Normal 1.6×10^{3}, 1.7×10^{4}
Passive current density for waste package inner overpack	1.00×10^{10}	—

Table 3-3. Parameters for Determining the Corrosion Failure of Waste Packages (continued)

Parameter	Mean Value	Distribution
Measured galvanic couple potential	0.00	—
Coefficient for localized corrosion of outer overpack	2.5×10^{4}	—
Exponent for localized corrosion of outer overpack	1.00	—
Coefficient for localized corrosion of inner overpack	1.00	—
Exponent for localized corrosion of inner overpack	1.00	—
Humid air corrosion rate	1.00×10^{15} m/yr	—
Fractional coupling strength	0.0	—
Factor for defining choice of critical potential	0.0	—
Critical chloride concentration for first layer (Alloy 22)	0.5 mol/L	—
Critical chloride concentration for second layer (316L SS)	1.00×10^{10} mol/L	—
Chloride multiplication factor	2.30	Uniform; 1.0, 3.6
Chloride multiplication factor prior to failure of the drip shield	1.0	—
Time of failure of the drip shield	7422.0	Lognormal 2700, 20400
Reference pH	9.0	—
Waste package surface scale thickness	0.0 m	—
Tortuosity of scale on waste package	1.0	—
Porosity of scale on waste package	1.0	—
Yield strength	370 MPa	—
Safety factor	1.4	—
Fracture toughness	1.00×10^{7} MPa/m^{2}	—

the mean value data set, 45 waste packages are initially defective at year zero. The number of initially defective failures ranges from 2 to 8 waste packages in the 10 subareas. No seismically induced failure occurs for the mean value data set. The first corrosion failures take place in Subareas 4, 5, 7, and 10 at 69,400 years, and the next corrosion failure occurs in Subareas 1, 2, 3, 6, 8, and 9 at 70,300 years. A total of 2,392 waste packages fail at the time of first failure, and 6,440 fail at the time of second failure. All waste packages in a subarea available for corrosion failure are assumed to fail simultaneously.

3.1.4 Releases from Waste Package

The main processes that control releases of radionuclides from the spent nuclear fuel to the boundary with the geosphere in the model are (i) protection of the spent nuclear fuel by cladding, (ii) degradation of the spent nuclear fuel by air and water vapor, (iii) contact of the spent nuclear fuel by liquid water, (iv) mobilization of radionuclides from the spent nuclear fuel to the liquid water, (v) transport of dissolved or otherwise mobilized (colloids) radionuclides in the water to the outside of the waste package, and (vi) transport of dissolved radionuclides in the water through the invert material to the outside of the engineered barrier subsystem.

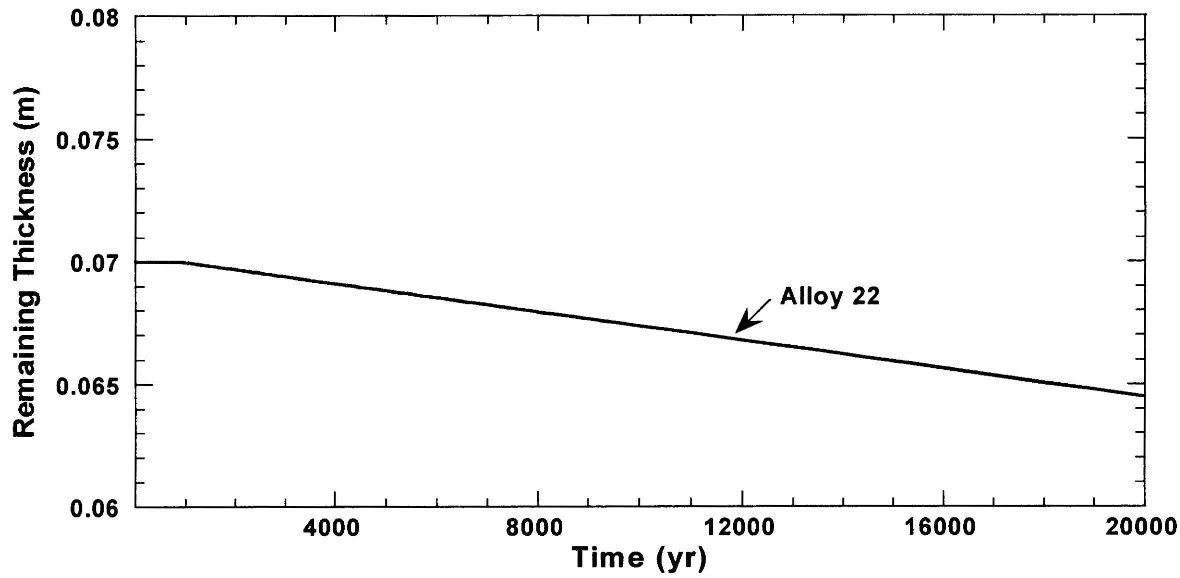

Figure 3-7. Waste Package Wall Thickness as a Function of Time for the Mean Value Data Set

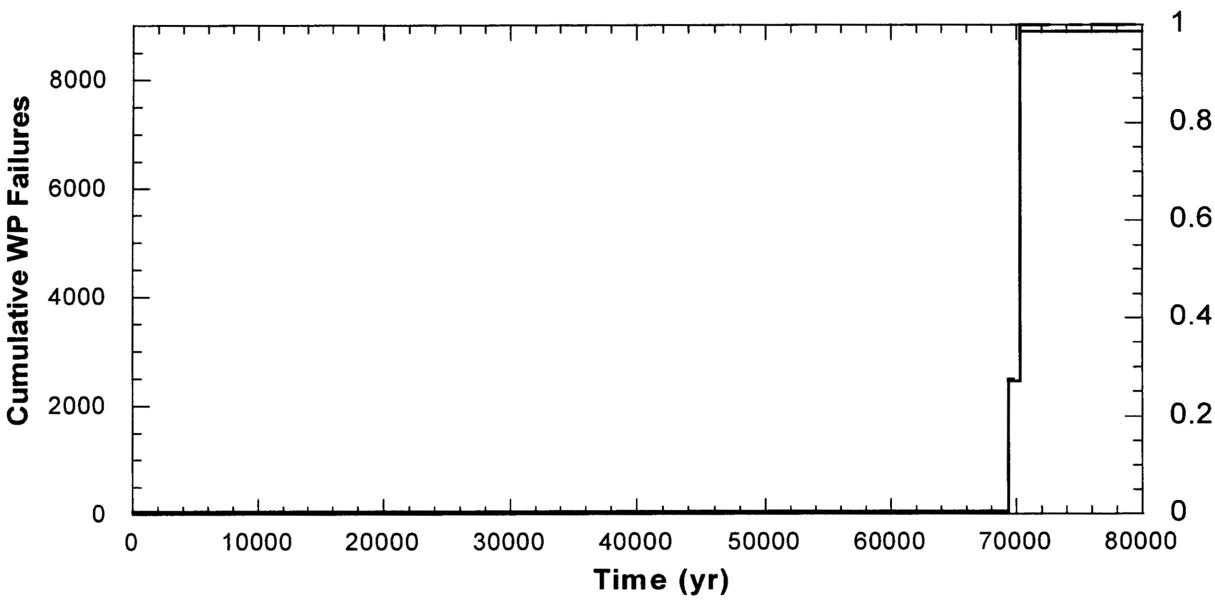

Figure 3-8. Cumulative Number of Failed Waste Packages for the Mean Value Data Set

Radionuclide releases are modeled assuming advective mass transfer out of the waste package from incoming water. The volume of water contacting the spent nuclear fuel is computed from a combination of flow in the near-field environment and three flow factors. The first flow factor represents the fraction of dripping water, which may be focused to reach the waste package. The second flow factor represents the fraction of the water that reaches the waste package, which enters the waste package. The first two factors are fixed, time-dependent variables read in from a data file; so a third factor, WastePackageFlowMultiplicationFactor, was added with an uncertainty distribution. The flow rate into the waste package is used in the bathtub model to determine radionuclide release rates. The mean value parameters used in the calculation of radionuclide release rates from the engineered barrier subsystem are presented in Tables 3-4 and 3-5.

Because radionuclides have different chemical, physical, and biological properties that affect the mobilization and radiotoxicity, not every radionuclide in the spent nuclear fuel is an important contributor to dose. Furthermore, because modeling all radionuclides in the spent nuclear fuel significantly increases the computation time, a screening process, employing criteria such as contribution to dose, was used to determine a list of 20 radionuclides. The 20 radionuclides and the decay chains evaluated in the total-system performance assessment analysis are presented in Table 3-6.

3.1.4.1 Cladding Degradation

Cladding must fail for water to contact the spent nuclear fuel. Because of inadequate knowledge, no explicit mechanism for cladding failure is included in the TPA Version 4.1 code. To capture the potential effect of cladding degradation, however, a fraction of the rods inside a waste package may be specified to have failed at the time of waste package failure. In the basecase, cladding failure is specified at 100 percent of the fuel rods, indicating no cladding protection for the spent nuclear fuel (see Table 3-4).

3.1.4.2 Spent Nuclear Fuel Dissolution and Mobilization

The spent nuclear fuel is present in the waste package in pellet form. Water must contact the pellet surface and the internal surfaces in the accessible fractures and pores. Spent nuclear fuel dissolution is modeled by defining rate equations for the spent nuclear fuel exposed after waste package failure and cladding degradation. Of the four spent nuclear fuel dissolution models, the one for which the rate equation is based on laboratory data in the presence of calcium and silicon is selected (Model 2). The data follow an Arrhenius-type trend that uses the time-varying temperature as the independent parameter. The dissolution rate is calculated from a mass balance on the water flowing into the waste package. Because the flow rate is subarea dependent, the dissolution rate varies from subarea to subarea.

The average temperature of the waste package surface, calculated in the drift-scale thermohydrology model, is used in the dissolution rate equation. This assumption that the temperature of the waste package surface is close to the temperature at the interior of the waste package is justified because, after the waste package failure, the temperature difference between the inside and outside of the waste package is expected to be small. The total surface area of the spent nuclear fuel available for dissolution is approximately 600 m^2 [6,460 ft^2] per

Table 3-4. Parameters Used in Determining Radionuclide Releases from the Engineered Barrier Subsystem		
Parameter	**Mean**	**Distribution**
Water contract mode for initial failure (0 = Bathtub, 1 = Flowthrough)	0	—
Water contract mode for faulting failure (0 = Bathtub, 1 = Flowthrough)	1	—
Water contract mode for volcanic failure (0 = Bathtub, 1 = Flowthrough)	1	—
Water contact mode for seismic failure interval1 (0 = Bathtub, 1 = Flowthrough)	0	—
Water contact mode for seismic failure interval2 (0 = Bathtub, 1 = Flowthrough)	0	—
Water contact mode for seismic failure interval3 (0 = Bathtub, 1 = Flowthrough)	0	—
Water contact mode for seismic failure interval4 (0 = Bathtub, 1 = Flowthrough)	0	—
Water contact mode for corrosion failure (0 = Bathtub, 1 = Flowthrough)	0	—
WastePackageFlowMultiplicationFactor	6	lognormal; 3.15×10^{-2}, 1.05×10^{3}
Subarea wet fraction	5.0×10^{-1}	Uniform; 0.0, 1.0
Initial failure time	0.00 yr	—
Defective fraction of waste packages per cell	5.05×10^{-3}	Uniform; 1.0×10^{-4}, 1.0×10^{-2}
Number of SEISMO waste package failure intervals	4.00	—
Beginning of seismic waste package failure intervals	0, 2000, 5000, 10,000 yr	—
Waste package internal volume	$4.83\ m^3$	—
Spent nuclear fuel density	$1.06 \times 10^{4}\ kg/m^3$	—
Surface area model	1.00	—
Spent nuclear fuel dissolution model	2.00	—
Oxygen partial pressure	2.10×10^{-1} atm	—
Negative log10 carbonate concentration	3.71 mol/L	—
User leach rate	$2.50 \times 10^{-6}\ kg/yr/m^2$	—
Preexponential factor for spent nuclear fuel dissolution rate from	$3.79 \times 10^{-4}\ (mg\ m^{-2} d^{-1})$	Log-uniform; 1.2×10^{3}, 1.2×10^{6}
Initial radius of spent nuclear fuel particle	1.85×10^{-3} m	Normal; 7.0×10^{-4}, 3.0×10^{-3}
Radius of spent nuclear fuel grain	1.25×10^{-5} m	—
Cladding correction factor	1.0	—
Subgrain fragment radius of UO_2 particle after transgranular fracture	1.25×10^{-6} m	Normal; 5.0×10^{-7}, 2.0×10^{-6}
Thickness of cladding	6.1×10^{-4} m	—
Spent nuclear fuel C-14 inventory of spent nuclear fuel	7.2×10^{-4} Ci/kg	—

Table 3-4. Parameters Used in Determining Radionuclide Releases from the Engineered Barrier Subsystem (continued)		
Parameter	**Mean**	**Distribution**
Clad C-14 inventory of spent nuclear fuel	4.89×10^{-4} Ci/kg	—
Zirconium oxide and crud C-14 inventory of spent nuclear fuel	2.48×10^{-5} Ci/kg	—
Gap and grain boundary inventory of spent nuclear fuel	6.2×10^{-6} Ci/kg	—
Spent nuclear fuel wetted fraction for all failure types	5.0×10^{-1}	Uniform; 0.0, 1.0
Invert bypass (0 = use ebsfilt, 1 = bypass ebsfilt)	0.00	—
Invert rock porosity	3.0×10^{-1}	—
Invert thickness	7.5×10^{-1} m	—
Invert diffusion coefficient	4.4×10^{-5} m^2/yr	—
Invert matrix permeability	2.0×10^{-17} m^2	Lognormal; 2.0×10^{-18}, 2.0×10^{-16}
Unsaturated zone minimum velocity change factor (fraction)	4.0×10^{-1}	
Maximum matrix longitudinal dispersivity specified as a fraction of layer thickness	0.06	—
Maximum fracture longitudinal dispersivity specified as a fraction of layer thickness	0.06	—
Invert RD		—
Am	3.00×10^3	—
C	6.10×10^1	—
Cl	1.00	—
Cm	6.00×10^3	—
Cs	1.21×10^2	—
I	7.00	—
Nb	6.10×10^2	—
Ni	6.10×10^1	—
Np	1.20×10^3	—
Pb	3.01×10^2	—
Pu	3.00×10^3	—
Ra	6.01×10^3	—
Se	1.00	—
Tc	1.00	—
Th	3.00×10^3	—
U	6.01×10^2	—

Table 3-5. Distributions of Solubility Limits		
Element	Mean Value (kg/m^3)	Distribution (kg/m^3)
Am	1.20×10^{-4}	Uniform; 2.4×10^{-8}, 2.4×10^{-4}
C	1.40×10^{1}	—
Cl	3.60×10^{1}	—
Cm	2.40×10^{-4}	—
Cs	1.35×10^{2}	—
I	1.29×10^{2}	—
Nb	9.30×10^{-7}	—
Ni	1.10×10^{-1}	—
Np	2.14×10^{-2}	Log triangular; 1.2×10^{-3}, 3.4×10^{-2}, 2.4×10^{-1}
Pb	6.60×10^{-5}	—
Pu	1.21×10^{-4}	Uniform; 2.4×10^{-6}, 2.4×10^{-4}
Ra	2.30×10^{-5}	—
Se	7.90×10^{1}	—
Tc	9.93×10^{1}	—
Th	2.30×10^{-4}	—
U	7.60×10^{-3}	—

Table 3-6. Radionuclide Decay Chains	
Chain Number	Chain
1	Cm-246 → U-238
2	Cm-245 → Am-241 → Np-237
3	Am-243 → Pu-239
4	Pu-240
5	U-234 → Th-230 → Ra-226 → Pb-210
6	Cs-135
7	I-129
8	Tc-99
9	Ni-59
10	C-14
11	Se-79
12	Nb-94
13	Cl-36

waste package based on the spent nuclear fuel particle size, grain density, and the spent nuclear fuel wetted fraction.

As with spent nuclear fuel dissolution, mobilization of spent nuclear fuel also depends on the initial inventory instantaneously released from the gap between spent nuclear fuel and cladding into the contacting water as soon as the waste package fails. The radionuclides available for instantaneous release are assumed held loosely on the grain boundaries, cladding/fuel gap, and cladding, referred to collectively as gap inventories. These inventories could be a major contributor to early dose. The gap and grain boundary inventories for each radionuclide are specified as input parameters as shown in Table 3-7.

Table 3-7. Initial Inventory, Gap Inventory, and Half-Life of Radionuclides in Spent Nuclear Fuel for Groundwater Release			
Radionuclide	Inventory at 10 Years from Reactor (Ci/WP)	Gap Inventory (%)	Half-Life (yr)
Am-241	16411.20	0.00	4.32×10^2
Am-243	208.30	0.00	7.38×10^3
C-14	11.36	10.00	5.73×10^3
Cl-36	0.09	12.00	3.01×10^5
Cm-245	2.89	0.00	8.50×10^3
Cm-246	0.60	0.00	4.73×10^3
Cs-135	4.23	6.00	2.30×10^6
I-129	0.28	6.00	1.57×10^7
Nb-94	6.69	0.00	2.03×10^4
Ni-59	19.25	0.00	8.00×10^4
Np-237	3.42	0.00	2.14×10^6
Pb-210	4.47×10^{-7}	0.00	2.23×10^1
Pu-239	2911.41	0.00	2.41×10^4
Pu-240	4292.16	0.00	6.54×10^3
Ra-226	3.24×10^{-6}	0.00	1.60×10^3
Se-79	0.21	6.00	1.10×10^6
Tc-99	114.41	1.00	2.13×10^5
Th-230	1.08×10^{-3}	0.00	7.70×10^4
U-234	9.31	0.00	2.45×10^5
U-238	2.49	0.00	4.47×10^9

3.1.4.3 Transport in the Engineered Barrier Subsystem

The TPA Version 4.1 code models advective transport out of the waste package and advective and diffusive transport through the invert below the waste package. Two different flow rates are used in these transport calculations. The volumetric flow rate of water into the waste package is calculated by multiplying the seepage flux into the drift by the surface area of the holes (pits, crevices, or patches). The volumetric flux through the invert is based on the volume of water entering the drift rather than on the volume of water entering the waste package.

Inside the waste package, high-solubility nuclides released from the solid matrix are transported out of the waste package. Low-solubility nuclides, however, precipitate out of solution if released from the solid matrix at a concentration exceeding the carrying capacity of water (or solubility limit of a particular nuclide). The volume of water available for dissolution of waste is the amount of water in the failed waste package and the difference between the volume of water flowing in and out of the failed waste package. Table 3-5 provides solubility limits of the radioelements evaluated in the TPA Version 4.1 code.

Releases from the waste package will travel through the invert before entering the tunnel wall. Current design shows the waste package on a pallet (consisting of two cradles and a steel support) over a porous invert made of sand or gravel ballast in between a carbon steel frame. Water running off or passing through the waste package would fall onto the invert. The invert material could sorb some of the radionuclide species, thereby providing an additional barrier to their release into the geosphere proper.

In the invert, advective and diffusive transport is modeled through 0.75 m [2.5 ft] of invert (slightly thicker than the value used in the Total System Performance Assessment–Site Recommendation) having a 30-percent porosity. The determination of whether flow through the invert occurs in the matrix or fractures is based on the invert matrix permeability and the average flow rate of water through the invert. Radionuclide sorption is modeled in the sand or gravel ballast invert, and the mean values of the Rds are presented in Table 3-4, together with values for other parameters used to compute transport in the engineered barrier subsystem. Colloidal transport of radionuclides is not considered in this calculation.

3.1.5 Unsaturated Zone Transport

Radionuclides released from the engineered barrier subsystem must pass (or be transported) through the unsaturated zone to reach the saturated zone. The main attributes of the unsaturated zone that control transport of radionuclides are (i) velocity of radionuclides in groundwater (fracture versus matrix flow), (ii) radionuclide sorption, (iii) matrix diffusion, and (iv) hydrologic stratigraphy. The transport velocity within a specific hydrostratigraphic unit (e.g., Calico Hills nonwelded zeolitic) is determined by assuming vertical flow below the repository and comparing the vertical flow to the saturated hydraulic conductivity of the matrix; if the vertical flow exceeds the saturated conductivity any time during the simulation, fracture transport velocities are used. Although this approach does not account for spatial variability of flow caused by heterogeneities in the hydrologic properties of the fractures and matrix, or the episodic nature of infiltration, the approach generally yields short traveltimes to the saturated zone, using current hydraulic properties and infiltration estimates.

In unsaturated zone transport calculations, the NEFTRAN II code (Olague, et al., 1991) models one-dimensional advection and retardation of radionuclides with chain decay. Inputs to the unsaturated zone transport model are the release rates of radionuclides from the engineered barrier subsystem, the time-varying flow results from the unsaturated zone shown in Figure 3-1, and the chemical and physical properties of the hydrostratigraphic units between the repository and the water table (see Figure 3-9 and Table 3-8). The water table elevation remains constant in the total-system performance assessment calculations. Thus, the thickness of the unsaturated zone does not change with time even during the pluvial climate. Sorption in fractures is neglected because of the fast traveltimes, whereas sorption in the matrix is modeled using the sorption coefficients presented in Table 3-8. The effects of matrix diffusion on transport in the unsaturated zone are not modeled.

Figure 3-10 shows the release rate for Cl-36. Because Cl-36 moves unretarded, comparison of the times of the release rates in this figure indirectly illustrates the unsaturated zone. The engineered barrier subsystem and unsaturated zone release rates are nearly the same, with only approximately 100 years difference, indicating the unsaturated zone does not significantly delay groundwater transport in those subareas where the Calico Hills vitric unit is absent.

3.1.6 Saturated Zone Flow and Transport

The transport of radionuclides from the location at which radionuclides from the unsaturated zone enter the water table immediately below the repository to a receptor location takes place in the saturated zone. Transport of radionuclides in the saturated zone is complicated by

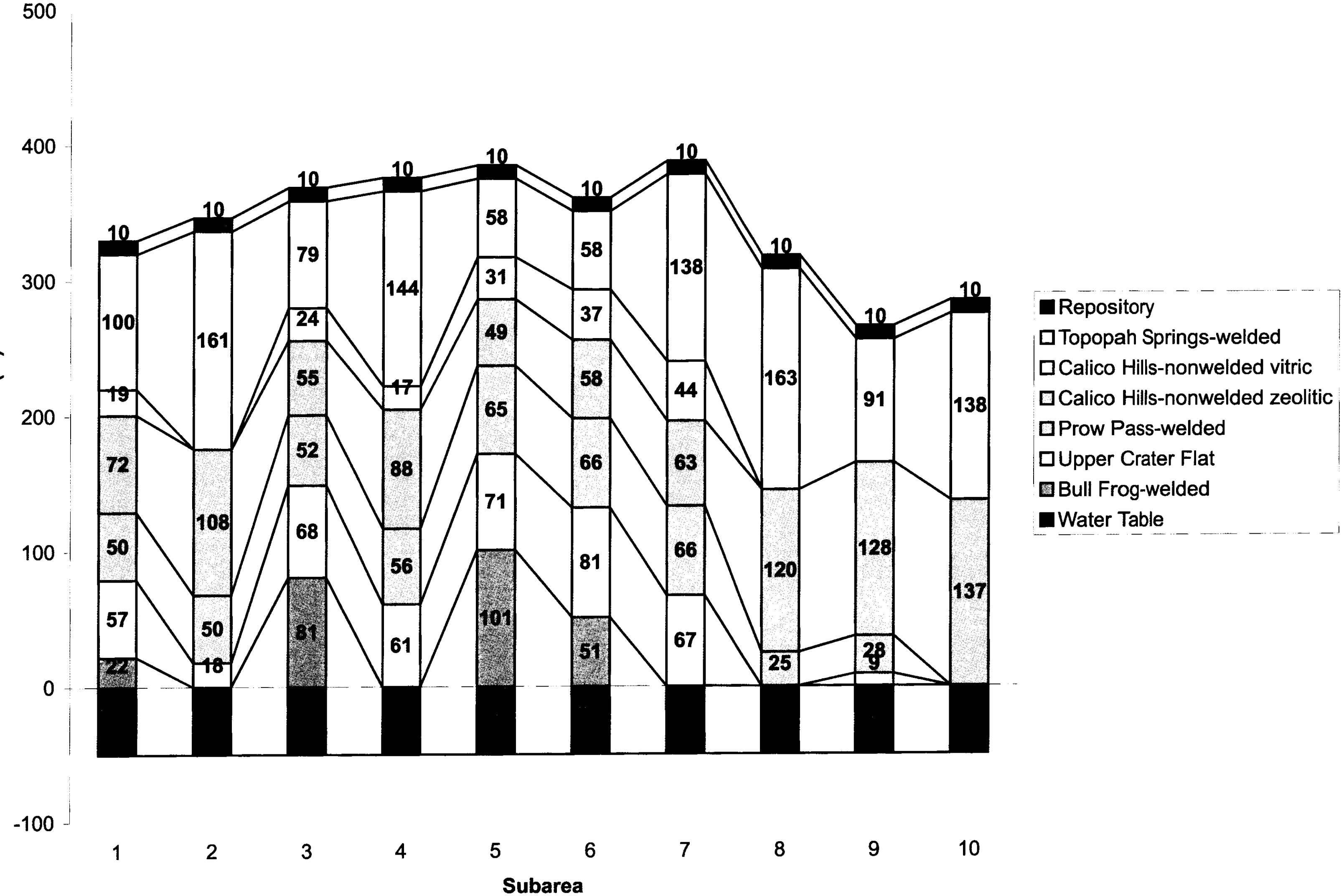

Figure 3-9. Thickness of Subara Stratigraphic Units

Table 3-8. Mean Values and Distributions of Sorption Coefficient, K_d (m^3/kg), Parameters (Other Parameters for Unsaturated Zone Radionuclide Transport Are Also Included; Dash in the Last Column Indicates a Constant Value for the Parameter Distribution.)

Element	Bull Frog Welded Unit	Calico Hills Nonwelded Vitric Unit	Calico Hills Nonwelded Zeolitic Unit	Prow Pass Welded Unit	Topopah Spring Welded Unit	Upper Crater Flat Unit
Am	10,993 (Lognormal; 1,699; 71,123)	34,549 (Lognormal; 5,340; 223,529)	31,410 (Lognormal; 4,855; 203,209)	25,912 (Lognormal; 4,005; 167,647)	11,386 (Lognormal; 1,760; 73,663)	27,090 (Lognormal; 4,187; 175,267)
C	0.00 —	0.00 —	0.00 —	0.00 —	0.00 —	0.00 —
Cl	0.00 —	0.00 —	0.00 —	0.00 —	0.00 —	0.00 —
Cm	0.00 —	0.00 —	0.00 —	0.00 —	0.00 —	0.00 —
Cs	0.51 (Uniform; 0.020, 1.0)	0.055 (Uniform; 0.010, 0.10)	2.75 (Uniform; 0.50, 5.0)	0.51 (Uniform 0.020, 1.0)	0.51 (Uniform 0.020, 1.0)	0.51 (Uniform 0.020, 1.0)
I	0.00 —	0.00 —	0.00 —	0.00 —	0.00 —	0.00 —
Nb	0.00 —	0.00 —	0.00 —	0.00 —	0.00 —	0.00 —
Ni	0.2500025 (Uniform; 5.0×10^{-6}, 0.50)	0.0500005 (Uniform; 1.0×10^{-6}, 0.10)	0.2500025 (Uniform; 5.0×10^{-6}, 0.50)	0.2500025 (Uniform; 5.0×10^{-6}, 0.50)	0.2500025 (Uniform; 5.0×10^{-6}, 0.50)	0.2500025 (Uniform; 5.0×10^{-6}, 0.50)
Np	9.408×10^{-3} (Lognormal; 3.04×10^{-3}, 2.71×10^{-2})	2.96×10^{-2} (Lognormal; 9.91×10^{-3}, 8.84×10^{-2})	2.690×10^{-2} (Lognormal; 9.01×10^{-3}, 8.03×10^{-2})	2.219×10^{-2} (Lognormal; 7.43×10^{-3}, 6.63×10^{-2})	9.740×10^{-3} (Lognormal; 3.26×10^{-3}, 2.91×10^{-2})	2.320×10^{-2} (Lognormal; 7.77×10^{-3}, 6.93×10^{-2})
Pb	0.3 (Uniform; 0.10, 0.50)	0.3 (Uniform; 0.10, 0.50)	0.3 (Uniform; 0.10, 0.50)	0.3 (Uniform; 0.10, 0.50)	0.3 (Uniform; 0.10, 0.50)	0.3 (Uniform; 0.10, 0.50)
Pu	1.036 (Lognormal; 0.36; 2.98)	3.252 (Lognormal; 1.13; 9.36)	2.961 (Lognormal; 1.03; 8.51)	2.443 (Lognormal; 0.85; 7.02)	1.068 (Lognormal; 0.37; 3.08)	2.556 (Lognormal; 0.89; 7.34)

Table 3-8. Mean Values and Distributions of Sorption Coefficient, K_d (m^3/kg), Parameters (Other Parameters for Unsaturated Zone Radionuclide Transport Are Also Included; Dash in the Last Column Indicates a Constant Value for the Parameter Distribution.) (continued)

Element	Bull Frog Welded Unit	Calico Hills Nonwelded Vitric Unit	Calico Hills Nonwelded Zeolitic Unit	Prow Pass Welded Unit	Topopah Spring Welded Unit	Upper Crater Flat Unit
Ra	0.3 Uniform; (0.1, 0.5)	0.075 (Uniform; 0.050, 0.10)	3 (Uniform; 1.0, 5.0)	0.3 Uniform; (0.1, 0.5)	0.3 Uniform; (0.1, 0.5)	0.3 Uniform; (0.1, 0.5)
Se	1.5×10^{-2} (Uniform; 3.0×10^{-7}, 3.0×10^{-2})	1.0×10^{-2} (Uniform; 2.0×10^{-7}, 2.0×10^{-2})	7.5×10^{-3} (Uniform; 1.5×10^{-7}, 1.5×10^{-2})	1.5×10^{-2} (Uniform; 3.0×10^{-7}, 3.0×-10^{-2})	1.5×10^{-2} (Uniform; 3.0×10^{-7}, 3.0×10^{-2})	1.5×10^{-2} (Uniform; 3.0×10^{-7}, 3.0×10^{-2})
Tc	0.00 —	0.00 —	0.00 —	0.00 —	0.00 —	0.00 —
Th	76.05 (Lognormal; 12; 482; 500 3.557×10^{-3})	240.0 (Lognormal; 38; 1,516; 1.064×10^{-2})	216.5 (Lognormal; 34; 1,378, 1.014×10^{-2})	178.4 (Lognormal; 28; 1,137, $8{,}380 \times 10^{-3}$)	77.46 (Lognormal; 12; 500, 3.682×10^{-3})	188.8 (Lognormal; 30; 1,188, 8.745×10^{-3})
U	$1.78 \times 10_5$ (Lognormal; 7.11×10^{-1})	5.58×10^{-5} (Lognormal; 5.58×10^{-5}, 2.03)	1.014×10^{-2} (Lognormal; 5.07×10^{-5}, 2.03)	4.18×10^{-5} (Lognormal; 1.68)	1.34×10^{-5} (Lognormal; 7.37×10^{-1})	4.37×10^{-5} (Lognormal; 1.75)

Table 3-8. Mean Values and Distributions of Sorption Coefficient, K_d (m^3/kg), Parameters. Other Parameters for Unsaturated Zone Radionuclide Transport Are Also Included. (continued)		
Parameter	**Mean**	**Distribution**
Matrix Permeability		
Topopah Spring—welded	2.00×10^{-19} m^2	Lognormal; 2.0×10^{-20}, 2.0×10^{-18}
Calico Hills—nonwelded vitric	2.00×10^{-14} m^2	Lognormal; 2.0×10^{-15}, 2.0×10^{-13}
Calico Hills—nonwelded zeolitic	5.00×10^{-18} m^2	Lognormal; 5.0×10^{-19}, 5.0×10^{-17}
Prow Pass—welded	1.00×10^{-17} m^2	Lognormal; 1.0×10^{-18}, 1.0×10^{-16}
Upper Crater Flat	3.00×10^{-18} m^2	Lognormal; 3.0×10^{-19}, 3.0×10^{-17}
Bull Frog—welded	2.00×10^{-19} m^2	Lognormal; 2.0×10^{-20}, 2.0×10^{-18}
Unsaturated Fracture Zone	1.94×10^{-17} m^2	Lognormal; 1.8×10^{-18}, 2.1×10^{-16}
Matrix Porosity		
Topopah Spring—welded	1.20×10^{-1}	—
Calico Hills—nonwelded vitric	3.30×10^{-1}	—
Calico Hills—nonwelded zeolitic	3.20×10^{-1}	—
Prow Pass—welded	2.80×10^{-1}	—
Upper Crater Flat	2.80×10^{-1}	—
Bull Frog—welded	1.20×10^{-1}	—
Unsaturated Fracture Zone	1.20×10^{-1}	—
Matrix Beta		
Topopah Spring—welded	1.5	—
Calico Hills—nonwelded vitric	1.3	—
Calico Hills—nonwelded zeolitic	2.30	—
Prow Pass—welded	1.50	—
Upper Crater Flat	1.40	—
Bull Frog—welded	1.70	—
Unsaturated Fracture Zone	2.30	—
Matrix Grain Density		
Topopah Spring—welded	2.46×10^3 kg/m^3	—
Calico Hills—nonwelded vitric	2.26×10^3 kg/m^3	—

Table 3-8. Mean Values and Distributions of Sorption Coefficient, K_d (m^3/kg), Parameters. Other Parameters for Unsaturated Zone Radionuclide Transport Are Also Included (continued)

	Parameter	Mean	Distribution
	Calico Hills—nonwelded zeolitic	2.40×10^3 kg/m^3	—
	Prow Pass—welded	2.54×10^3 kg/m^3	—
	Upper Crater Flat	2.42×10^3 kg/m^3	—
	Bull Frog—welded	2.57×10^3 kg/m^3	—
	Unsaturated Fracture Zone	2.63×10^3 kg/m^3	—
Fracture Permeability			
	Topopah Spring—welded	8.00×10^{-13} m^2	Lognormal; 8.0×10^{-15}, 8.0×10^{-11}
	Calico Hills—nonwelded vitric	8.00×10^{-13} m^2	Lognormal; 8.0×10^{-15}, 8.0×10^{-11}
	Calico Hills—nonwelded zeolitic	6.00×10^{-13} m^2	Lognormal; 6.0×10^{-15}, 6.0×10^{-11}
	Prow Pass—welded	6.00×10^{-13} m^2	Lognormal; 6.0×10^{-15}, 6.0×10^{-11}
	Upper Crater Flat	6.00×10^{-13} m^2	Lognormal; 6.0×10^{-15}, 6.0×10^{-11}
	Bull Frog—welded	3.00×10^{-13} m^2	Lognormal; 3.0×10^{-15}, 3.0×10^{-11}
	Unsaturated Fracture Zone	1.00×10^{-12} m^2	Lognormal; 1.0×10^{-13}, 1.0×10^{-11}
Fracture Porosity			
	For Topopah Spring—welded and Unsaturated Fracture zone	3.16×10^{-3}	Lognormal; 1.0×10^{-3}, 1.0×10^{-2}
	For all other units	3.16×10^{-4}	Lognormal; 1.0×10^{-4}, 1.0×10^{-3}
	Fracture beta		
	For all units	2.00	—
	For unsaturated fracture zone	1.60	—
	Dispersivity		
	Matrix and fracture longitudinal dispersivity as a fraction of unit	0.06	—

Note: Dash in last column indicates a constant value for the parameter distribution

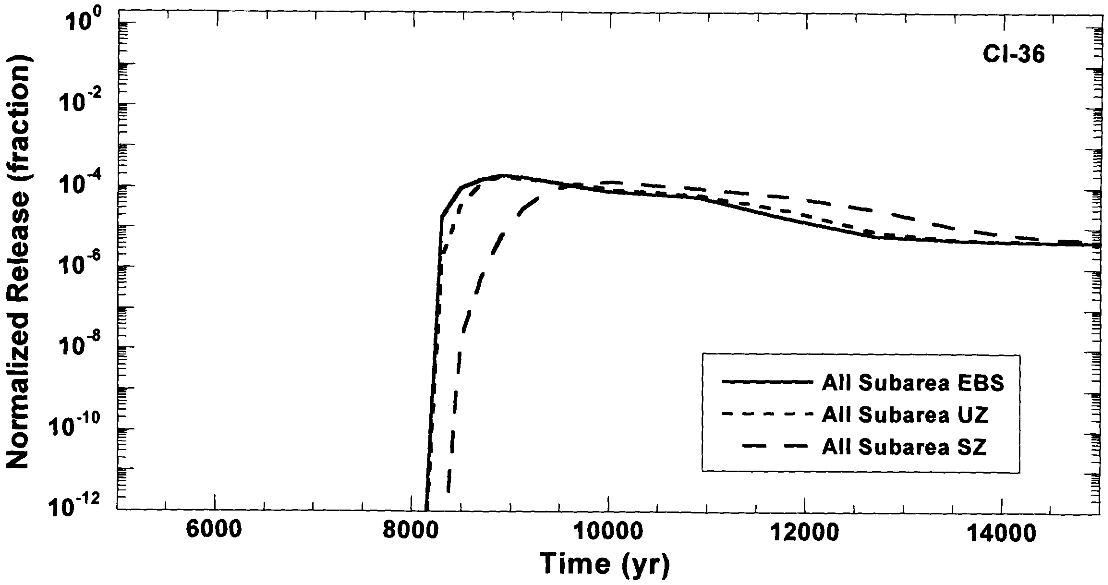

Figure 3-10. Cl-36 Normalized Release Rates from the Engineered Barrier Subsystem, Unsaturated Zone, and Saturated Zone

(i) spatial variability in the geochemical properties of the fracture surfaces and rock matrix, (ii) heterogeneity in formation-scale transport pathways, (iii) temporal variations in the flow field caused by climatic change and pumping for water use, and (iv) variability in the rate at which radionuclides transiting the unsaturated zone reach the water table. Although the abstracted model neglects many of the high-resolution spatial and temporal variations in transport processes, the model does include (i) advective transport through the tuff and alluvial aquifers, (ii) longitudinal dispersion during transport, (iii) chemical sorptive processes that retard the transport of radionuclides in the alluvial aquifer and in the matrix of the tuff aquifer, and (iv) diffusion of radionuclides from the fractures to the matrix in the tuff aquifer. Three one-dimensional streamtubes originating at the water table below the repository and terminating at a receptor location connecting to one or more unsaturated zone streamtubes are used for representing saturated zone transport. Radionuclide transport is simulated using the NEFTRAN II code (Olague, et al., 1991), which calculates the radionuclide release rate (Bq/yr) at the down-gradient receptor location. For each subarea, radionuclide transport out of the engineered barrier subsystem and into the unsaturated and saturated zones is conceptualized as occurring in a single streamtube that originates in the repository, extends to the water table, and continues to the receptor location. Streamtubes begin at the water table directly below the repository and continue to the receptor location. Each subarea in the repository is assigned to the nearest streamtube. Subareas 1, 2, 3, 4, and 8 are mapped to streamtube 2; subareas 5, 6, and 7 are mapped to streamtube 1; and subareas 9 and 10 are mapped to streamtube 3. Figure 3-11 shows the subareas and streamtubes used for the saturated zone transport model, and Table 3-9 provides the length of the saturated zone flow path by subarea. The groundwater traveltimes from the point where the radionuclides enter the saturated zone to the receptor location are 536 years for subareas 1, 2, 3, 4, and 8 (streamtube 2); 596 years for subareas 5, 6, and 7 (streamtube 1); and 766 years for subareas 9 and 10 (streamtube 3) for

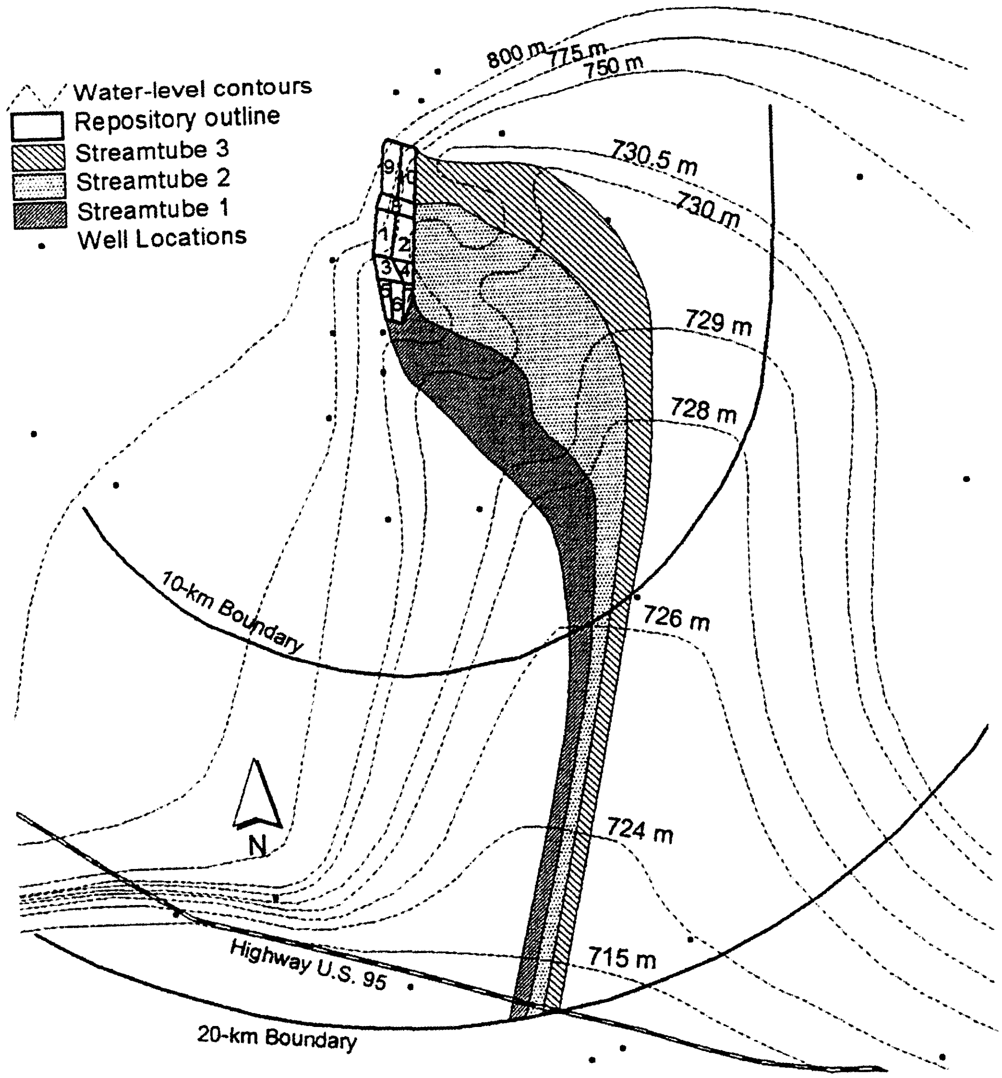

Figure 3-11. Saturated Zone Streamtubes Assigned to Each Subarea

Table 3-9. Mean Values and Distributions Used for Saturated Zone Flow and Radionuclide Transport in Total System Performance Assessment		
Parameter	**Mean**	**Distribution**
Mixing zone dispersion fraction	1.00×10^{-2}	—
Tuff dispersion fraction	1.00×10^{-2}	—
Alluvium dispersion fraction	1.00×10^{-1}	—
Tuff fracture porosity	3.16×10^{-3}	Log-uniform; 1.0×10^{-3}, 1.0×10^{-2}
Alluvium matrix porosity	1.25×10^{-1}	Uniform; 1.0×10^{-1}, 1.5×10^{-1}
Immobile R_d for tuff		
Am	1.80×10^{4}	—
Np	19.00	—
I	1.00	—
Tc	1.00	—
Cl	1.00	—
Cm	1.8×10^{4}	—
U	37.00	—
Pu	1.8×10^{3}	—
Th	1.8×10^{4}	—
Ra	5.4×10^{3}	—
Pb	5.4×10^{3}	—
Cs	9.0×10^{3}	—
Ni	1.8×10^{3}	—
C	1.00	—
Se	55.00	—
Nb	1.8×10^{4}	—
Immobile porosity for tuff	2.00×10^{-1}	—
Diffusion rate for tuff	0.00	—
Fracture R_d for tuff for all nuclides	1.00	—
Minimum residence time for tuff	1.00×10^{1} yr	—
Minimum residence time for alluvium	1.00×10^{1} yr	—
Distance to tuff alluvium interface	14.95 km	Uniform; 10.0, 19.9
Distance to receptor group	20.00 km	—
Pluvial well pumping rate at receptor group 20 km [gal/day]	6.215×10^{6}	Uniform; 3.2×10^{6}, 9.23×10^{6}
Pluvial switch time	13000.00	—
Well pumping rate at receptor group at 20 km	8.75×10^{6} gal/day	Uniform 4.5×10^{6}, 1.3×10^{7}
Mixing zone thickness at 20 km	1.25×10^{2} m	Uniform 50.00, 200.0
Alluvium Matrix R_d (For Correlations See Table 3-11)		
Am	7.14×10^{7}	Lognormal; 7.5×10^{4}, 6.8×10^{10}
C	1.00	—
Cl	1.00	—
Cm	7.50×10^{4}	—
I	1.00	—
Np	6.24×10^{1}	Lognormal; 1.0, 3.9×10^{3}
Pu	1.28×10^{4}	Lognormal; 4.2×10^{2}, 3.9×10^{5}

Table 3-9. Mean Values and Distribution Used for Saturated Zone Flow and Radionuclide Transport in Total System Performance Assessment (continued)			
Parameter		Mean	Distribution
Se		2.24×10^1	Log-uniform; 1.0, 500.0
Tc		1.00	—
Th		9.25×10^3	Lognormal; 1.9, 4.5×10^7
U		1.38×10^2	Lognormal; 1.0, 1.9×10^4
Ra		4.0×10^3	Log-uniform; 2.0×10^3, 8.0×10^3
Pb		4.0×10^3	Log-uniform; 2.0×10^3, 8.0×10^3
Cs		9.49×10^4	Log-uniform; 9.0×10^4, 1.0×10^5
Ni		8.94×10^1	Log-uniform; 1.0×10^0, 8.0×10^3
Nb		7.75×10^3	Log-uniform; 2.0×10^3, 3.0×10^4
Streamtube Flow Properties			
	Subarea	**Saturated Zone Streamtube**	**Length (m)**
	1	2	26,900
	2	2	26,100
	3	2	26,900
	4	2	25,900
	5	1	22,500
	6	1	22,200
	7	1	21,800
	8	2	26,600
	9	3	30,000
	10	3	29,300

the mean value data set. Variations in the groundwater traveltimes are primarily the result of variations in the streamtube length, width, and flow rates. The total saturated zone flow rate in all the streamtubes is 1.78×10^5 m^3/yr [6.29×10^6 ft^3/yr]. The relative contributions of streamtubes 1, 2, and 3 to the total saturated zone flow are 33, 41, and 26 percent. The release rate at the outlet of the streamtubes is determined using the sum of the release rates from all the streamtubes and is dependent on the time-varying concentration at the inlet. Figure 3-10 shows the saturated zone release rates for Cl-36, which is not retarded in the saturated zone.

The source term for the saturated transport model is the time-varying radionuclide release rate from the unsaturated zone calculations. Other inputs to the saturated zone transport model include the physical and chemical properties of the tuff and alluvium and the streamtube flow rates, widths, and lengths. The mean values for the saturated zone input parameters are presented in Table 3-9. The correlation coefficients for the alluvium matrix retardation factors are presented in Table 3-10.

3.1.7 Dose to the Receptor Group

The radionuclide concentrations in groundwater in the saturated zone at the receptor location are used to calculate the annual total effective dose equivalent to a reasonably maximally exposed individual. The groundwater concentrations are converted to doses by taking into consideration (i) the location of the receptor group, (ii) the lifestyle characteristics of the

Table 3-10. Correlated Parameters and Correlation Coefficients for the Multiple Realizations		
Correlated Parameter 1	**Correlated Parameter 2**	**Correlation**
SubAreaWetFraction	ArealAverageMeanAnnualInfiltrationAtStart[mm/yr]	0.631
SubAreaWetFraction	MatrixPermeability_TSw_[m2]	-0.623
AlluviumMatrixRD_SAV_Am	AlluviumMatrixRD_SAV_Pu	0.964
AlluviumMatrixRD_SAV_Am	AlluviumMatrixRD_SAV_U	0.346
AlluviumMatrixRD_SAV_Am	AlluviumMatrixRD_SAV_Np	0.837
AlluviumMatrixRD_SAV_Am	AlluviumMatrixRD_SAV_Th	0.112
AlluviumMatrixRD_SAV_Pu	AlluviumMatrixRD_SAV_U	0.489
AlluviumMatrixRD_SAV_Pu	AlluviumMatrixRD_SAV_Np	0.881
AlluviumMatrixRD_SAV_Pu	AlluviumMatrixRD_SAV_Th	0.109
AlluviumMatrixRD_SAV_Np	AlluviumMatrixRD_SAV_Th	0.260
AlluviumMatrixRD_SAV_Np	AlluviumMatrixRD_SAV_U	0.610
AlluviumMatrixRD_SAV_Th	AlluviumMatrixRD_SAV_U	0.165

receptor group and the exposure pathways, (iii) processes that determine fate and transport of contaminants in the biosphere, (iv) calculation of human doses from factors that convert exposure to contaminated media to effective dose equivalents, and (v) well pumping rates. The activity released from the saturated zone per unit time is converted to activity per unit volume of water by dividing by the pumping rate. Dose conversion factors are then calculated and used to determine dose to the reasonably maximally exposed individual. At each timestep, total doses are the sum of the product of each radionuclide concentration and dose conversion factor within and among groundwater pathways.

The receptor location for the basecase data set is 20 km [12.4 mi] from the repository. At 20 km [12.4 mi], the mean value for the pumping rate is 1.21×10^7 m^3/yr [4.3×10^8 ft^3/yr], which is sufficient to capture the entire contaminant plume.[3,4] Because the TPA Version 4.1 code assumes the volume of water pumped is constant throughout the simulation period, values for the concentration of the well water exhibit the same behavior as the saturated zone release rates. For example, to convert from Cl-36 release rates in Figure 3-10 to concentration, the release rates are divided by the well pumping rate to compute the wellwater concentrations. Note that in the saturated zone transport model, the well pumping rate does not change the velocity field, thus does not alter the rate of radionuclide transport.

The groundwater dose is determined by multiplying the concentration of the nuclides in the pumped water with the dose conversion factor. The mass of radionuclides captured by pumping is diluted in the volume of water extracted from the pumping well and converted from a groundwater concentration to a dose using dose conversion factors. The dose to an individual of the receptor group originates from drinking and irrigation waters used by an

[3]Plume thickness is assumed uniformly distributed between 10 and 100 m [32.8 ft and 328 ft]. The smallest pump discharge rate considered {1.5×10^4 gallons/day [5.7×10^4 L/day]} creates a capture zone more than150 m [492 ft] thick.

[4]Current regulation specifies well pumping at a constant value of 3,000 acre-ft/yr [1.01×10^4 m^3/day].

average adult living in Amargosa Valley. The groundwater pathway dose conversion factors for the 20 radionuclides used in the basecase mean value data set are summarized in Table 3-11.

3.2 Results From The Mean Value Data Set

This section describes the behavior of the total system and explains how the individual dose is influenced by the various subsystem models and parameters. Time history plots of key system parameters for both doses and release rates at various subsystem boundaries are presented in this section for the mean value, single-realization case.

The dose to an average individual residing 20 km [12.4 mi] downgradient of the repository is presented in Figure 3-12 for radionuclides with doses greater than 10^{-8} mSv/yr [10^{-6} mrem/yr] for 10,000 and 100,000 years. The period of 100,000 years is chosen so the effects of one cycle of the pluvial climate and the effects of waste package corrosion, which occur after the 10,000-year simulation period, can be studied.

A peak total dose of 3.5×10^{-4} mSv/yr [0.035 mrem/yr] occurred during the 10,000-year simulation period. The dose is dominated in the 10,000-year simulation period by I-129, Tc-99, and, to some extent, Cl-36. These nuclides are nonsorbing and have relatively long half-lives.

For the 100,000-year simulation period, a peak total dose of 3.8×10^{-2} mSv/yr [3.8 mrem/yr] occurred at 100,000 years, and the dose was dominated by Np-237, but also had significant contributions from I-129 and Tc-99. To 28,000 years, dose contribution is primarily from Tc-99 and I-129. At 28,000 years, Np-237 starts contributing noticeably to dose and immediately becomes the dominant contributor. The average breakthrough time for Np-237 from the engineered barrier subsystem and unsaturated zone is approximately 8,700 years. The average breakthrough time for Np-237 from the saturated zone is 31,400 years with its earliest breakthrough occurring at 25,300 years. The ramp-up in dose between 30,000 and 40,000 years is related to the delayed breakthrough of Np-237 released from initially defective waste packages. The peak occurring near 70,000 years is a result of the waste packages failing from corrosion at 69,400 years. The main contributors to this peak are I-129, Tc-99, and, to a lesser extent, Cl-36. The peak near 100,000 years is from the delayed release of Np-237 from failed waste packages from corrosion at 70,000 years. A discussion of the total-system performance assessment results from the 10,000- and 100,000-year simulation periods, with and without the faulting and igneous activity disruptive events, follows in the next two sections.

3.2.1 10,000-Year Releases and Dose

As evident from Figure 3-8 and as explained in Section 3.1.3.2, all basecase releases in 10,000 years are from the initially defective waste package failures. Although the initially defective failures take place at the zero year, releases do not occur until 8,100 years later. Before 8,100 years, the drip shield fails at 7,422 years and then refluxing water enters and fills the failed waste package. Water accumulates in the failed waste package with time and eventually overflows, releasing radionuclides.

Table 3-11. Biosphere Dose Conversion Factors for Groundwater at the 20-km Receptor Location		
Radionuclide	Nonpluvial Dose Conversion Factor (rem/year)/(Ci/m^3)	Pluvial Dose Conversion Factor (rem/year)/(Ci/m^3)
Ac-227	1.53×10^7	2.64×10^5
Ag-108m	8.26×10^3	3.79×10^6
Am-241	3.91×10^6	3.44×10^6
Am-242m	3.78×10^6	3.61×10^6
Am-243	3.89×10^6	3.29×10^6
C-14	2.93×10^3	2.92×10^5
C-36	5.09×10^3	5.62×10^5
Cm-243	2.69×10^6	1.39×10^6
Cm-244	2.16×10^6	5.60×10^6
Cm-245	4.02×10^6	2.57×10^6
Cm-246	3.97×10^6	3.71×10^6
Cs-135	7.62×10^3	3.63×10^6
Cs-137	5.38×10^4	2.74×10^5
I-129	2.95×10^5	1.09×10^7
Mo-93	1.92×10^3	1.45×10^7
Nb-94	7.80×10^3	3.84×10^6
Ni-59	2.42×10^2	7.02×10^4
Ni-63	6.64×10^2	3.74×10^6
Np-237	4.75×10^6	4.55×10^6
Pa-231	1.14×10^7	2.98×10^5
Pb-210	5.88×10^6	3.71×10^6
Pd-107	1.81×10^2	2.06×10^6
Pu-238	3.44×10^6	3.63×10^6
Pu-239	3.79×10^6	2.76×10^5
Pu-240	3.79×10^6	1.36×10^6
Pu-241	7.35×10^4	4.00×10^2
Pu-242	3.60×10^6	5.14×10^4
Ra-226	1.47×10^6	7.27×10^3
Se-79	9.43×10^3	2.82×10^5
Sm-151	4.20×10^2	2.06×10^4
Sn-121m	1.95×10^3	1.82×10^3
Sn-126	2.18×10^4	7.87×10^3
Sr-90	2.07×10^5	1.67×10^2
Tc-99	1.91×10^3	1.74×10^3
Th-229	3.89×10^6	1.71×10^3
Th-230	5.88×10^5	7.44×10^3
U-232	1.44×10^6	1.71×10^3
U-233	3.15×10^5	1.83×10^5
U-234	3.09×10^5	8.99×10^3
U-235	2.90×10^5	6.23×10^2
U-236	2.93×10^5	2.26×10^2
U-238	2.80×10^5	4.45×10^3
Zr-93	1.79×10^3	2.60×10^3

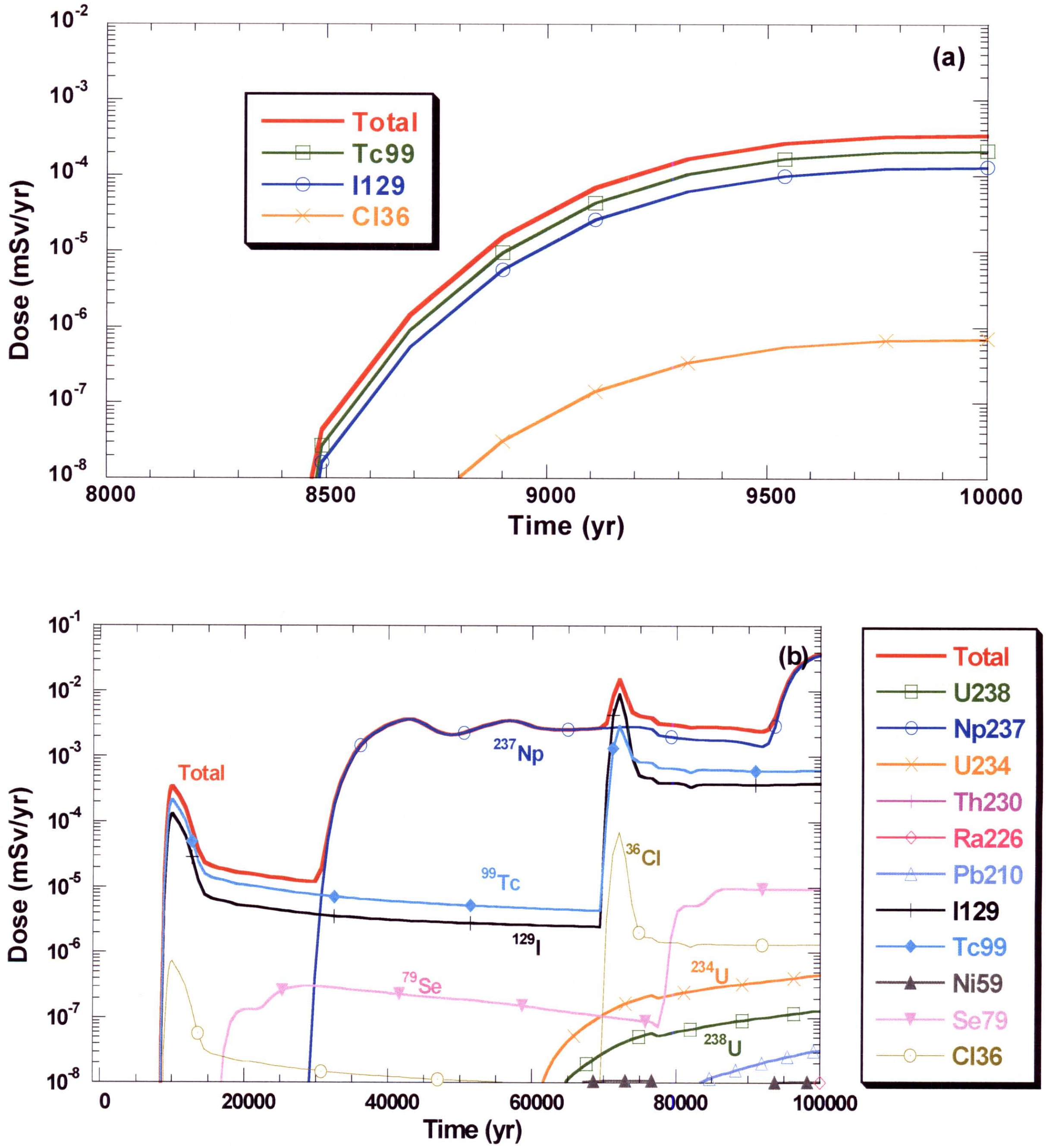

Figure 3-12. Groundwater Dose to an Average Individual as a Function of Time at the Receptor Location 20 km [12.4 mi] Downgradient of the Repository, for the Mean Value Data Set in the (a) 10,000-Years, and (b) 100,000-Years Simulation Period

Time histories of radionuclide releases at the outflow boundaries of the engineered barrier subsystem, the unsaturated zone, and the saturated zone are shown in Figure 3-13. In general, the release rates from the engineered barrier subsystem in Figure 3-13(a) for the soluble radionuclides drop after the peak release is reached because of radioactive decay and because the removal of radionuclides from the waste package decreases the inventory available for release. Other radionuclides, such as U-238, U-234, Np-237, Pu-239, Nb-94, and Th-230, which are less soluble and have relatively longer half-lives, exhibit increasing release rates throughout the 10,000-year simulation period. Am-241 also has low solubility; however, with a half-life of only 432 years, the inventory decreases rapidly.

There is only a small increase {~ 1.0×10^{-5} mSv/yr [1.0×10^{-3} mrem/yr]} in the engineered barrier subsystem release rates from the instantaneous release of the gap fraction inventory. The increase in infiltration rate for the 10,000-year simulation period shown in Figure 3-1 is only marginal compared with the period beyond 10,000 years. Therefore, climatic change from current to pluvial conditions is a key event that affects release rates only beyond 10,000 years.

The similarity between engineered barrier subsystem and unsaturated zone releases shown in Figures 3-13(a) and (b) indicates the unsaturated zone as modeled apparently does not significantly delay the releases into the saturated zone for the mean value data set. One might expect the unsaturated zone to delay the transport of radionuclides because the radionuclides must be transported 300 m [984 ft] from the repository to the water table.

The unsaturated zone releases are directly related to the presence of the Calico Hills vitric layer. The groundwater travel time through the unsaturated zone is 11–21 years for subareas 2, 8, 9, and 10 (i.e., fracture flow); the remaining subareas are between 200 and 700 years (i.e., matrix flow). Subareas 2, 8, 9, and 10 show a fast path because, in the absence of the Calico Hills nonwelded vitric layer, the flow is predominately in fractures. Consequently, for subareas 2, 8, 9, and 10, which encompass almost 48.3 percent of the spent nuclear fuel inventory, the unsaturated zone does not delay radionuclide transport subsequent to release from the engineered barrier system. For the remaining 51.7 percent of the spent nuclear fuel inventory, the 200–700 years of groundwater traveltime somewhat delays the non-retarded radionuclides, however, retarded radionuclides will be effectively held up for greater than 10,000 years in those subareas where the Calico Hills vitric unit is present.

The saturated zone release illustrated in Figure 3-13(c) reveals releases of only non-retarded Tc-99, I-129, and Cl-36 in the 10,000-year simulation period. The saturated zone release rates presented in Figure 3-13(c) also can be compared with Figure 3-13(b) to evaluate the effects of flow and transport in the saturated zone. The groundwater traveltime computed using the streamtube flow rates and lengths in the saturated zone is 570 years (see Table 3-12). However, sorption in the alluvium significantly increases the traveltime for most radionuclides.

As illustrated in Figure 3-12(a), the groundwater pathway dose at 10,000 years is dominated by I-129, Tc-99, and Cl-36. These nuclides contribute the most to dose because of no retardation during transport in alluvium, a large initial inventory {1.32×10^{9}, 5.37×10^{11}, and 4.26×10^{8} Bq/MTU [0.0357, 14.5, and 0.0115 Ci/MTU]}, long half-lives compared with the 10,000-year timeframe of interest (1.57×10^{7}, 2.13×10^{5}, 3.01×10^{5} year), moderate to high dose conversion factors, and moderate to high solubilities {129, 99.3, and 36 kg/m^3 [8.05, 6.20, and 2.25 lb/ft^3]}. Tables 3-5 and 3-7 through 3-10 provide a summary of the mean values for these parameters corresponding to all radionuclides. To obtain a perspective of the magnitude

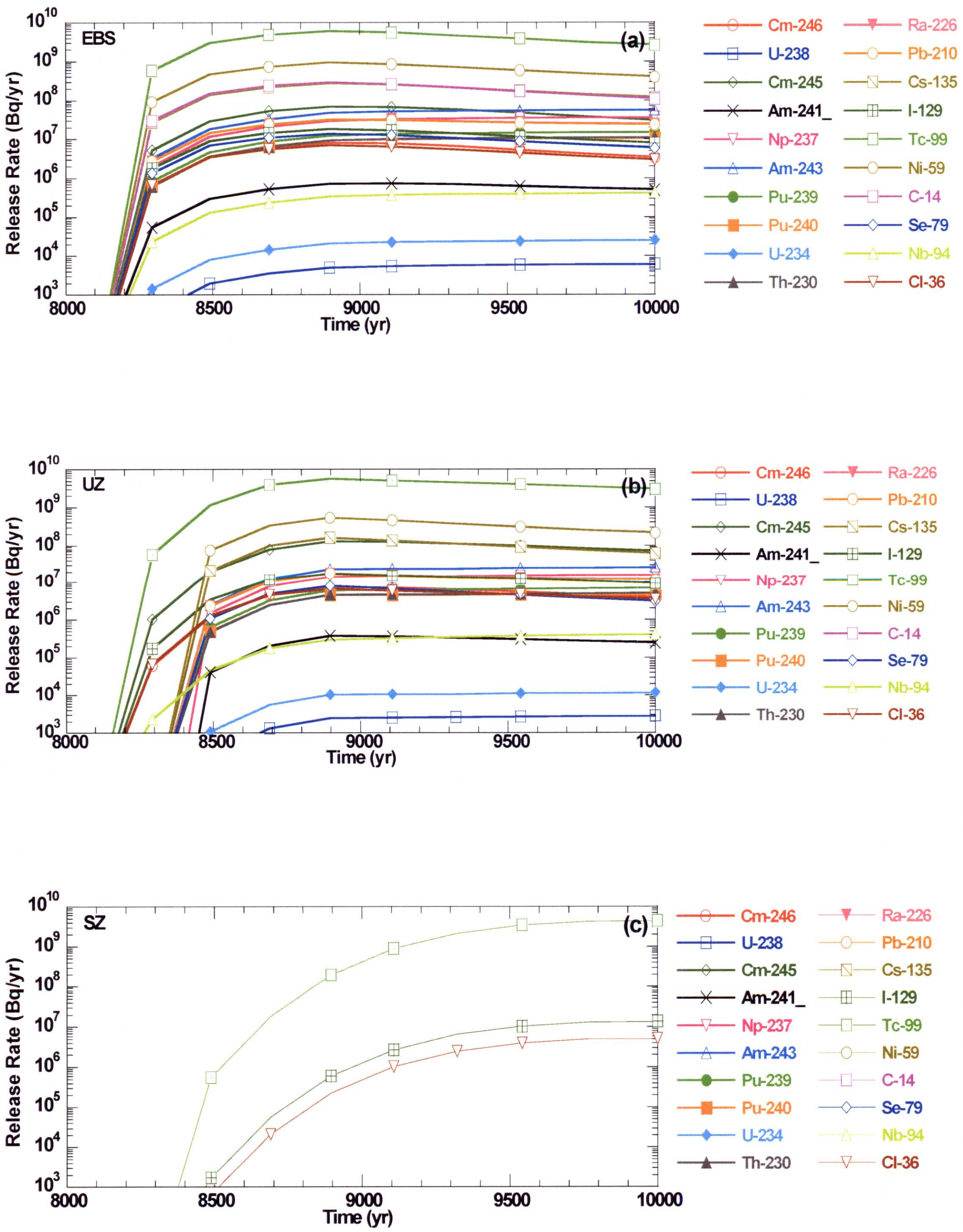

Figure 3-13. Release Rates in the 10,000-Year Time Period of Interest from the (a) Engineered Barrier Subsystem, (b) Unsaturated Zone, and (c) Saturated Zone for the Mean Value Data Set

Table 3-12. Average, Maximum, and Minimum Saturated Zone Groundwater Traveltimes and the Average from 350 Realizations				
		Groundwater Traveltimes (yr)		
Streamtube	Subarea	Minimum	Maximum	Average
1	5	58	1,356	629
	6	57	1,352	627
	7	57	1,350	626
2	1	76	1,261	592
	2	72	1,234	578
	3	74	1,249	586
	4	72	1,234	578
	8	72	1,239	581
3	9	80	1,790	821
	10	78	1,781	816
Average (all subareas)		70	1,385	644

of the dose, a total dose of 10^{-11} Sv/yr [1 nanorem/yr] does not appear until 8,490 years in the time evolution of the dose curve in Figure 3-12(a). Furthermore, the saturated zone release rate for I-129 corresponding to 74,000 Bq/yr [2 μCi/yr] occurs at 8,300 years, at which time there is no measurable dose from any nuclide. The only nuclides that contribute more than 10^{-11} Sv/yr [1 nanorem/yr] to dose in 10,000 years are I-129, Tc-99, and Cl-36, which exhibit the peak doses at the end of the 10,000-year simulation period.

The dose histories for a particular faulting event and a particular igneous event are presented in Figures 3-14(a) and (b). The purpose of the following discussion is not to compare the incremental risk posed by the faulting or the igneous event, but rather to illustrate the behavior of the underlying model abstractions for faulting and igneous activity. To determine the risk, one would need to multiply the additional doses caused by faulting and igneous activity by their respective annual probabilities of occurrence [5×10^{-6} and 1×10^{-7}(see Mohanty, et al., 2002, pp. 12-2 and 14-2, respectively for details)]. For the mean value data set, there are no faulting events because the mean value of the threshold displacement is greater than the mean value of the credible displacement along a fault. If the threshold is made smaller than the mean value of the credible displacement, however, the faulting event occurs at approximately 4,900 years and causes the failure of 208 waste packages. Figure 3-14(a) shows that the compliance period peak groundwater dose from the forced faulting event occurs approximately 1,400 years earlier and more than 2.5 times the basecase compliance period peak dose. The earlier release is because waste packages failed from faulting events do not experience bathtub behavior and thus have rapid release. The difference between the results arises solely from the release of spent nuclear fuel from waste packages failed by faulting.

The groundwater dose from igneous activity in Figure 3-14(b) behaves similarly to the dose from faulting events. The increase in groundwater dose from igneous activity is smaller than that for faulting events because only 53 waste packages are failed by the intrusive igneous activity compared with 208 waste packages failed by the faulting event in the mean value,

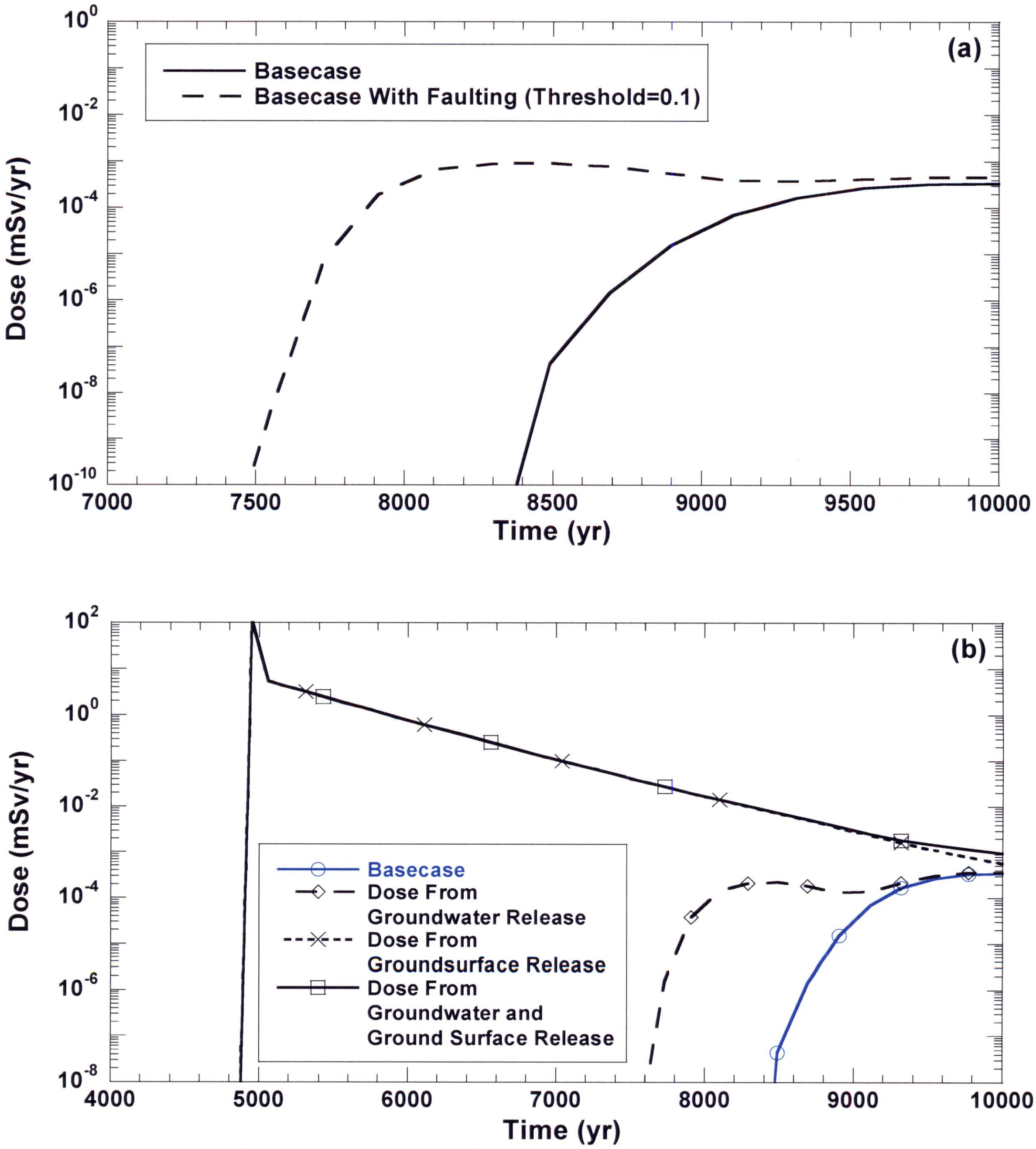

Figure 3-14. Groundwater Dose in 10,000-Year Simulation Period With and Without (a) Faulting; and (b) Igneous-activity Disruptive Events, for the Mean Value Data Set, Without Probability Weighting. (The Ground-Surface Dose Is Shown for Releases Caused by Extrusive Igneous Activity.)

single-realization case. Extrusive igneous events also result in a peak ground surface dose of approximately 0.1 Sv/yr [10,000 mrem/yr] at 4,900 years, which is the time of the volcanic event, and the dose exponentially decreases thereafter.

3.2.2 Releases and Dose 100,000-Year Simulation Period

This section presents a discussion of the total-system performance assessment results from the 100,000-year simulation period for dose, release rates, and other intermediate values such as corrosion failure time using the mean value data set. The results for the 100,000-year simulation period are different from the results for the 10,000-year simulation period, in part because waste packages fail from corrosion only after 10,000 years.

Calculations beyond 10,000 years help us understand the effect of processes beyond the anticipated behavior of the repository for the regulatory period (e.g., failure of the waste packages by corrosion, wetter environment).

Figure 3-8 provides the performance of the engineered barrier subsystem showing the number of failed waste packages during the 100,000-year simulation period. Initially defective failures in all subareas account for 45 waste packages, whereas, of those remaining, 2,392 waste packages in subareas 4, 5, 7, and 10 fail from corrosion at 69,400 years; and 6,440 waste packages in subareas 1, 2, 3, 6, 8, and 9 fail from corrosion at 70,300 years (i.e., 900 years after the first corrosion failure). Thus, all 8,877 waste packages in the repository fail by 70,300 years. Table 3-3 provides a summary of the total-system performance assessment input parameters that determine the waste package failure time.

The release rate histories for all 20 radionuclides at the three boundaries (i.e., engineered barrier subsystem, unsaturated zone, and saturated zone presented in Figure 3-15) reflect the time required for the drip shield to fail, and initially defective waste packages to fill with water (8,300 years) and release radionuclides, together with the final corrosion failure time of 70,300 years. The waste packages failed by corrosion fill relatively faster and release radionuclides relatively faster than the initially defective failures because the thermal reflux period has passed, the drip shields have failed, and the pluvial period has taken effect. The first peak releases begin at approximately 8,300 years, corresponding to the initially defective failure, and the second peak begins just after 70,000 years, corresponding to the corrosion failure of waste packages. Just as with the 10,000-year simulation period in Figure 3-13, release rates for radionuclides are impacted by sorption coefficients, half-lives, initial inventories, gap inventories, solubilities, and dose conversion factors. Values for these parameters are presented in Tables 3-5 and 3-7 through 3-10. The gap fraction inventory has a longer impact on dose in the 100,000-year simulation period (a 300 percent increase in dose at the time of corrosion failure of waste package) compared with the 10,000-year simulation period (a 12 percent increase in the peak expected dose. This is primarily the result of a proportionately larger gap inventory being available after the corrosion failure than the initially defective failure. The gap fraction inventory, however, influences the 10,000-year simulation period peak while it does not affect the 100,000-year simulation period peak.

For the waste package failure modes in which the waste package behaves as a bathtub, the releases of Tc-99, I-129 and the other highly soluble radionuclides represent the accumulation of the radionuclides in water that occurs as the waste package fills. In the nominal case

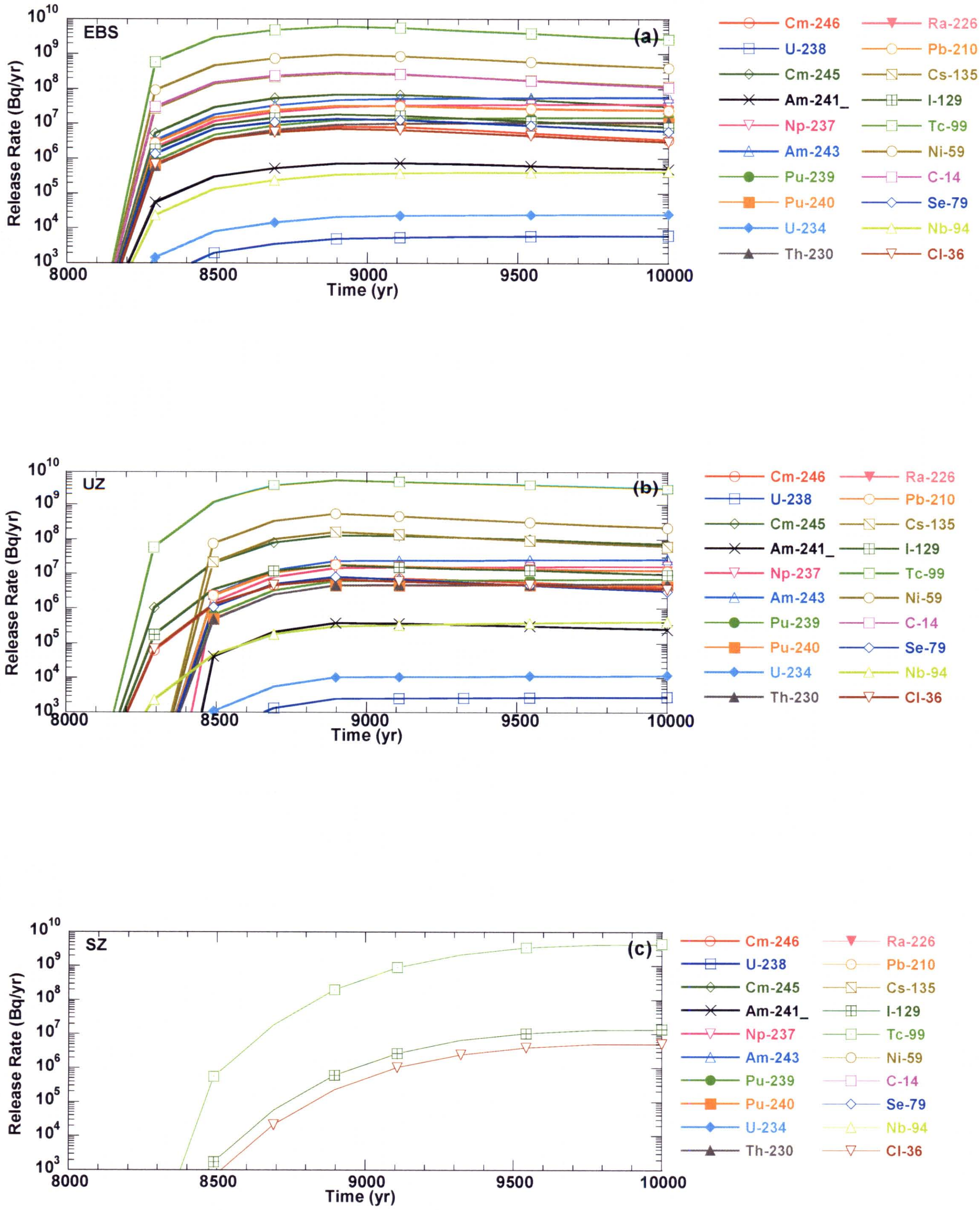

Figure 3-15. Release Rates up to 100,000 Years from the (a) Engineered Barrier Subsystem, (b) Unsaturated Zone, and (c) Saturated Zone for the Mean Value Data Set

scenario, bathtub behavior occurs for initially defective, corrosion, and seismic failures. Because seismic failure does not occur with the mean value data set, bathtub behavior occurs before 10,000 years because of initially defective failure and after 10,000 years because of corrosion failure. The peak releases for these highly soluble radionuclides occur after the waste package fills with water at 8,300 years. As Figure 3-15 shows for the less soluble radionuclides such as Np-237, the release rate peaks at 17,000 years. This time delay of 8,700 years after the Tc-99 and I-129 peak release is because the solubility limit controls the release rate. Because Np-237 leaves the waste package at the solubility limit, the release rate from the waste package is proportional to the rate of water flow through the waste package. Further discussions on the impact of solubility limits on Np-237 can be found in Chapter 7. With a half-life of 2.14×10^6 years and an initial inventory of 3.42 Ci per waste package, the Np-237 inventory is available for release throughout the simulation period. After 17,000 years, the solubility limits control on release rate decreases as the flow rate increases (because of the reduced rate of radionuclide mass accumulation in the bathtub), implying that the release becomes more controlled by the dissolution rate. Therefore, the decrease in the Np-237 release rate until the next waste package failure time can be attributed to a higher infiltration rate during the pluvial period. This effect is observable in Figure 3-15(a), from 17,000 years to the corrosion failure time at 70,000 years. After 70,000 years, radionuclide releases decrease (i.e., not solubility-limited) following the peak releases at approximately 70,000 years. The decrease in release rates for the radionuclides with low solubilities can also be attributed to high flow rates during the pluvial period that switches the release mode from solubility limited to dissolution limited. Pu-239 is another actinide that is solubility limited in ambient Yucca Mountain pore waters. Therefore, its release rates from the engineered barrier subsystem should be similar to Np-237, as Figure 3-15(a) shows.

The plot in Figure 3-15(b) represents the release rates at the water table for each radionuclide summed over all 10 subareas. A comparison of the engineered barrier subsystem and unsaturated zone release rates in Figures 3-15(a) and (b) shows that the unsaturated zone has little delaying effect, not only on the transport of Tc-99, a nonsorbing nuclide, but also on the transport of the other 19 radionuclides. Those subareas that do not contain the Calico Hills vitric layer do not significantly affect the release rates because for those subareas, transport occurs mainly in fractures. However for the subareas containing the Calico Hills vitric layer, release rates would be significantly lowered, especially for retarded radionuclides.

Figure 3-15(c) illustrates the performance of the saturated zone in the 100,000-year simulation period. In the saturated zone, sorption significantly affects the release rates. The only radionuclides that arrive at the receptor location with a release rate greater than 37 Bq/yr [10^{-6} Ci/yr] are Tc-99, Np-237, I-129, Se-79, Cl-36, Ni-59, and U-234. Either retardation of the remaining 13 radionuclides in the alluvium delays the time of arrival past the 100,000-year simulation period or the inventory decays during transit because the half-lives are short relative to the transport time. The saturated zone alluvium sorption coefficients for all radionuclides are provided in Table 3-9.

The radionuclides dominating the 100,000-year dose are different from those dominating the 10,000-year dose. For the 100,000-year simulation period, the dose shown in Figure 3-12(b) is dominated by Np-237, Tc-99, and I-129, with smaller contributions from Cl-36, Se-79, and others. The radionuclides contributing the most to the peak dose at 72,000 years are I-129, Np-237, and Tc-99, with minor contributions from Cl-36. Although Cl-36 has a relatively long half-life at 3.01×10^5 years, the inventory is small (see Table 3-7). Thus, although contributing significantly to peak dose at 72,000 years, Cl-36 rapidly becomes an insignificant contributor to dose. Figure 3-12(b) also illustrates the impact of retardation in the alluvium portion of the saturated zone on the arrival of radionuclides at the 20-km [12.4-mi] receptor location. The retardation factors for Cl-36, I-129, Tc-99, Se-79, and Np-237 are 1.0, 1.0, 1.0, 22.4, and 62.4 respectively. The reasons Tc-99 and I-129 dominate the dose in Figure 3-12(b) are (i) high solubility in the water contacting the spent nuclear fuel, (ii) no retardation, (iii) long half-lives, and (iv) relatively large dose conversion factors. Np-237 has comparatively low solubility, but has a relatively large dose conversion factor. Tables 3-5 and 3-7 through 3-10 provide summaries of the values for these parameters. Note that the flow in the remainder of the saturated zone (i.e., tuff) is in fractures which are assumed to have no retardation. Retardation in the tuff occurs only after radionuclides diffuse into the matrix but the effect is much smaller compared to the retardation in the alluvium.

Figures 3-16 and 3-17 show the Tc-99 and Np-237 release rates and the Tc-99 dose, by individual subarea and the entire repository. The engineered barrier subsystem release rates for Tc-99 and Np-237 in Figure 3-16(a) and (b) exhibit similar behavior with the subareas having the largest inventory contributing the most to the total release. The number of waste packages in each subarea, which are directly related to the inventory, are 1,455; 1,568; 775; 426; 760; 851; 323; 846; 977; and 896 for subareas 1–10, respectively. Subareas 1 and 2 contain the most waste packages and show the highest release rates, whereas subareas 4 and 7 contain the fewest waste packages and have the lowest release rates.

The plots of the unsaturated zone releases in Figure 3-16(c) indicate that the Tc-99 release rates are the same as the engineered barrier subsystem releases in Figure 3-16(a). Np-237 release rates [Figure 3-16(d)] vary considerably between unsaturated zone release and engineered barrier subsystem release especially in subareas 1, 3, 4, 5, 6, and 7, which have the Calico Hills nonwelded vitric unit (Figure 3-9) that has relatively high matrix permeability compared with other units. At the infiltration rate corresponding to the mean value data set, only matrix flow can occur in this unit. Flow occurs in the fractures for subareas 1, 2, 8, 9, and 10 with groundwater traveltimes of approximately 20 years and no retardation. For subareas 1, 3, 4, 5, 6, and 7, however, the transport of Np-237 is retarded in the matrix and the effects of the time-varying unsaturated zone flow change the Tc-99 and Np-237 release rates. As evident in Figure 3-16(b), (c), and (d), retardation in the matrix produces a greater effect on the Np-237 unsaturated zone release rates than on those radionuclides that are not retarded.

The saturated zone release rates for Tc-99 in Figure 3-16(e) exhibit a delay when compared with the Tc-99 unsaturated zone release rates in Figure 3-16(c). The general characteristics of the engineered barrier and unsaturated zone releases are preserved insofar as the peak releases arising from initially defective failures and corrosion failures are apparent in the plot. The variability by subarea is also consistent for the Tc-99 release rates. There is lower Np-237 release from the saturated zone because of retardation in the saturated zone alluvium.

The groundwater doses for Tc-99 by subarea are shown in Figure 3-17. The characteristics of these dose curves are identical to the corresponding saturated zone release rate curves for Tc-99 in Figure 3-16(e) because the dose is obtained from the release rates using several multipliers. For 100,000 years, the subareas with the largest Tc-99 release rates and doses (shown in Figure 3-17) contain the greatest amount of spent nuclear fuel (i.e., the subareas listed from the largest to the smallest amount of spent nuclear fuel are subareas 2, 1, 9, 10, 6,

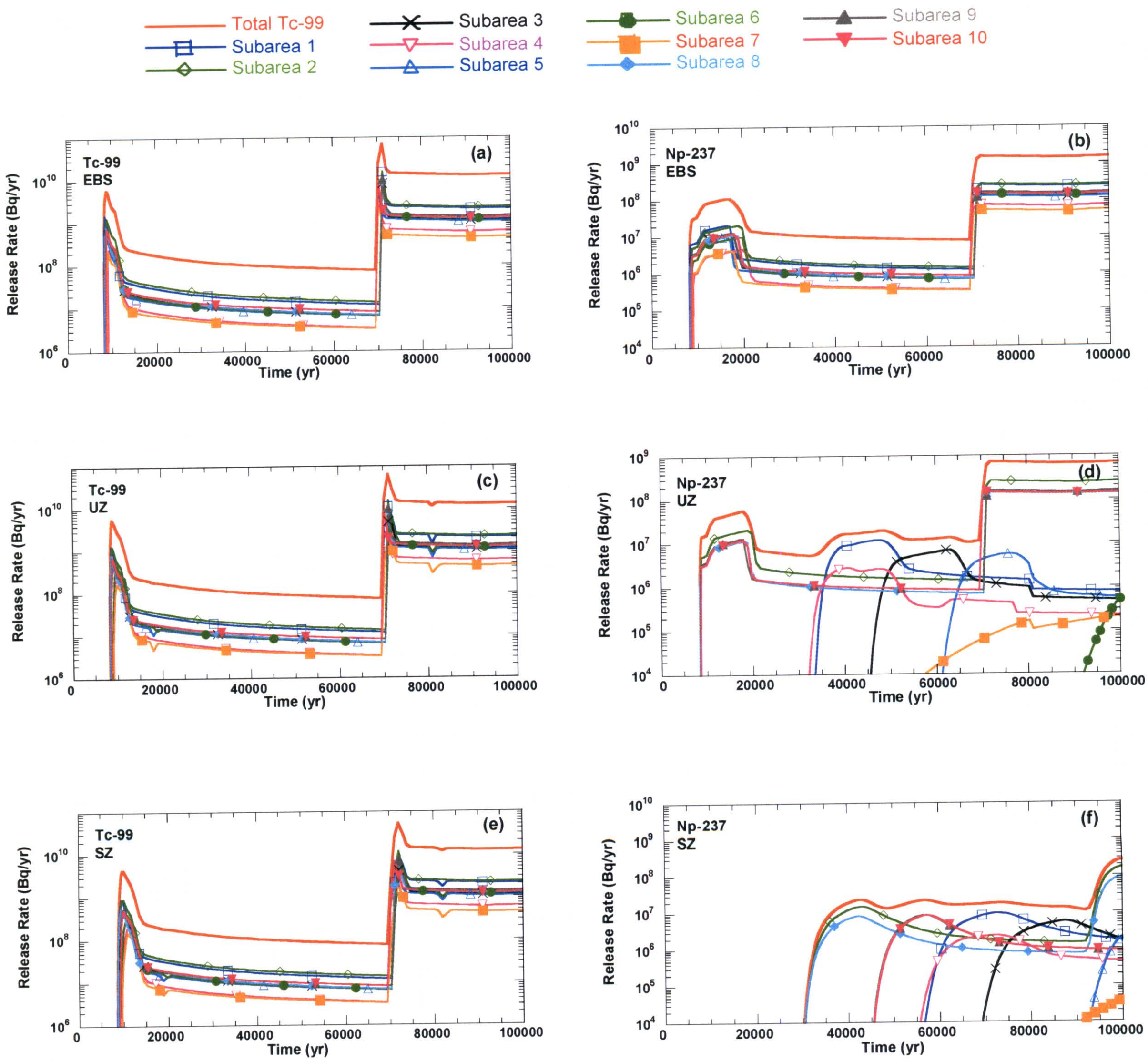

Figure 3-16. Np-237 and Tc-99 Total Releases by Subarea in 100,000 Years from the (a) and (b) Engineered Barrier Subsystem, (c) and (d) Unsaturated Zone, and (e) and (f) Saturated Zone for the Mean Value Data Set

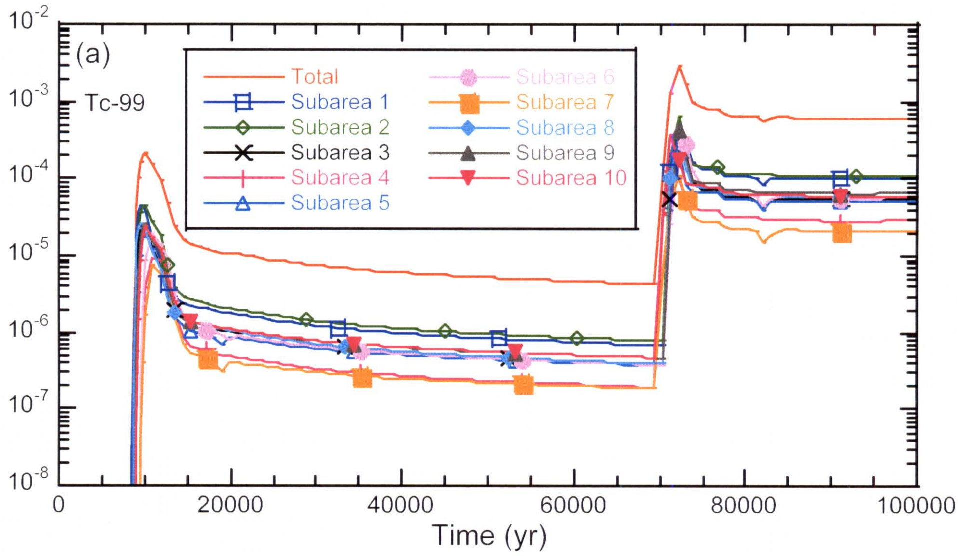

Figure 3-17. Tc-99 Groundwater Doses, Total and by Subarea, in 100,000 Years, for the Mean Value Data Set

8, 3, 5, 4, and 7). The saturated zone traveltimes vary by subarea because groups of subareas are connected to different streamtubes. Subareas 1, 2, 3, 4, and 8 are connected to streamtube 2 and exhibit the shortest saturated zone traveltimes, whereas subareas 5, 6, and 7 are assigned to streamtube 1, and subareas 9 and 10 use streamtube 3. The longest traveltimes are found in streamtube 3 (see Table 3-9 for streamtube lengths), which is at the outer edge of the saturated zone pathway. The groundwater doses for all radionuclides by subarea are shown in Figure 3-18. The combined effects of retardation, solubility limit and groundwater travel time are evident in the variations shown in the figure. The dose history for faulting events and igneous activity[5] for 100,000 years is presented in Figure 3-19. As with the results for the 10,000-year simulation period, the mean value data set results show no faulting events because the mean value of the threshold displacement is greater than the mean value of the credible displacement along a fault. But if a faulting event were to occur (i.e., emulated by making the threshold smaller than the credible displacement), the faulting event would occur at approximately 4,900 years and fail 208 waste packages. Figure 3-19(a) shows the groundwater dose from the faulting event (before probability weighting) is greater than the dose without a faulting event from approximately 10,000 to 18,000 years.

The groundwater dose from igneous activity for the 100,000-year simulation period [shown in Figure 3-19(b)] behaves similarly to the dose from faulting events. As with the results for the 10,000-year simulation period, the increase in groundwater dose from igneous activity for

[5]These results are presented only to show the process-level trends and must be used in proper context. Because these results are not weighted by appropriate probabilities, the dose values are much larger than they should be when appropriately weighted by the event probability The annual probability for the faulting event is 5×10^{-6} and for the igneous event is 1×10^{-7} years^{-1}(Mohanty, et al., 2002).

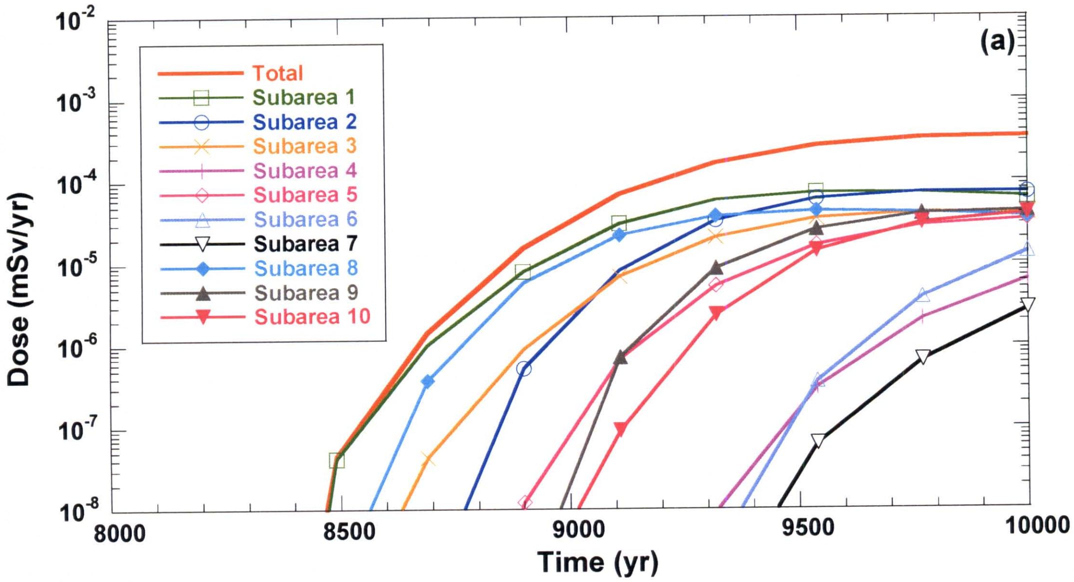

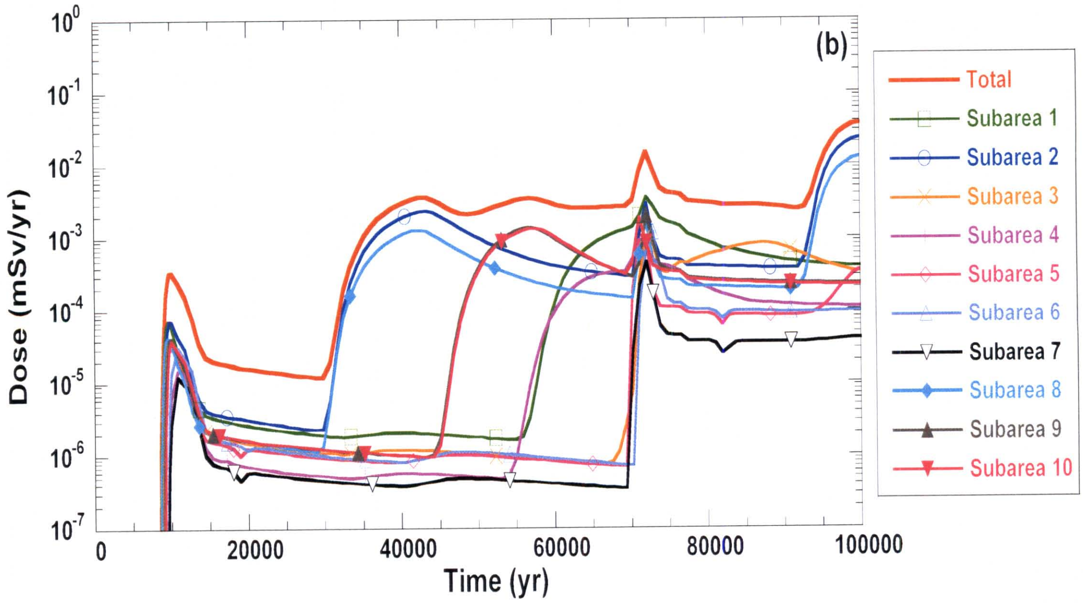

Figure 3-18. Groundwater Dose, Total and by Subarea, in (a) 10,000, and (b) 100,000 Years, for the Mean Value Data Set

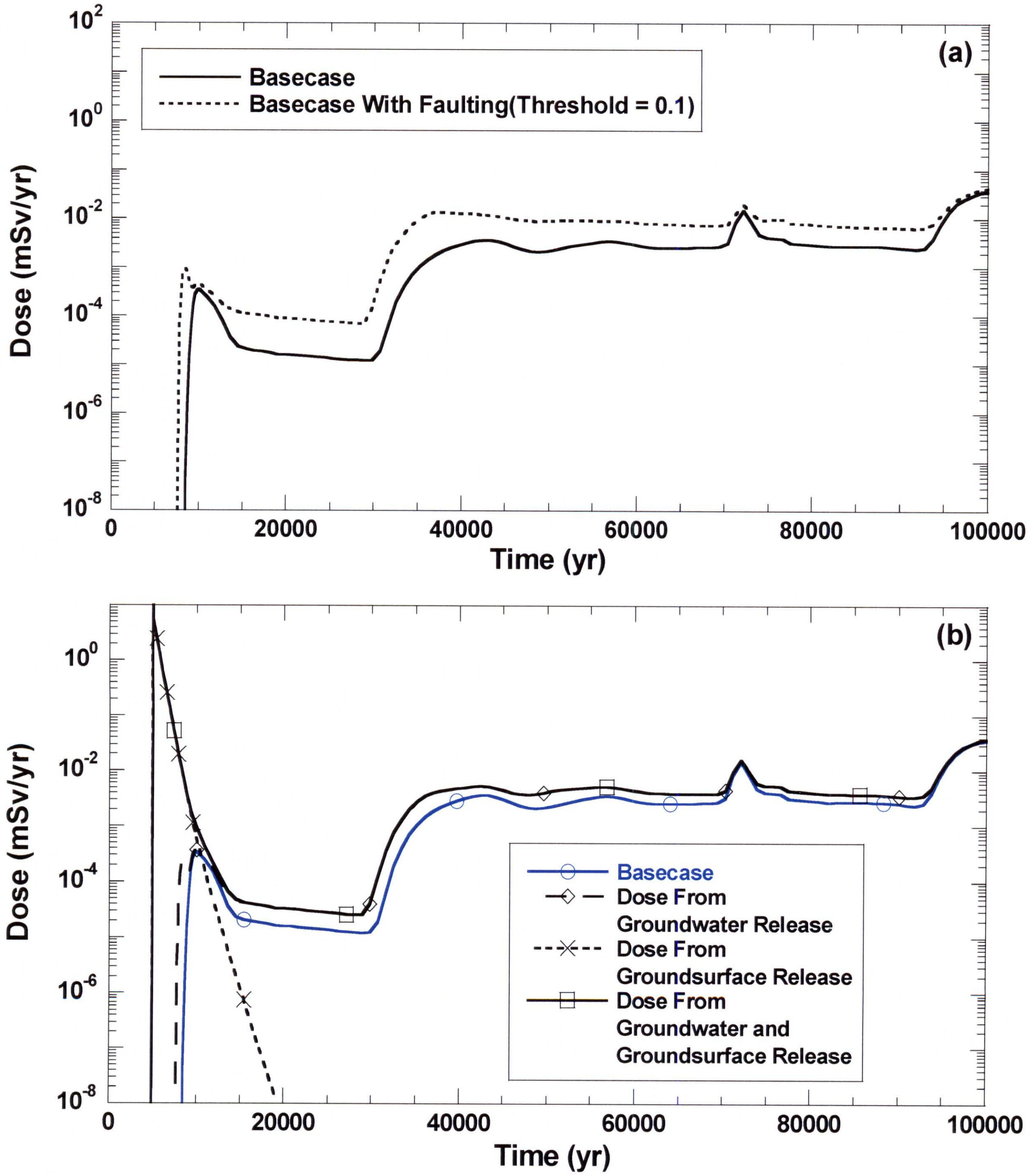

Figure 3-19. Groundwater Dose in 100,000 Years With and Without (a) Faulting and (b) Igneous Activity Disruptive Events for the Mean Value Data Set, Without Probability Weighting. (The Ground-Surface Dose Is Shown for Releases Caused by Extrusive Igneous Activity.)

100,000 years is smaller than that for faulting events because only 53 waste packages are failed by the intrusive igneous activity, compared with 208 waste packages failed by the faulting event. Extrusive igneous events also result in a ground-surface dose that peaks at approximately 100 mSv/yr [10,000 mrem/yr] when the volcanic events occur at 4,900 years and exponentially decreases thereafter. At approximately 12,000 years, the groundwater and ground-surface contributions to dose are equal. For the remainder of the 100,000 year period, the igneous activity groundwater doses stay above the basecase (except for a short period corresponding to the corrosion failure at 70,000 years) because of the release from the 53 waste packages that failed from intrusive igneous activity. The doses presented in Figure 3-19 are not probability weighted.

3.3 Multiple-Realization Analysis

The performance of the Yucca Mountain repository is evaluated with a probabilistic (i.e., stochastic) approach that averages the results from multiple realizations. This approach uses the probabilistic sampling of input data to compute dose at a receptor location 20 km [12.4 mi] from the repository during 10,000 and 100,000 years. Although the deterministic approach (runs with the mean value data described in the previous section) was presented to illustrate in detail how the behavior of the various components or processes influences other components or dose, the probabilistic analysis provides results that show the variation in the output resulting from the combined effects of the uncertainty and variability in the input data. Also, trends and relationships not evident in the results from the deterministic simulation are revealed in the probabilistic results.

Probabilistic sampling is conducted using Latin Hypercube Sampling (Iman, et al., 1980) for the 350 realizations, which is theoretically large enough to obtain convergence in results while maintaining computational efficiency (see Appendix H for further discussion on convergence). Each realization uses a set of values generated from probability distribution functions specified in the total-system performance assessment input file. Probability distribution functions are constructed for the input parameters whose true values are uncertain or vary spatially and temporally. Uncertainty arises from a lack of complete information, whereas variability is the natural or inherent variance in the value of a parameter.

In the basecase data set, of the 950 parameters, 620 are defined as constants, and 330 are defined by probability distribution functions. The basis for assigning a constant value or a probability distribution to the parameter depends on various factors. For example, constant values are assigned to parameters that are either well characterized or have negligible variability. Probability distribution functions are assigned to parameters not well known or where variability has been observed in data. The subject matter experts have provided a valid basis to assign a constant value or a probability distribution function to a parameter though no formal elicitation process was used. Selection of the particular distribution type, such as normal, uniform, or beta, depends on the information available for the parameter and may involve either the best fit of data to a distribution or a reasonable assumption of the distribution type. Specification of a probability distribution function in the TPA Version 4.1 code consists of a distribution type and limits (e.g., uniform with a minimum of 0 and a maximum of 100, or log-triangular, with a minimum of 1.0×10^{-5}, a maximum of 1.0×10^{-1}, and a peak of 1.0×10^{-3}). The limits are set at 0.01^{th} percentile and at the 99.99^{th} percentile for unbounded distributions. These values are required by the Latin Hypercube Sampling model in the TPA Version 4.1 code. The impact of assuming a particular distribution for a parameter is evaluated in Chapter 5.

When the TPA Version 4.1 code is executed for a realization of the parameters, dose to the receptor is calculated for that realization. The results from all Monte Carlo realizations using Latin Hypercube Sampling are plotted to evaluate the repository performance. For example, dose to the receptor is presented in a scatterplot of peak dose versus time of peak dose, a time history of dose for all realizations, and a complementary cumulative distribution function of peak dose. The expected dose is computed by averaging the doses at each time step from all realizations. The resulting curve is a time-dependent curve that represents the expected dose. The peak expected dose is the largest expected dose obtained from the expected dose curve versus time. For example, groundwater dose from a single realization using the mean value data set is shown in Figure 3-18 (total dose curve), and the expected dose from multiple realizations is presented in Figure 3-20, which also shows the dose from individual realizations. Peak dose obtained from the expected dose curve is shown in Figure 3-20. Additionally, the relationship between dose and intermediate results, such as waste package failure time, flow of water into a waste package, and radionuclide release rates, is presented for all realizations.

3.3.1 Unsaturated Zone Flow

The variation in the mean, minimum, and maximum infiltration rates is illustrated in Figure 3-21. For the mean infiltration rates, a present-day climate exists from 0 to approximately 13,000 years, and 87,000 to 100,000 years, with the pluvial climate occurring between 13,000 and 87,000 years. Figure 3-21 shows that the infiltration rate ranges between 4 and 30 mm/yr [0.16 and 1.2 in/yr] in the first 10,000 years, with the infiltration rate steadily rising from 0^{th} year to $10{,}000^{th}$ year. The average infiltration is 8 mm/yr [0.31 in/yr] at the 0^{th} year and doubles in the first 10,000 years. The peak infiltration rate ranges two orders of magnitude {4–96 mm/yr [0.16–3.8 in/yr]} in the 100,000-year simulation period. This range is related to the total-system performance assessment input parameter for the present-day areal average mean infiltration rate, which has a uniform distribution from 4 to 13 mm/yr [0.158 to 0.512 in/yr].

As shown earlier using the mean value data set, subarea 1 exhibits the largest infiltration rates (see Figure 3-2) because of higher infiltration at the ground surface above subarea 1, which is attributable to near-surface processes such as elevation and soil depth. Subareas 4, 6, and 7, however, have the lowest infiltration rates. In any single realization, the subarea-to-subarea variability in infiltration rates is substantial. The largest subarea-to-subarea variation observed in 10,000 and 100,000 years are $0.040 m^3/yr$ and $0.134 m^3/yr$ [$1.42 ft^3/yr$ and $4.73 ft^3/yr$], respectively. The minimum and maximum pluvial infiltration rates, which occur between approximately 13,000 and 87,000 years, vary from approximately 10 to 85 mm/yr [0.394 to 3.35 in/yr] for all realizations and subareas.

3.3.2 Near-Field Environment

The time history of average waste package temperature for each subarea is shown in Figure 3-22(a). The subarea-to-subarea variability in the waste package temperature from 0 to 400 years and from 10,000 to 100,000 years is less than 10 °C [50 °F]. The subarea-to-subarea variability in the waste package temperature in the 400- to 10,000-year time period is

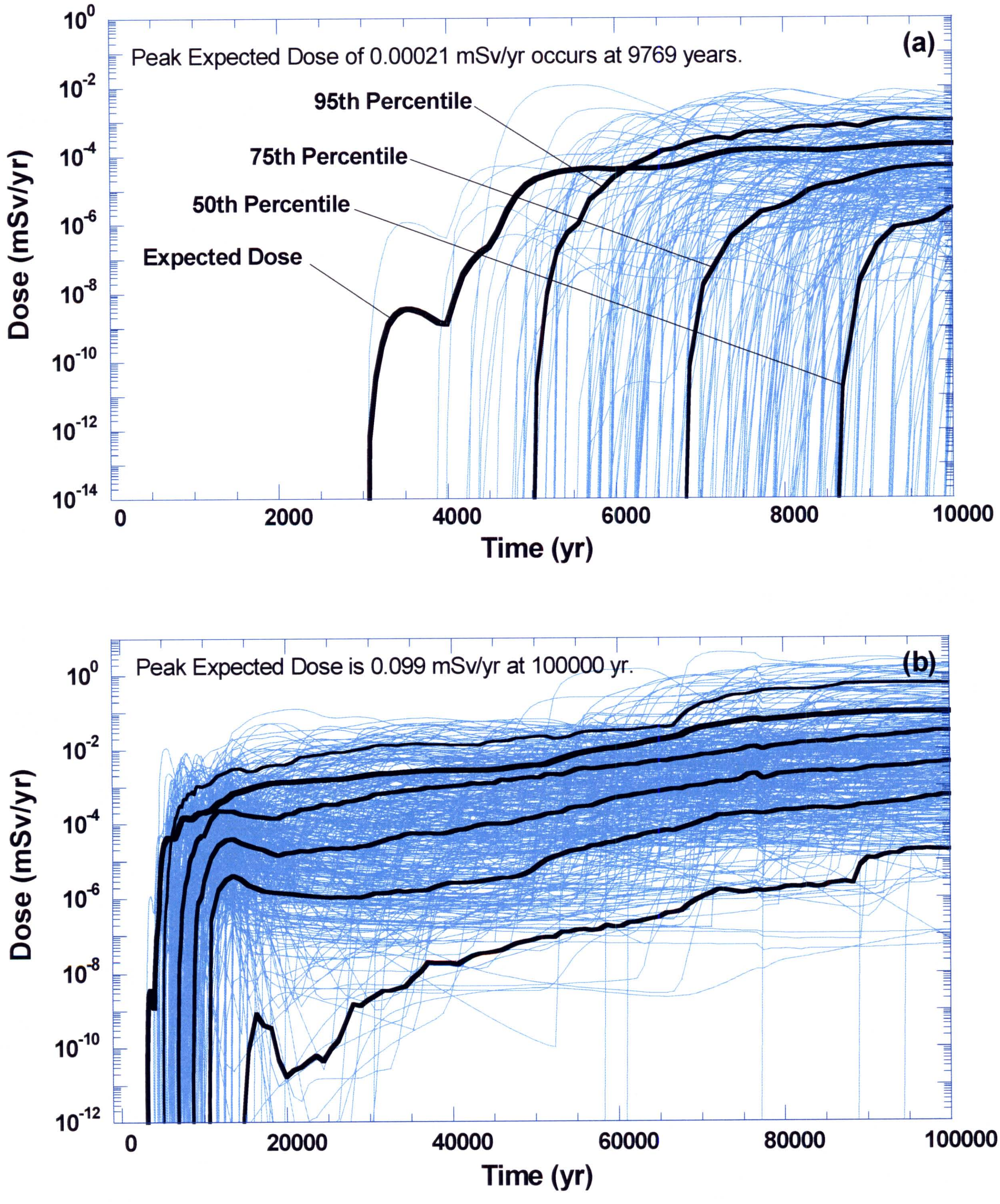

Figure 3-20. Groundwater Dose in (a) 10,000 and (b) 100,000 Years, Including the Average Dose for 350 Realizations

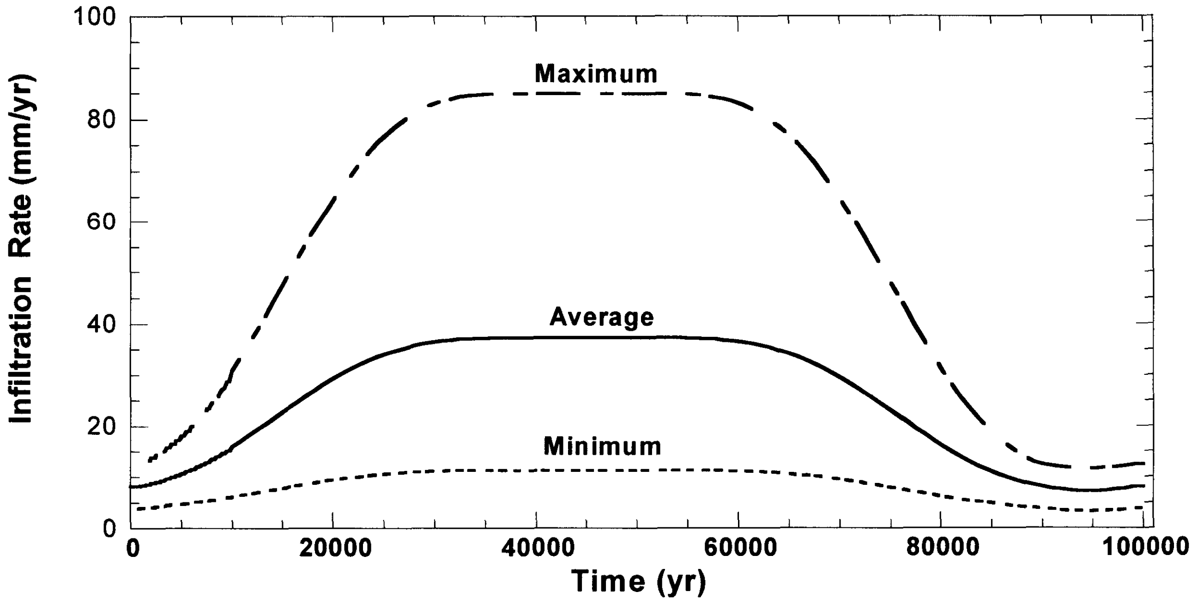

Figure 3-21. Mean, Maximum, and Minimum Infiltration Rates in the Unsaturated Zone for All Subareas. (The Subarea Average Infiltration Rate Is Obtained by Averaging Over All 350 Realizations.)

greater than 10 °C [50 °F] with a maximum temperature difference of 20 °C [68 °F] at 1,600 years. This period corresponds to the greatest amount of heat generated from the radioactive decay of spent nuclear fuel. Note that the subarea-to-subarea variability in temperature shown here may not be fully reflective of the edge effect (i.e., heat losses at the periphery of the subarea) because of the limited number of subareas used and the temperature is estimated only at the center of each subarea.

Figure 3-22(b) shows the average, minimum, and maximum waste package temperatures for subarea 1. The range between the minimum and maximum temperatures is approximately 20 °C [68 °F] for the time period of 100–1,000 years. Subareas 2–10 exhibit the same general variability in the average, minimum, and maximum waste package temperatures as subarea 1. The largest minimum to maximum difference within a subarea for all 350 realizations is 25 °C [77 °F] for all subareas, and this difference occurs around 90 years. These large differences indicate the parameters sampled in the basecase data set (e.g., thermal conductivity of the rock surrounding the repository) have an influence on the range of computed waste package temperatures. This difference could affect the spent nuclear fuel dissolution and corrosion calculations because the corrosion rate is sensitive to the waste package temperature especially if localized corrosion is a possibility.

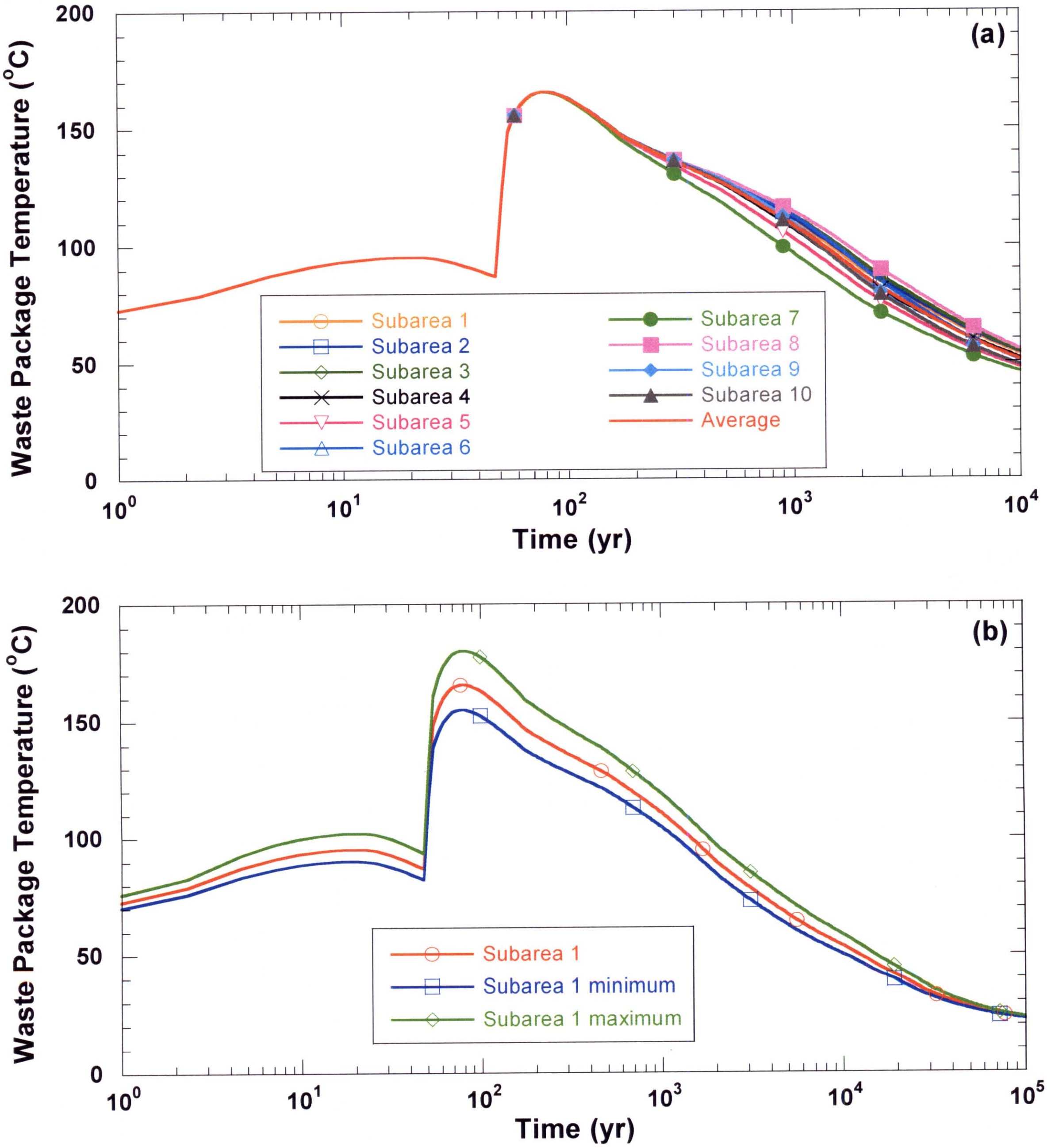

Figure 3-22. Waste Package Surface Temperature: (a) Averaged Over the Repository and for Each Subarea; and (b) in Subarea 1, the Average, Minimum, and Maximum Values, for 350 Realizations

3.3.3 Waste Package Degradation

Figure 3-23 presents results from all realizations and the expected failure curve of waste packages failed by corrosion. The time of waste package failure by corrosion ranges from approximately 37,900 to beyond 100,000 years, with an average corrosion failure time for 350 realizations of approximately 68,000 years. For the computation of the average waste package failure time, it is assumed that all waste packages lasting longer than 100,000 years also failed at 100,000 years. Based on the models used and the assumption made in the TPA 4.1 code, even with 4,000 realizations, the earliest failure time is 37,900. It should be noted that effects of failure at welds and closures, which could substantially decrease waste package failure time, have not been considered in this calculation.

The variability in the peak groundwater dose ranges 6 orders of magnitude, compared to the average waste package failure time range of 37,900–100,000 years. Note that not all waste packages fail from corrosion in 100,000 years. When the waste package failure time is delayed, more of the spent fuel inventory decays, and the transport time through the unsaturated zone and saturated zone is delayed. Thus, the peak groundwater dose is generally expected to be lower for a longer waste package life. In most instances, the peak groundwater dose occurs after the average waste package failure time for the 100,000-year analyses. For 27 percent (95 out of 350) of the realizations, however, the peak groundwater dose occurs at times equal to or greater than 100,000 years. Because the waste package does not fail until 37,900 years, no groundwater peak dose corresponding to the corrosion failure of waste package is observed in 10,000 years.

3.3.4 Radionuclide Release

Water transports radionuclides out of the waste package and into the unsaturated and saturated zones to the receptor location. The release from the engineered barrier subsystem should be positively correlated with the flow rate of water in the unsaturated zone above the repository. Higher flow rates into the waste package lead to early release from the bathtub formed in the waste package and promotes dissolution-limited release. Higher release rates contribute to greater peak groundwater doses, as shown in Figure 3-24, for Tc-99 and Np-237, in subarea 1. The subarea 1 release rates presented in these figures are representative of release rates from subareas 2–10. Factors that influence the radionuclide transport from the engineered barrier subsystem to the receptor location, such as retardation, cause greater variability in the groundwater dose than the release rate from the engineered barrier system.

Figure 3-25 shows the release rate of Tc-99 from subarea 1 for 10,000 and 100,000 years. The figure shows a large variability in the engineered barrier subsystem release rates. The peak release rates corresponding to initially defective failure at the 0^{th} year are spread from 3,700 to 32,000 years and beyond, and the peaks corresponding to the corrosion failure are spread from 41,000 to 100,000 years. The variability can be attributed to factors such as lower flow rates at times less than 40,000 years, retardation of radionuclides, time of waste package failure, and time to fill the waste package. The variability in the magnitude of the releases extends more than six orders of magnitude

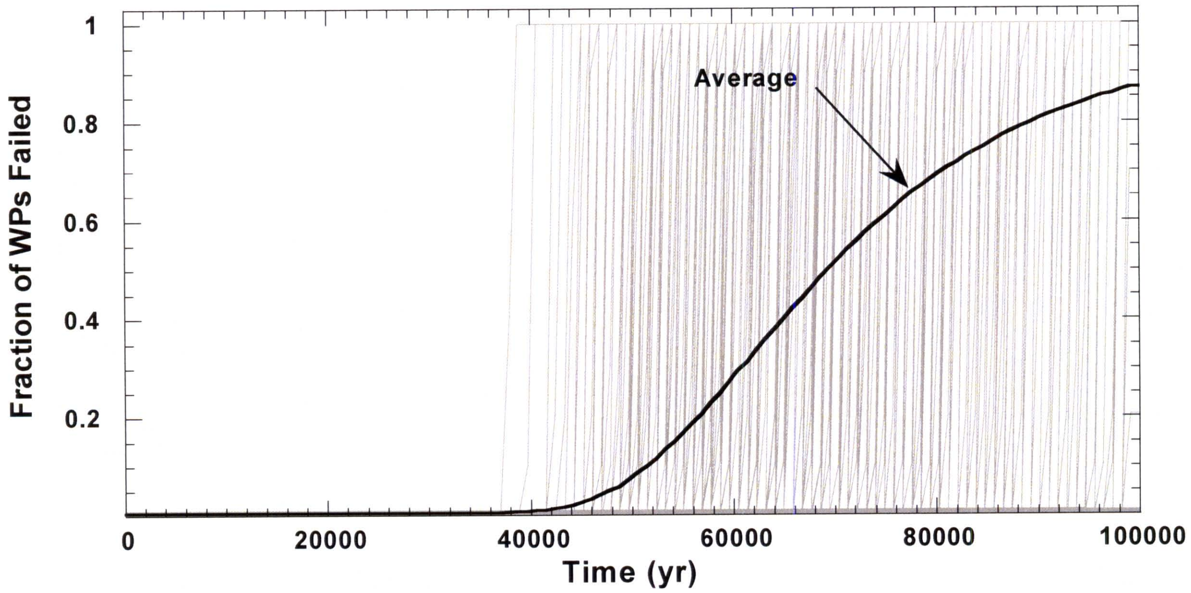

Figure 3-23. Fraction of Waste Packages Failed by Corrosion for Each of the 350 Realizations, and the Average Fraction of Failed Waste Packages

The cumulative release of radionuclides from the engineered barrier subsystem as a function of time is plotted in Figure 3-26 along with the initial inventory, the unsaturated and saturated zone releases, and the expected failure curve of waste packages failed from corrosion with its own axis displayed at the right hand axis. This graph shows a sharp rise in the activity level at less than 5,000 years, which corresponds to the initially defective failure. An increase in activity level after 45,000 years is caused by the waste packages failing from corrosion. Radionuclides with a combination of higher solubility, half-life, initial inventory and gap fraction (e.g., Tc-99) contribute to the largest release rates. The figure shows approximately 1.11×10^{13} Bq [300 Ci] of radionuclides have been released in 10,000 years at the engineered barrier subsystem, of which approximately 5.9×10^{12} Bq [160 Ci] has been released from saturated zone (which is 5×10^{-5} percent of the initial inventory). The figure also shows that at the end of 100,000 years, 1.33×10^{15} Bq [36,000 Ci] have been released from the saturated zone, which is 0.01 percent of the initial inventory and 1.25 percent of the 100,000-year no-release inventory. No-release inventory is the remaining inventory at any given time up to which decay and ingrowth take place but no releases occur.

3.3.5 Unsaturated Zone Transport

Figure 3-27 presents the Tc-99, Np-237, and Pu-239 average release rates and the expected failure curve of waste packages failed from corrosion for the basecase data set. In the first 37,900 years, releases result from initial waste package failures. The failure of waste packages from corrosion begins at approximately 37,900 years, and a corresponding increase in the release rates is evident in Figure 3-27, after 40,000 years, with the peak average release rate for 350 realizations occurring at approximately 80,000 years.

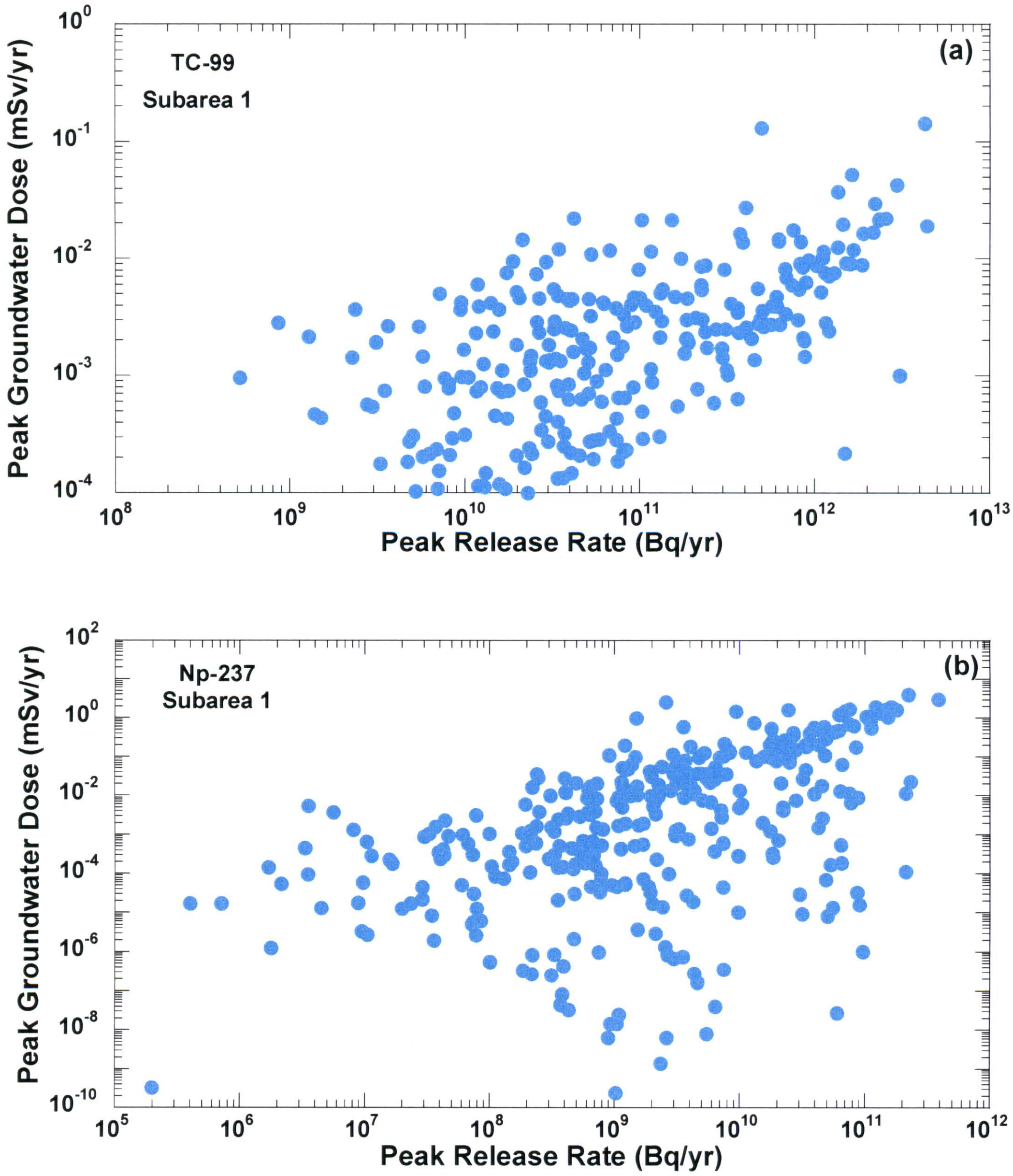

Figure 3-24. Peak Groundwater Dose and the (a) Tc-99 and (b) Np-237, Peak Release Rates from Subarea 1, for 350 Realizations

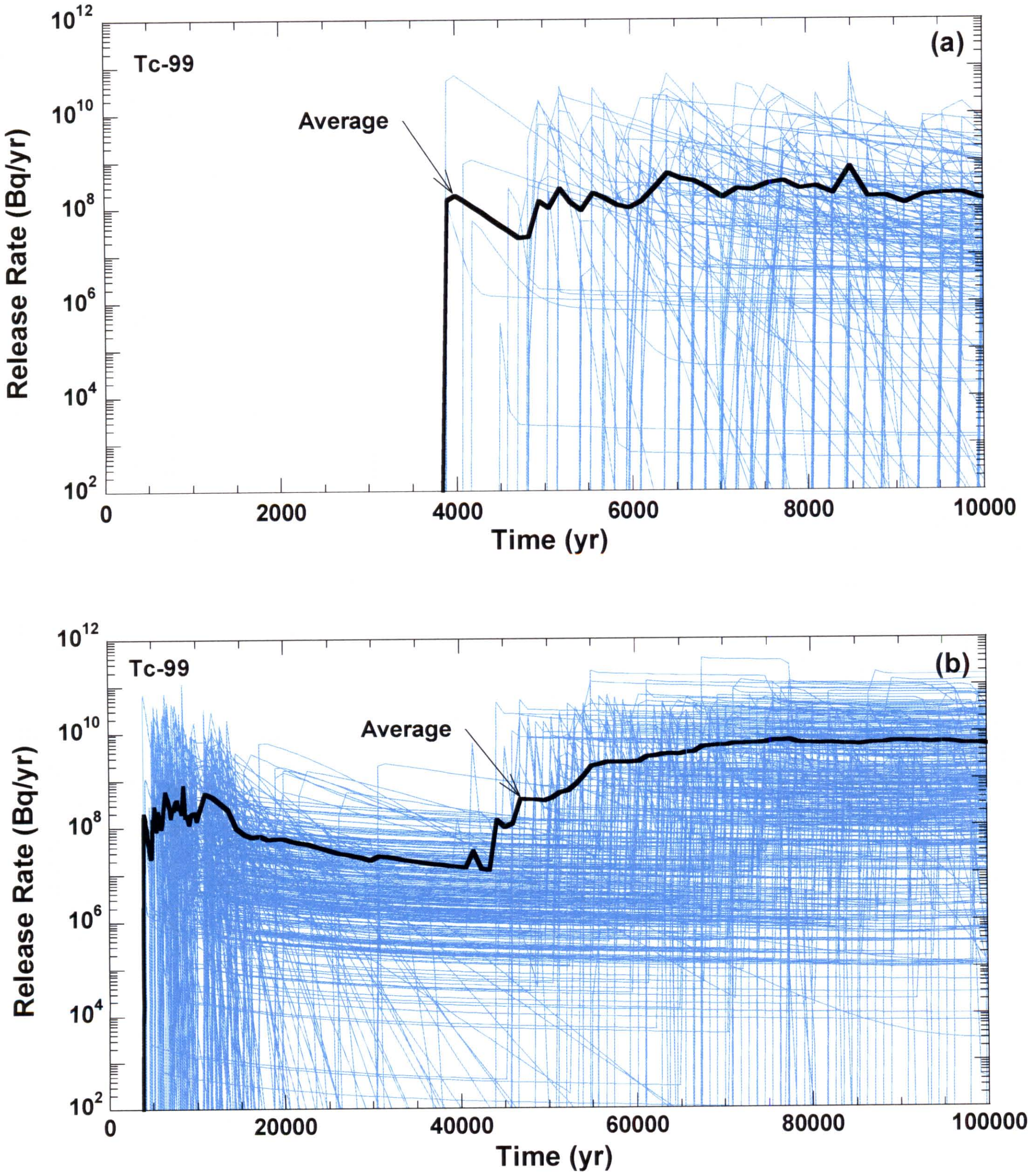

Figure 3-25. Tc-99 Release Rates from the Engineered Barrier Subsystem Over (a) 10,000 and (b) 100,000 Years Including the Average Release Rate, in Subarea 1 for 350 Realizations.

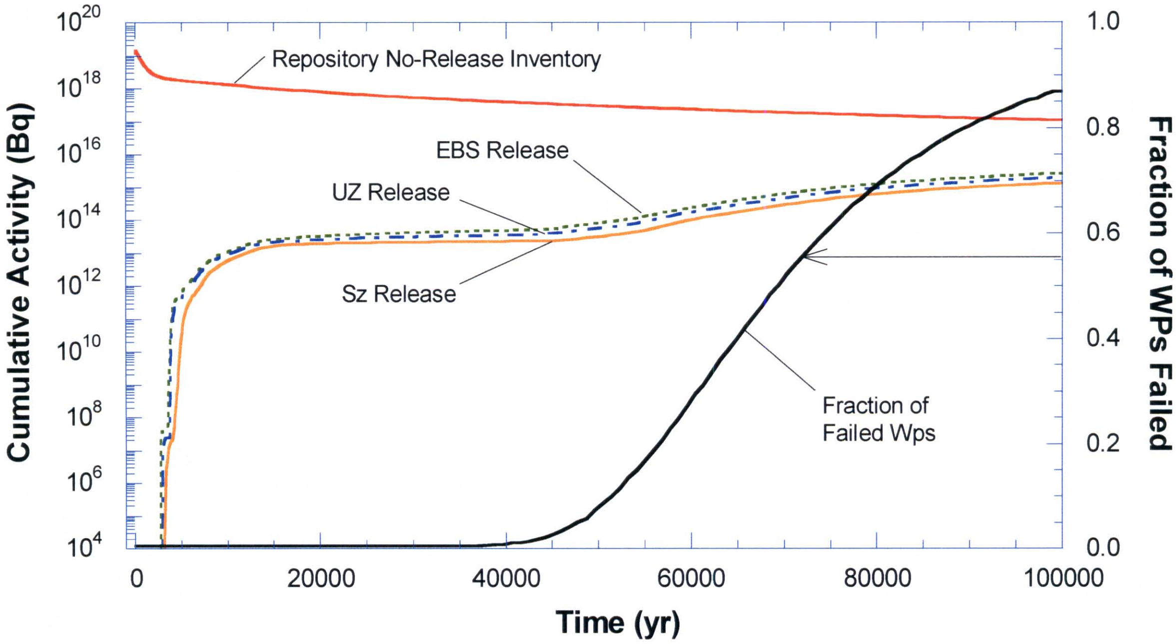

Figure 3-26. Cumulative Releases from the Engineered Barrier Subsystem, the Unsaturated Zone, and the Saturated Zone Together with the Initial Inventory in the Repository

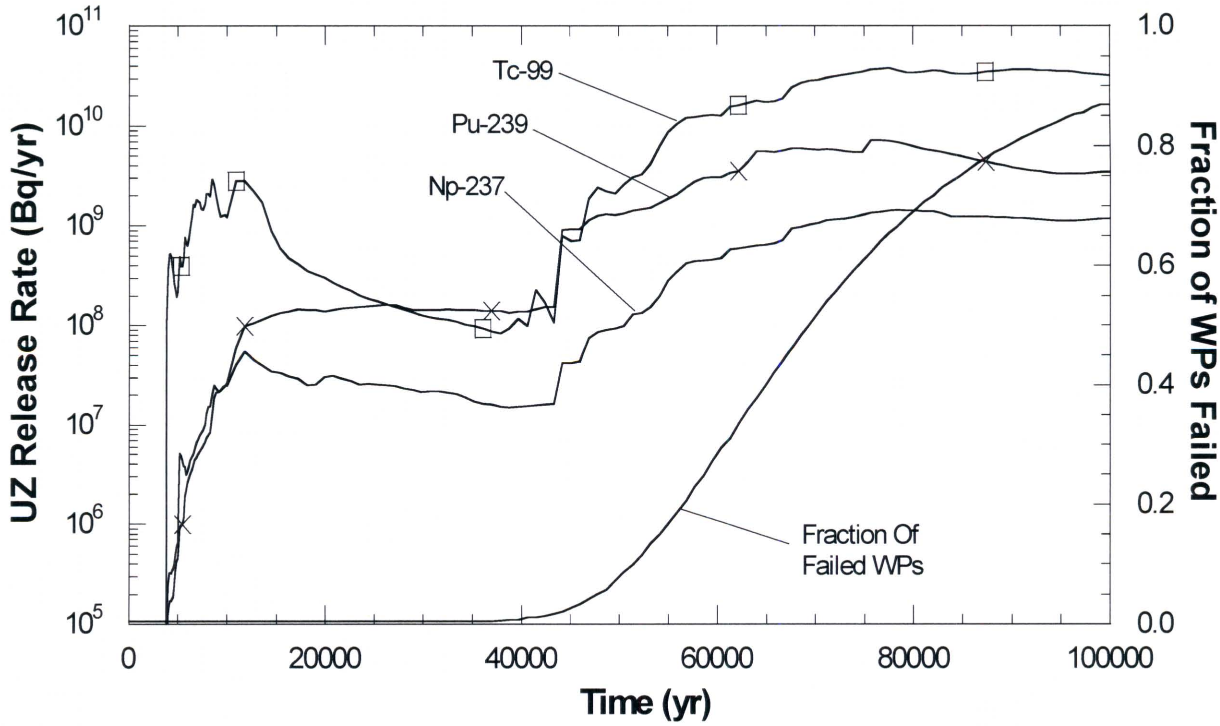

Figure 3-27. Unsaturated Zone Average Release Rates of Tc-99, Np-237, and Pu-239, for 350 Realizations

The results in Figure 3-26 indicate that the simulated unsaturated zone releases are only slightly less than the engineered barrier subsystem releases. Such a small difference between the two curves suggests the effects of the hydrostratigraphic units beneath the repository on the radionuclide release rates are not significant. Although there is significant hold-up of radionuclides in the subareas where the Calico Hills vitric layer is present, most of the release to the saturated zone comes from the subareas where the unit is thin or missing.

Figure 3-28 shows the Tc-99 release rate from the unsaturated zone from subarea 1 over 10,000 and 100,000 years. Figure 3-29 is a composite plot of the average engineered barrier subsystem, unsaturated zone and saturated zone release and shows that the average release rate versus time curve for Tc-99 for the unsaturated zone does not significantly lag behind the release rate curve for the engineered barrier subsystem. As with the engineered barrier subsystem, releases from the unsaturated zone before 40,000 years are from initially failed waste packages, whereas the peak releases observed after 40,000 years result mainly from corrosion failures. The magnitude of the releases extends six to seven orders of magnitude and arises partly from the variability in the flow rate, retardation in the unsaturated zone, and matrix versus fracture flow.

The conclusion that the unsaturated zone reduces by only a small amount the engineered barrier subsystem release rates is further supported by Figure 3-30, which shows the complementary cumulative distribution function of the unsaturated zone traveltimes. The average unsaturated zone traveltime is approximately 282 years with a range of 150–800 years, which is small, compared with the 10,000- and 100,000-year simulation periods. Subareas 2, 8, 9, and 10 exhibit the fastest groundwater traveltimes with averages varying from 12 to 27 years. The remaining subareas (1, 3, 4, 5, 6,and 7) exhibit average groundwater traveltime from 245 to 769 years. Differences in the traveltimes arise mainly from the presence of the Calico Hills vitric layer.

3.3.6 Saturated Zone Flow and Transport

Average release rates from the saturated zone are presented in Figure 3-31 for Tc-99, Np-237, and Pu-239. The Tc-99, Np-237, and Pu-239 unsaturated zone and saturated zone release rates can be significantly different because of the flow path length and retardation in the saturated zone alluvium. The path length in the saturated zone alluvium ranges from 5,500 to 5,700 m [18,045 to 18,701 ft], whereas the unsaturated zone path length is approximately 350 m [984 ft]. The TPA Version 4.1 code currently does not vary alluvium path length as a function of the sampled values of tuff-alluvium contact. The average retardation factors for Tc-99, Np-237, and Pu-239 are 1; 137; and 14,900 in the unsaturated zone matrix and 1; 62; and 13,000 in the saturated zone alluvium where saturated zone retardation occurs. Consequently, the longer flow path, combined with greater retardation, has a larger effect on the saturated zone release rates than on the unsaturated zone release rates. These effects can be seen in the unsaturated zone and saturated zone release rates plotted in Figures 3-27 and 3-31. Compared with the releases from the unsaturated zone, Tc-99 and Np-237 releases are smaller from the saturated zone and, because of a larger retardation factor, Pu-239 is released from the saturated zone in 100,000 years.

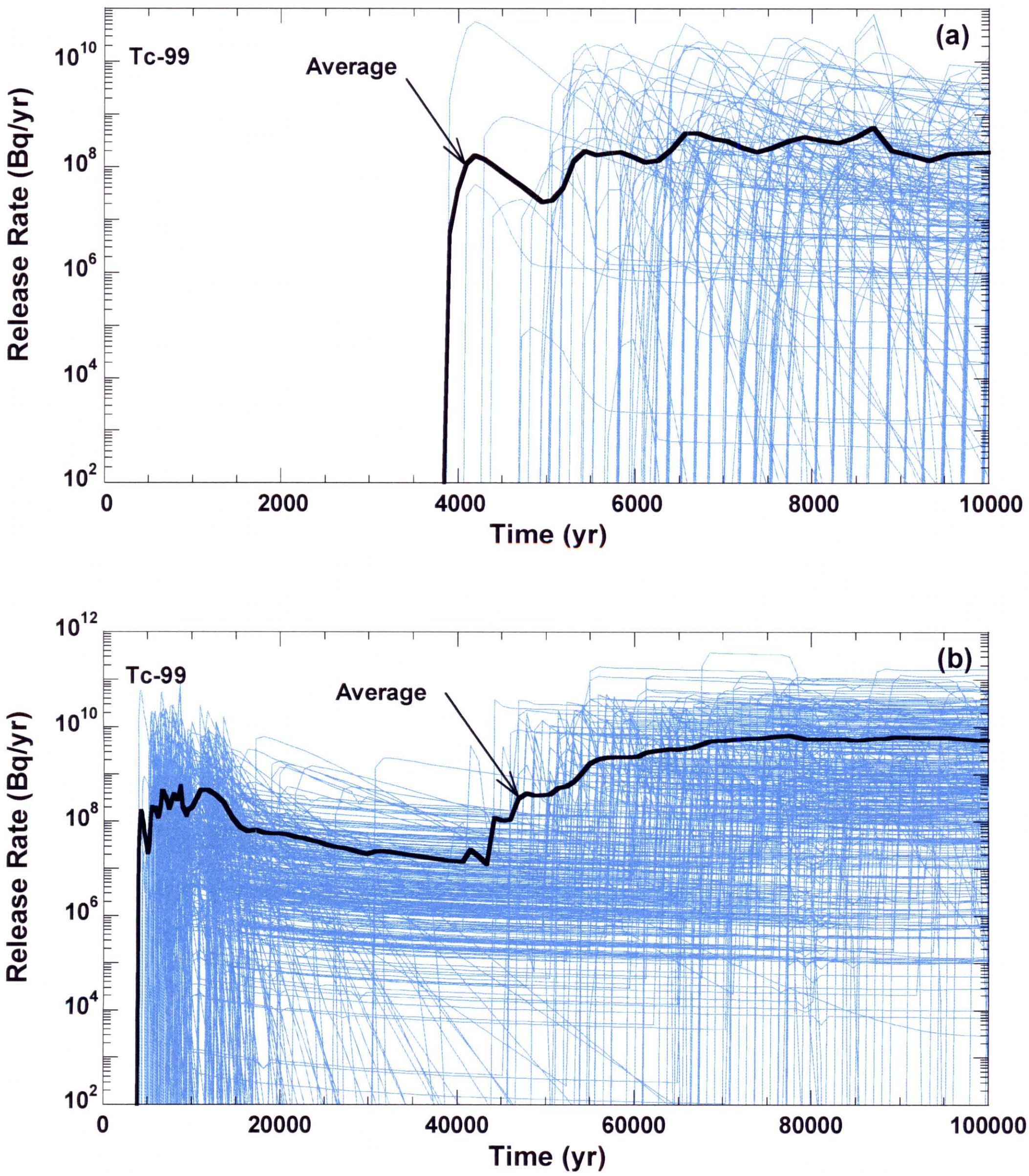

Figure 3-28. Unsaturated Zone Release Rates of Tc-99 Over (a) 10,000 and (b) 100,000 Years, Including the Average Release Rate in Subarea 1, for 350 Realizations

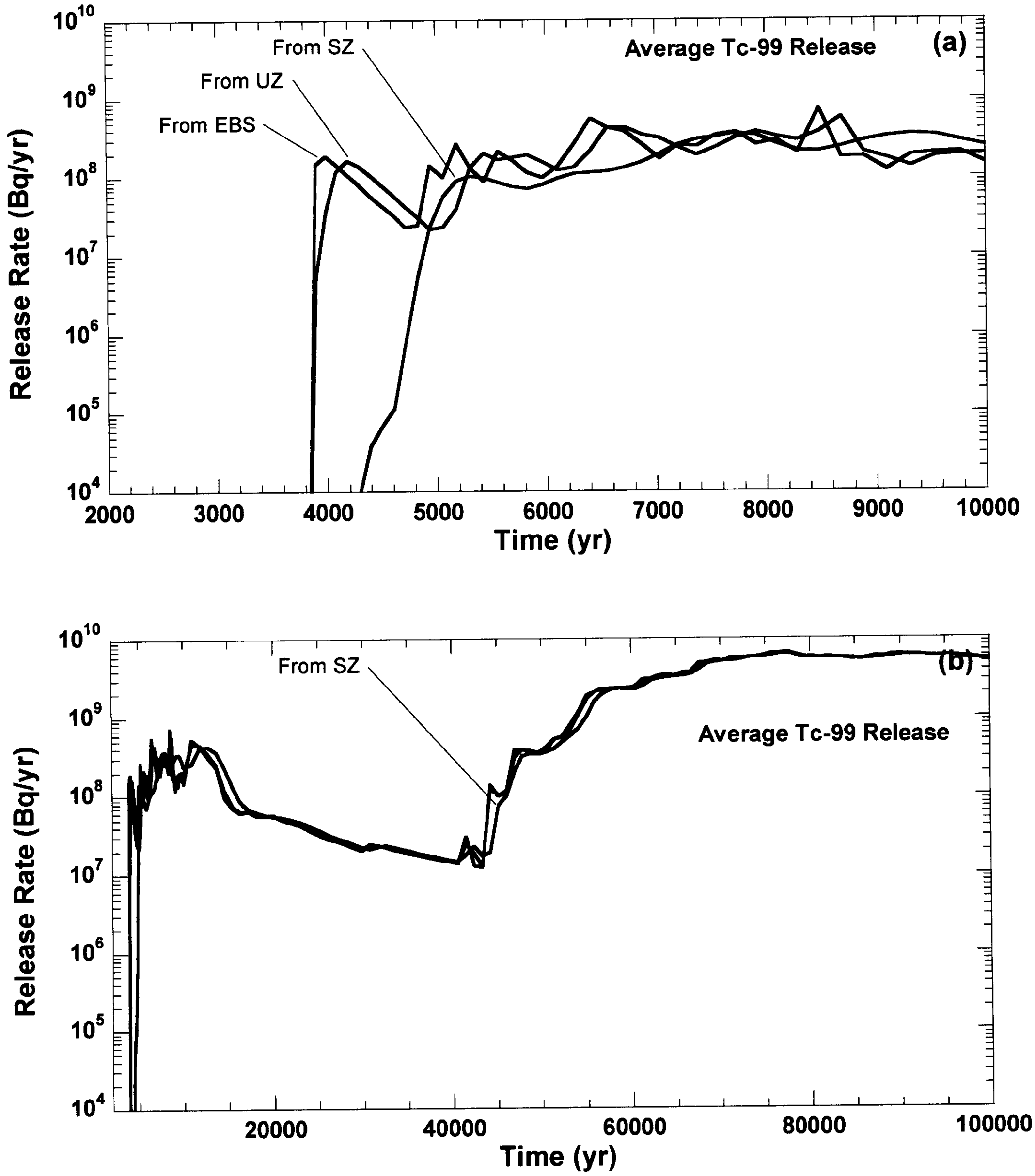

Figure 3-29. Tc-99 Average Release Rate from the Engineered Barrier Subsystem, the Unsaturated Zone and the Saturated Zone Over (a) 10,000 and (b) 100,000 Years in Subarea 1 for 350 Realizations

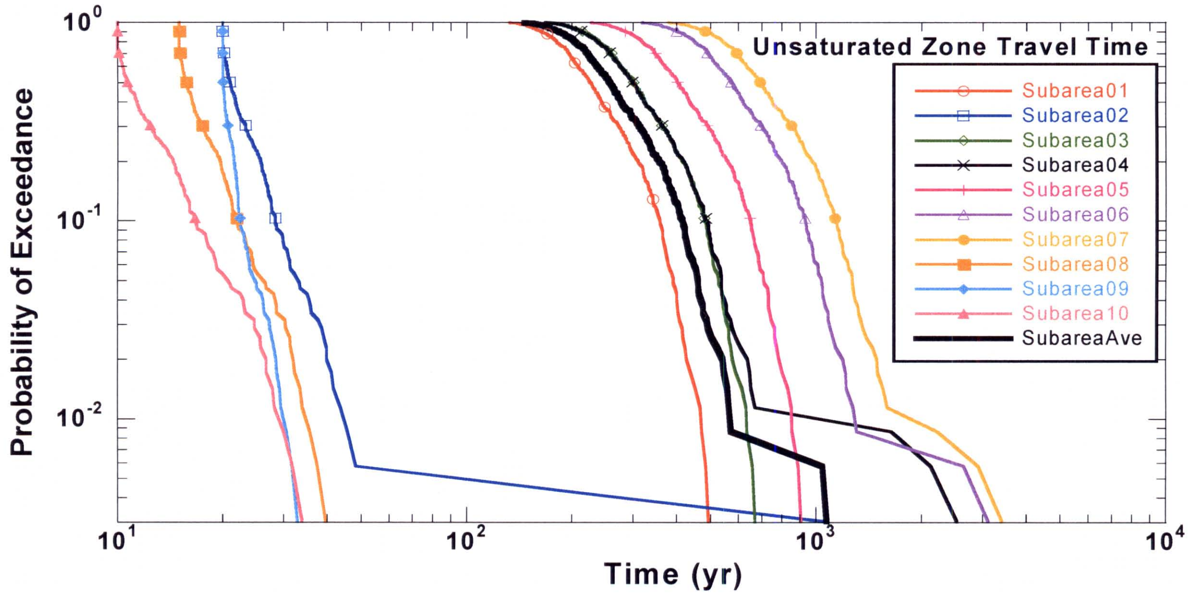

Figure 3-30. Complementary Cumulative Distribution Function of Unsaturated Zone Groundwater Travel Times for 350 Realizations

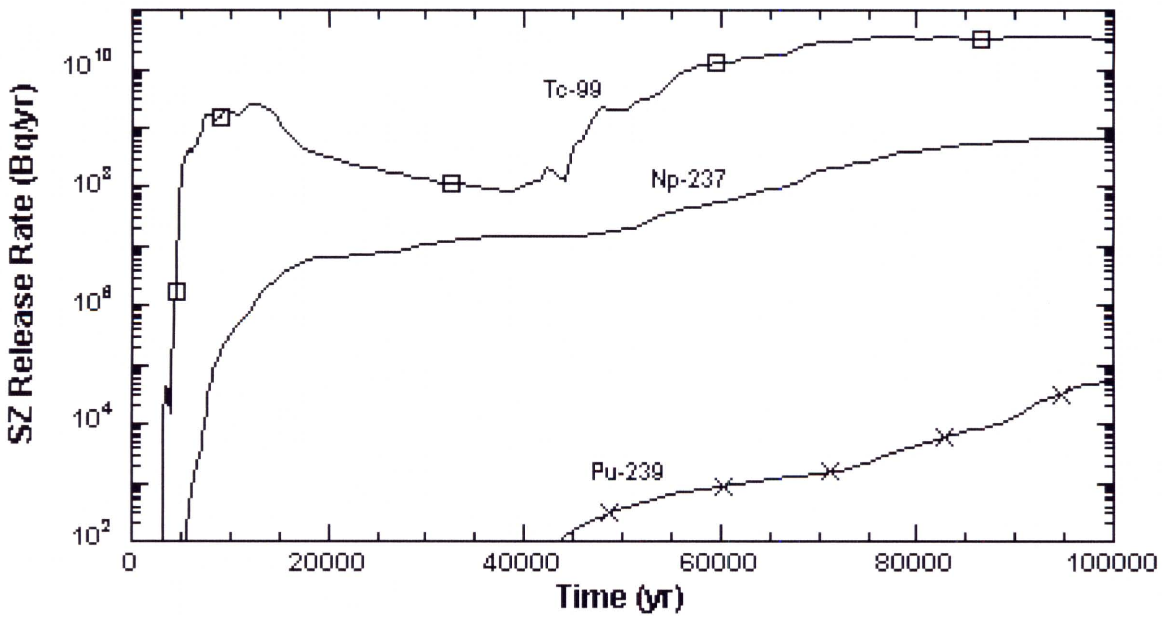

Figure 3-31. Saturated Zone Average Release Rates of Tc-99, Np-237, and Pu-239, for 350 Realizations

Figure 3-32 shows the saturated zone release rate and average release rate for Tc-99 in subarea 1. The effect of the flow path length on the Tc-99 saturated zone release rates for subarea 1, from 10,000 and 100,000 years, is evident when comparing the saturated zone release with the unsaturated zone release rates in Figure 3-29. Groundwater traveltime release is delayed until a later time.

The complementary cumulative distribution function of the saturated zone average groundwater traveltimes for all 350 realizations and for each subarea is presented in Figure 3-33. The groundwater traveltime in the saturated zone ranges between 57 and 1,790 years, with an average of 640 years (see Figure 3-33), compared with the approximately 280-year average groundwater traveltime for the unsaturated zone (see Figure 3-30). The streamtube connections given in Table 3-9 are clearly evident in Figure 3-33 because the subarea groundwater traveltime falls into three distinct groups corresponding to the saturated zone streamtubes. Variation in groundwater traveltime among subareas connected to the same streamtube are because of the subarea location in the repository footprint; the subareas located further west have the longest traveltime. The subarea-to-subarea variation in the minimum traveltimes ranges between 57 to 80 years, whereas the maximum traveltimes range between 1,234 and 1,790 years. Table 3-12 provides a summary of the average (of all realizations), minimum, and maximum saturated zone groundwater traveltimes for the repository and for each subarea. The average for each subarea is obtained using equal weighting of groundwater traveltimes from each realization. Similarly, the repository average (from all subareas and realizations) is the mean of subarea averages. The subarea-to-subarea variability in the average (from 350 realizations) saturated zone traveltimes is approximately three times less than for the unsaturated zone. The realization-to-realization variation in the repository averaged saturated zone groundwater traveltimes ranges between 580 to 820 years; for the unsaturated zone, the range is 12 to 770 years.

3.4 Dose to the Receptor Group from Multiple Realization Set

The peak expected dose for the multiple realization case for the 10,000-year simulation period is 2.1×10^{-4} mSv/yr [0.021 mrem/yr]. For the 100,000-year simulation period, the peak expected dose is 9.9×10^{-2} mSv/yr [9.9 mrem/yr]. Table 3-13 provides the primary radionuclides contributing to peak expected dose for the 10,000- and 100,000-year simulation periods. The main contributors to the dose for both simulation periods are Np-237, I-129, and Tc99. Np-237 is the third largest contributor at 10,000 years but becomes the dominant contributor at the 100,000-year simulation period.

The variability in dose among all 350 realizations is shown in Figure 3-20, for 10,000 and 100,000 years, together with the average dose and the 5th, 25th, 50th, 75th, and 95th percentiles. The minimum and maximum peak doses vary from no release {i.e., < 1.0×10^{-22} mSv/yr [1.0×10^{-20} mrem/yr]} to 1.15×10^{-2} mSv/yr [1.15 mrem/yr], for 10,000 years, and 2.9×10^{-6} mSv/yr [2.9×10^{-4} mrem/yr] to 4.10 mSv/yr [410 mrem/yr] for 100,000 years. The doses occurring before 37,900 years are from initially defective waste packages. After 37,900 years, corrosion failures occur and contribute to increased dose.

The groundwater dose from each of the radionuclides considered for groundwater transport (Cm-246, U-238, Cm-245, Am-241, Np-237, Am-243, Pu-239, Pu-240, U-234, Th-230, Ra-226, Pb-210, Cs-135, I-129, Tc-99, Ni-59, C-14, Se-79, Nb-94, and Cl-36) is illustrated in

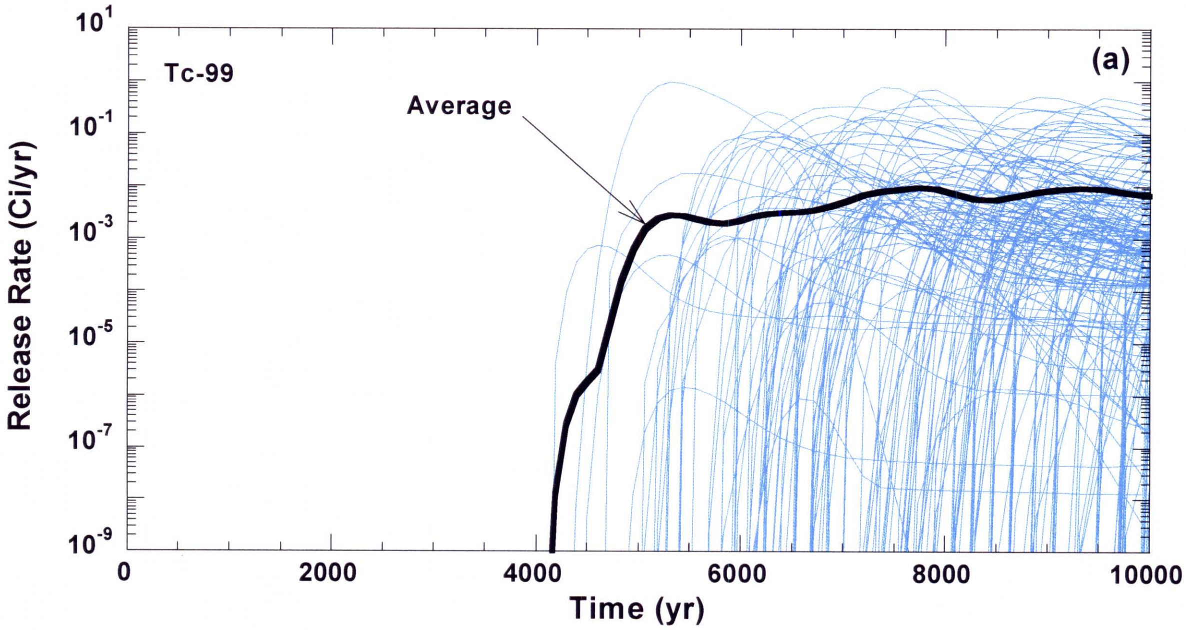

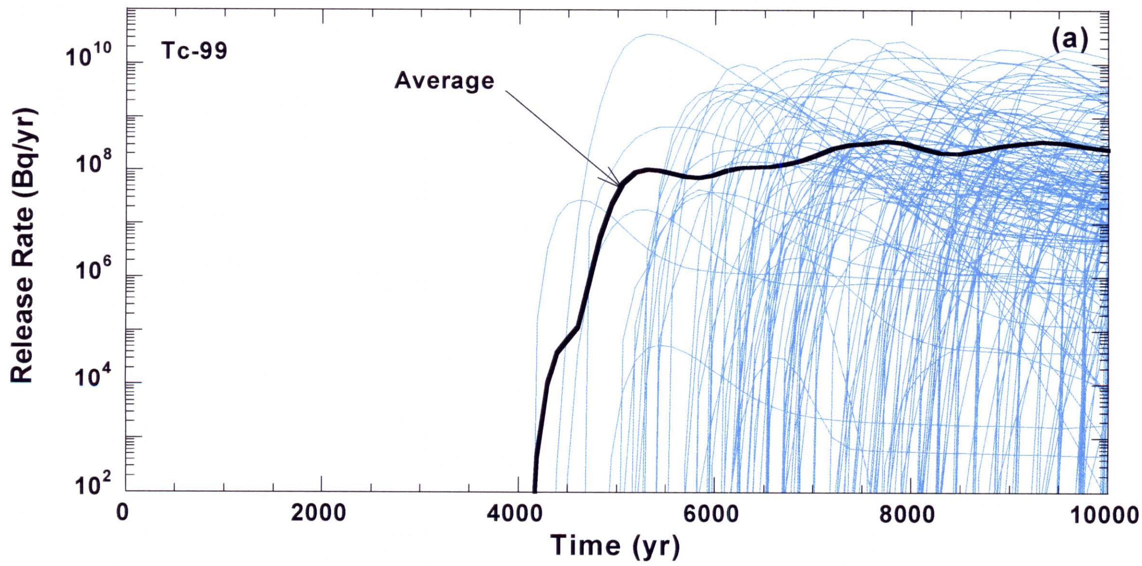

Figure 3-32. Saturated Zone Release Rates of Tc-99 over (a) 10,000 and (b) 100,000 Years, Including the Average Release Rate, in Subarea 1 for 350 Realizations

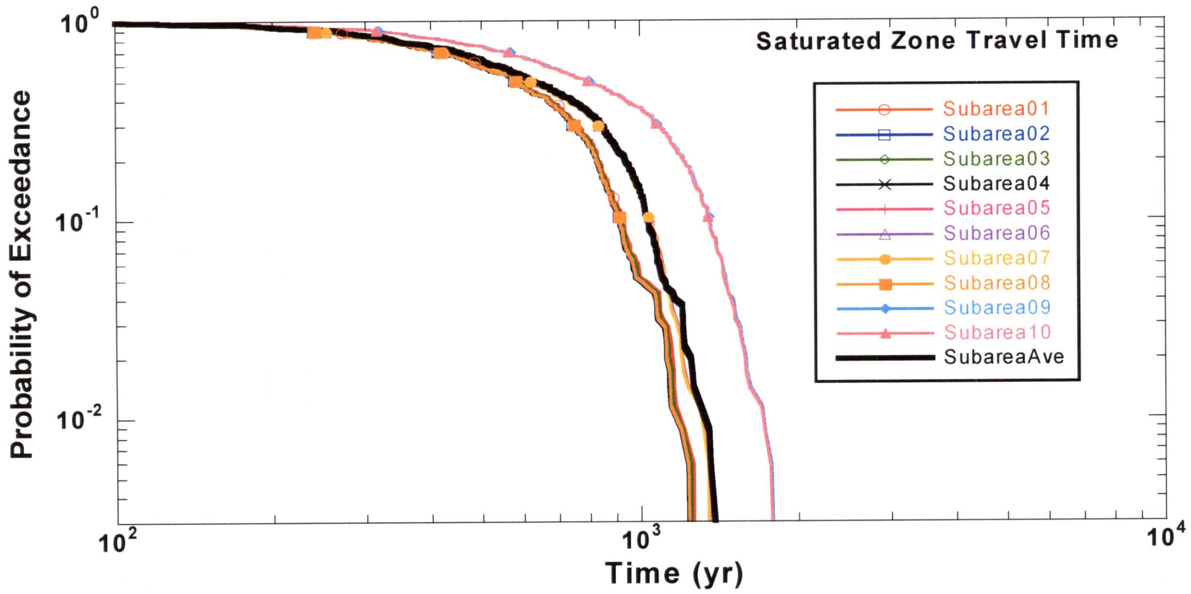

Figure 3-33. Complementary Cumulative Distribution Function of Saturated Zone Groundwater Travel Times for 350 Realizations

Table 3-13. Primary Radionuclides Contributing to Peak Expected Dose

Radionuclide	10,000 Years		100,000 Years	
	Mean Value Data Set (mSv/yr)	Multiple-Realization Data Set (mSv/yr)	Mean Value Data Set (mSv/yr)	Multiple-Realization Data Set (mSv/yr)
Np-237	0	4.29×10^{-5}	3.69×10^{-2}	9.54×10^{-2}
I-129	1.30×10^{-4}	5.34×10^{-5}	3.90×10^{-4}	1.33×10^{-3}
Tc-99	2.15×10^{-4}	1.09×10^{-4}	6.17×10^{-4}	2.09×10^{-3}
U-234	0	1.77×10^{-9}	4.6×10^{-7}	6.80×10^{-5}
Cl-36	7.11×10^{-7}	2.64×10^{-7}	1.35×10^{-6}	5.10×10^{-6}
Se-79	0	3.74×10^{-8}	9.31×10^{-6}	1.14×10^{-5}

Figure 3-34 for all 350 realizations. Figure 3-34 is a box plot representation of each radionuclide contribution to the total dose as a percentage. Each box encloses half of a radionuclide percentage values with the top and bottom lines of the box showing the ±25 percent limits of the values. The median radionuclide percentage value is represented by the horizontal line inside the box. Values in the data set that remain within a specified limit (e.g., 95th percentile) are indicated by the line extending from the top of the box. The circles are labeled “outliers” by the statistical test, which are values beyond three standard deviations from the mean, but are nevertheless significant values. In Figure 3-34a, all Np-237 values are outliers, because, of the 350 realizations, 286 realizations (82 percent) have no contribution from Np-37. Eleven of the realizations have Np-237 contributions that exceed 80 percent. Of

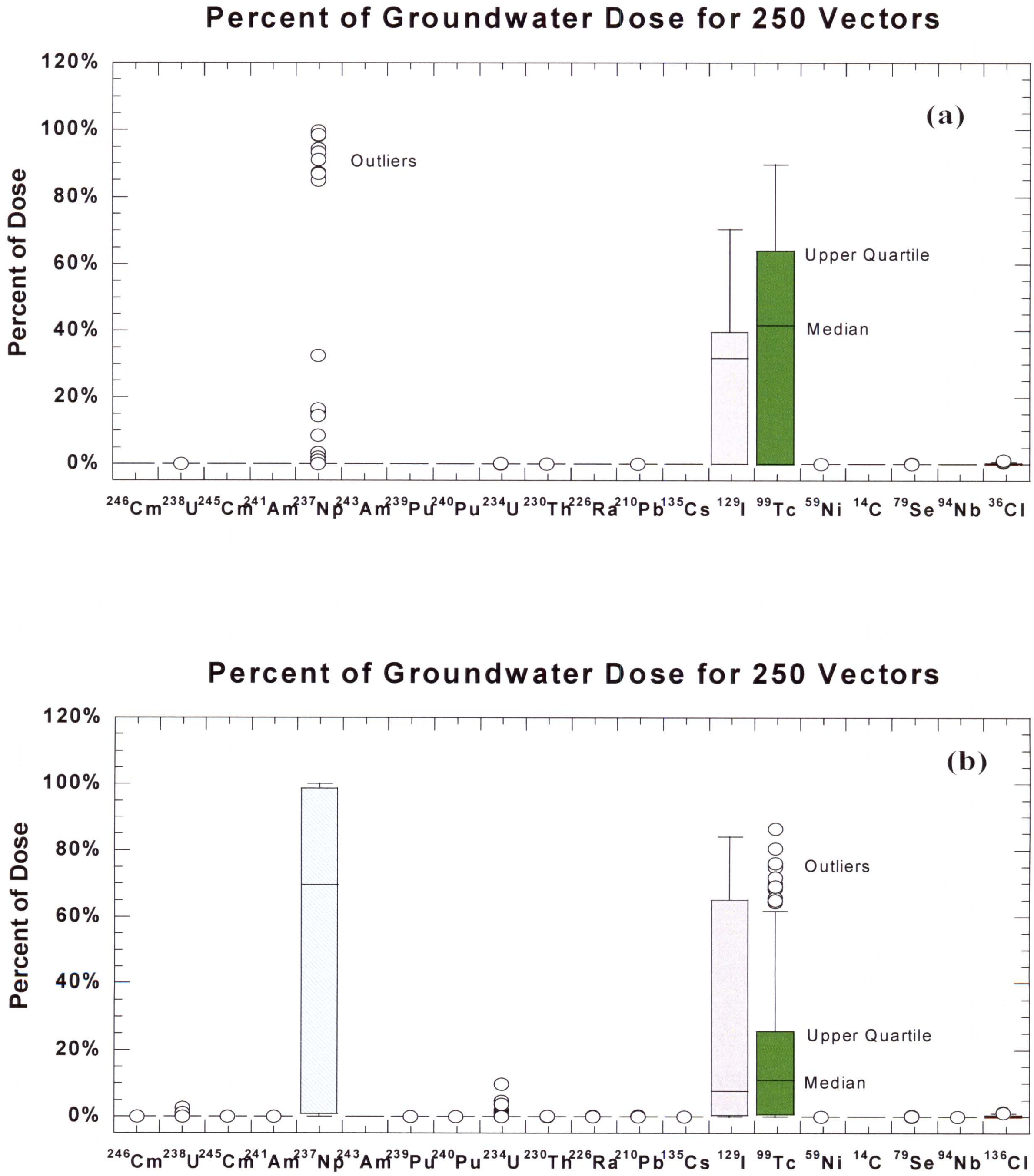

Figure 3-34. Percent Each Radionuclide Contributes to the Peak Groundwater Dose in (a) 10,000 Years and (b) 100,000 Years for 350 Realizations

the 350 realizations, the highest percentage contribution of I-129 to total dose is 70 percent. In 3 of the realizations, Tc-9 contributes at least 80 percent to the total dose. The median value for I-129 is 31.7 percent and for Tc-99 is 41.6 percent. In Figure 3-34b, representing the 100,000-year case, Np-237, I-129, and Tc-99 contribute at least 1 percent to the groundwater dose for any single realization. Of the 350 realizations, Np-237 exceeds 80 percent of the contribution for 177 realizations and exceeds 90 percent of the contribution in 166 of those realizations. Contributions to total dose exceeds 80 percent in only 7 realizations for I-129, and in only 2 realizations for Tc-99. The median values for Np-237, I-129 and Tc-99, are 69.6, 7.7 and 11 percent. Radionuclides U-238, U-234, Se-79, and Cl-36 contribute at least 0.01 percent to the total. The remaining nuclides (Cm-246, Cm-245, Am-241, Am-243, Pu-239, Pu-240, Th-230, Ra-226, Pb-210, Cs-135, Ni-59, C-14, and Nb-94) contribute negligibly to the groundwater dose. The radionuclides with the greatest consistency in contributing to peak dose in all realizations are I-129 and Tc-99 for 10,000 years and Np-237, followed by I-129 and Tc-99, for 100,000 years. The results (plotted in Figure 3-35) of the expected dose for each nuclide show similar behavior for the 10,000- and 100,000-year simulation periods, as does Figure 3-34, with the same nuclides having the largest contribution to the groundwater dose.

3.5 Alternative Conceptual Models

This section compares repository performance, as measured by expected dose, for the basecase data set, with the expected dose computed for the alternative conceptual models described in Section 2.3. Only the general trends in the groundwater dose of the alternative models relative to the basecase are described in this section. Additional discussion of the sensitivity of TPA output to a conceptual model, using multiple realizations, is provided in Section 4.4.

Conceptual models can be activated with flags in the TPA Version 4.1 code input file, by modifying TPA input parameters, or by a combination of both setting appropriate flags and changing TPA input parameters. All three approaches are used in this section to specify a conceptual model and to analyze the influence of the conceptual model on the expected dose. Conceptual models activated with flags in the TPA input file include the four dissolution rate models, bypassing invert transport, and the particle and grain surface-area models. Conceptual models evaluated by modifying the parameter values in the TPA input file are the focused flow, matrix diffusion, and no retardation module. Conceptual models activated using a combination of flags and changes to TPA input parameters include the flow through models and cladding protection.

Figures 3-36 through 3-38 present expected groundwater dose in 10,000 and 100,000 years for the basecase data set, together with expected groundwater doses from the total-system performance assessment alternative conceptual models. For the conceptual models evaluated using the basecase data set, peak expected dose spans 4 orders of magnitude for the 10,000-year simulation period. The general trend in groundwater expected dose exhibited in Figures 3-36 through 3-38 indicates a wide range in the sensitivity of groundwater expected dose to the conceptual model. The alternative models with the most deviation from the basecase data set peak dose are the no-retardation case, which is 2 orders of magnitude greater than the basecase peak dose, and the schoepite and Clad-M1 cases, which are 2 orders of magnitude less than the basecase peak dose, for 10,000- and 100,000-year

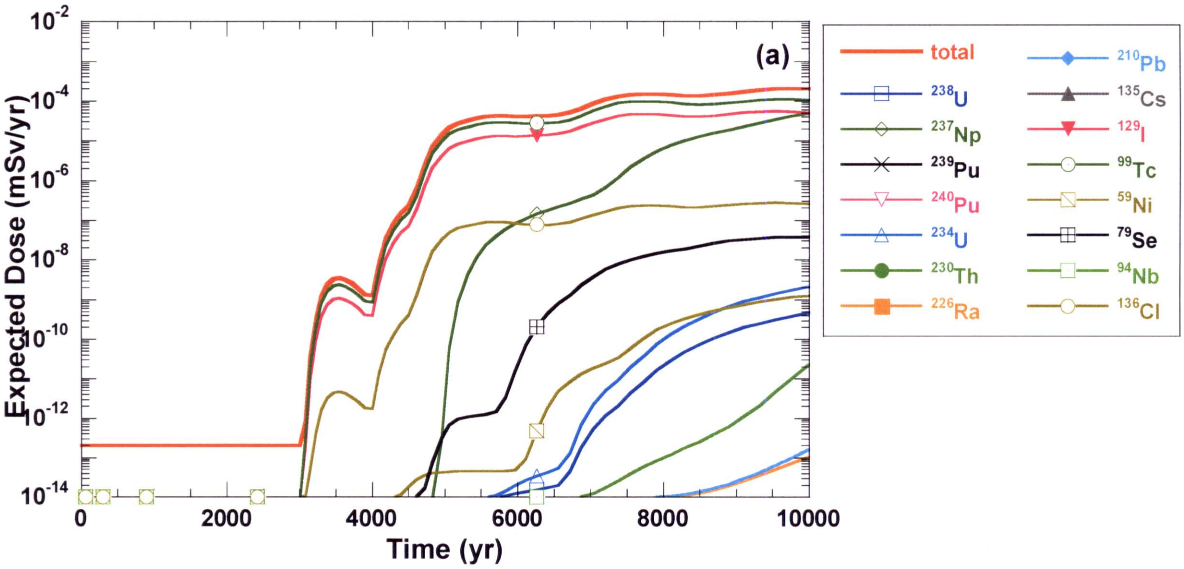

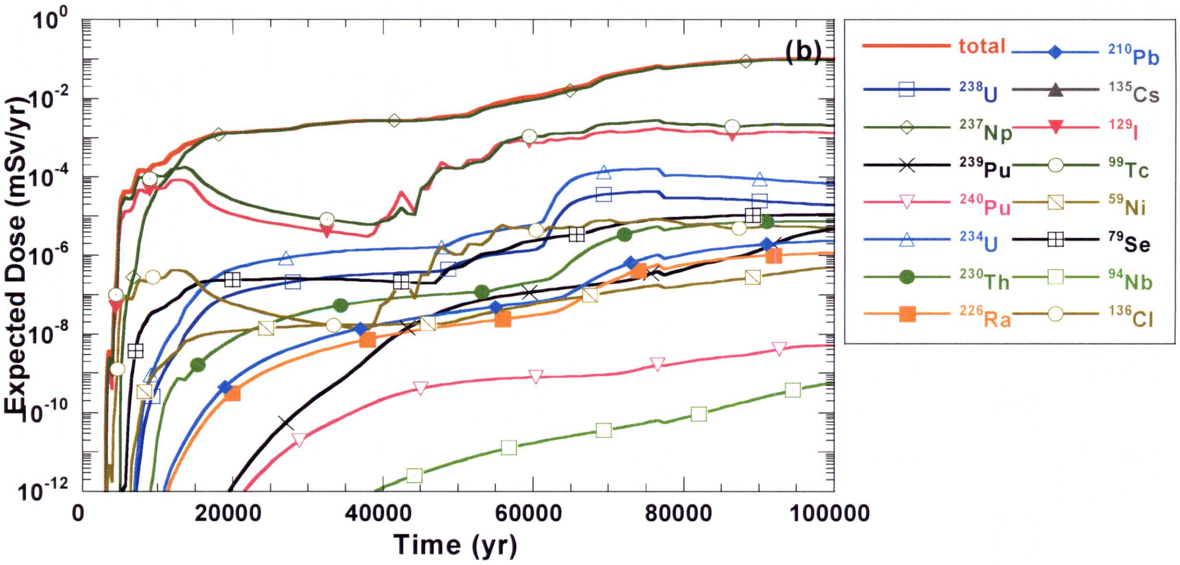

Figure 3-35. Average Groundwater Dose in (a) 10,000 and (b) 100,000 years for Each Nuclide, Including the Total Dose, for 350 Realizations

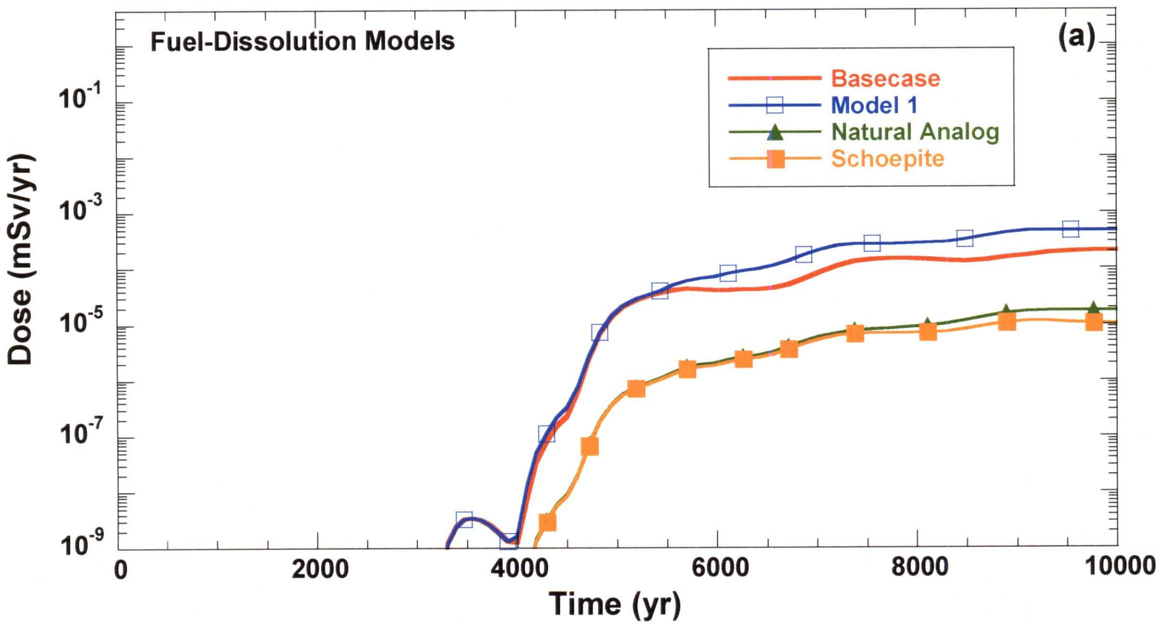

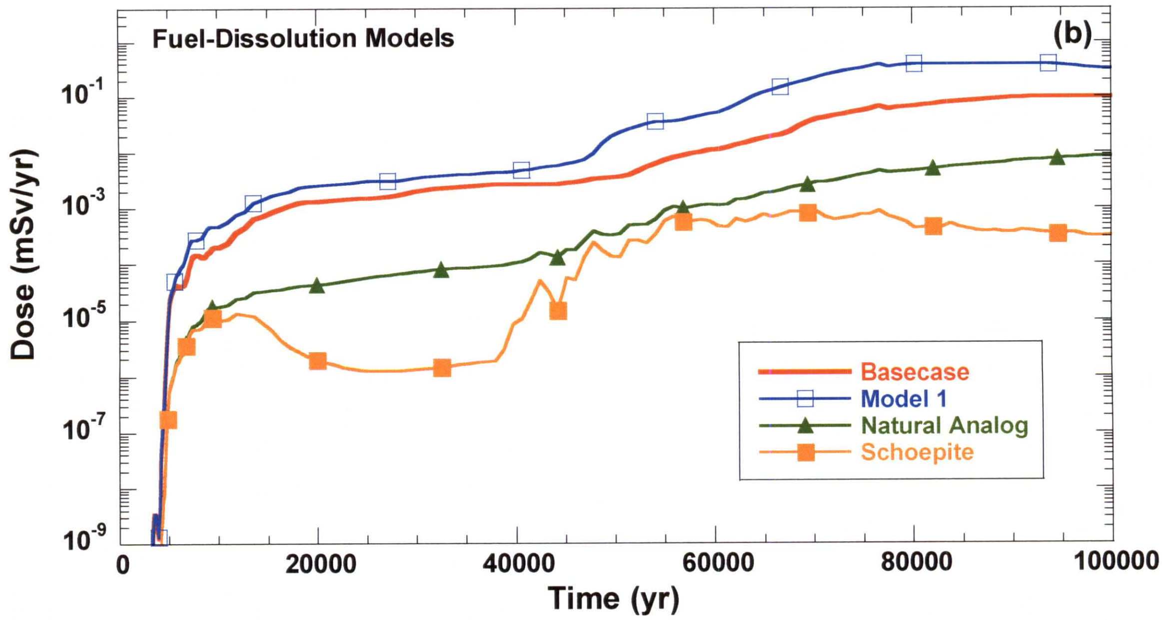

Figure 3-36. Groundwater Dose from the Basecase and the Fuel-Dissolution Alternative Conceptual Models for (a) 10,000 and (b) 100,000 Years, Using the Mean Value Data Set

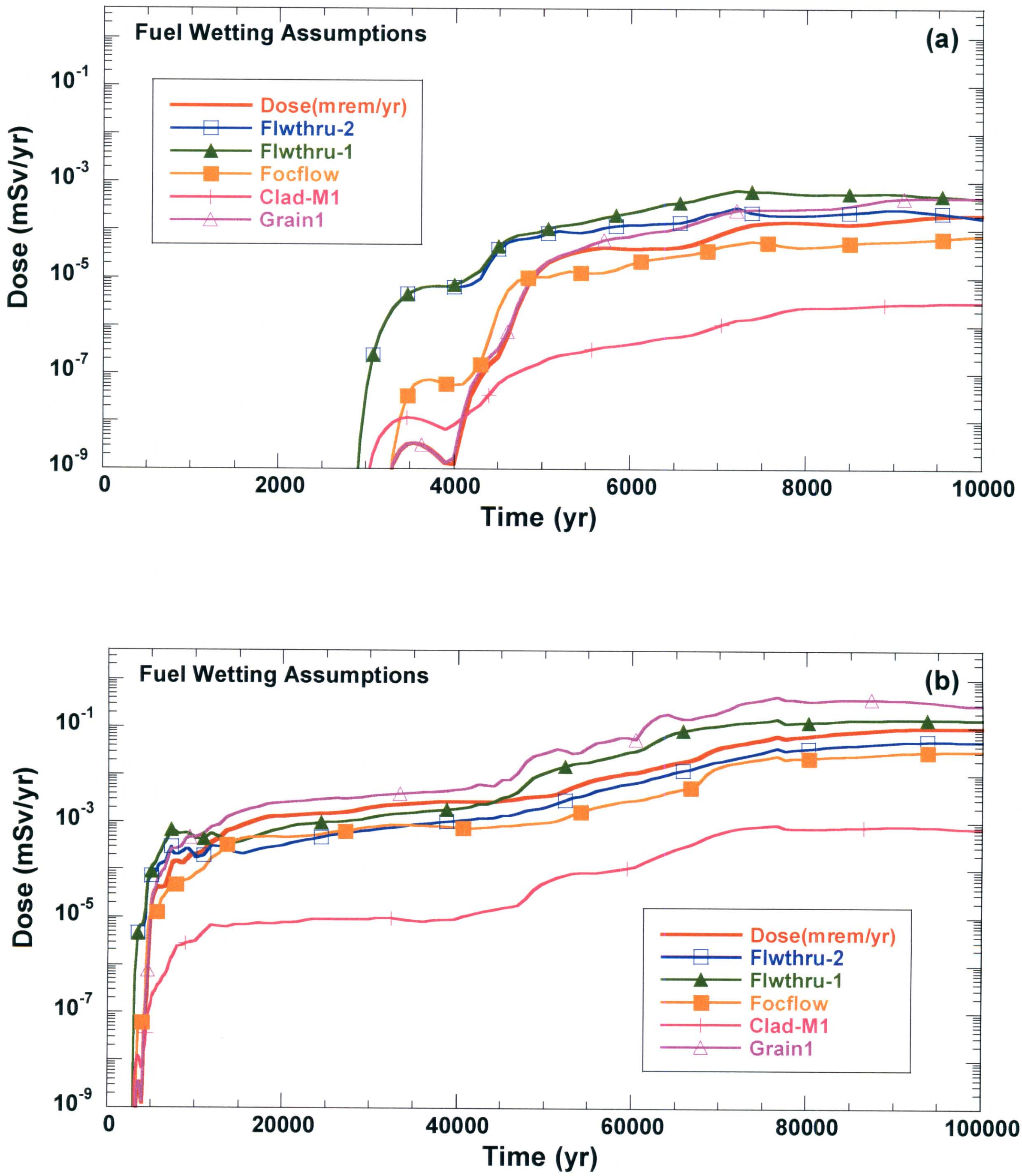

Figure 3-37. Groundwater Dose from the Basecase and the Fuel-Wetting Alternative Conceptual Models for (a) 10,000 and (b) 100,000 Years, Using the Mean Value Data Set

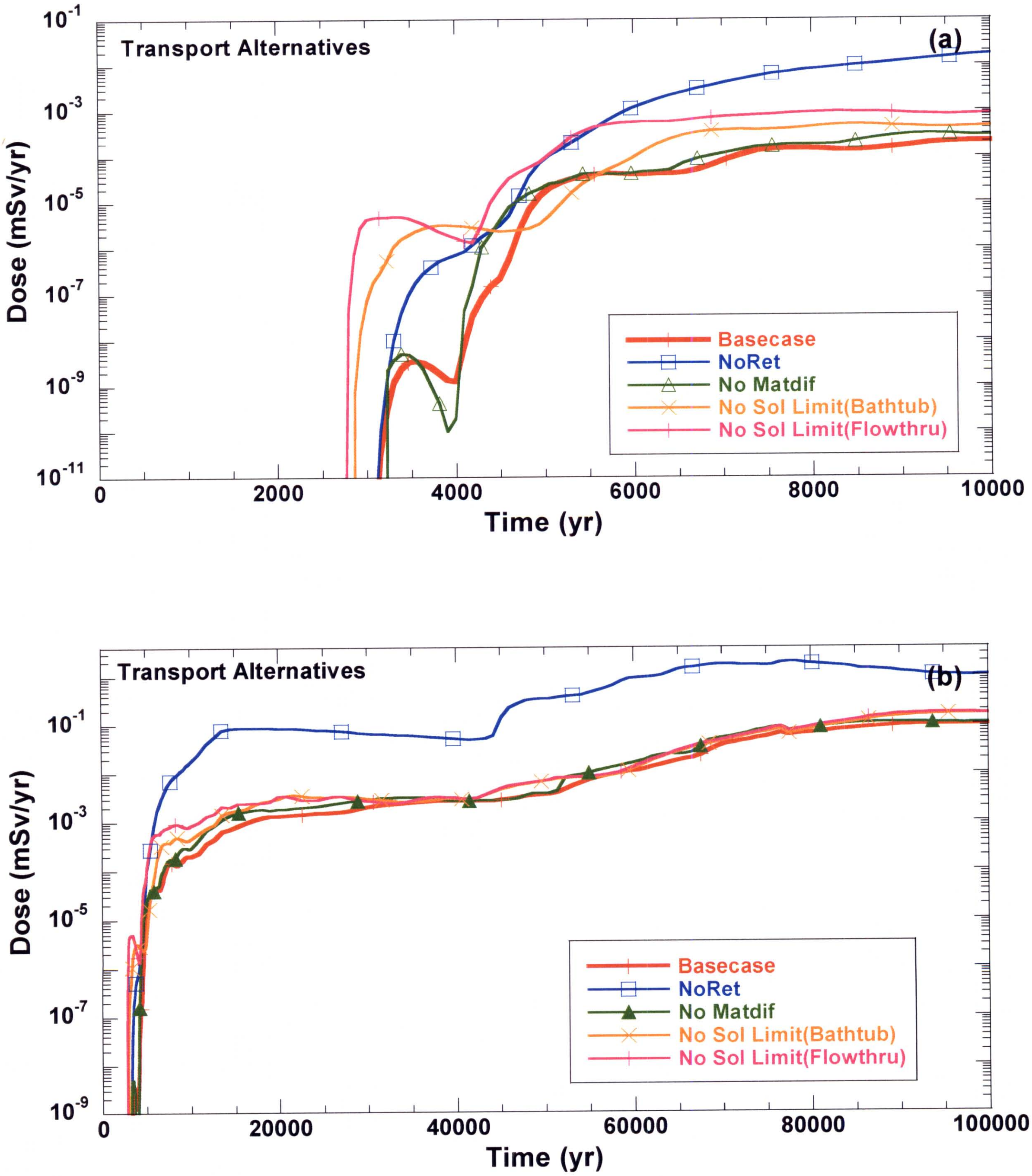

Figure 3-38. Groundwater Dose from the Basecase and the Transport Alternative Conceptual Models for (a) 10,000 and (b) 100,000 Years, Using the Mean Value Data Set

simulation periods. The following sections discuss the alternative conceptual models grouped by fuel dissolution, fuel wetting, and transport assumptions and compare the groundwater expected dose for the basecase. The TPA Version 4.1 code user's guide presents a description of these models.

3.5.1 Fuel-Dissolution Models

Results from total-system performance assessment simulations, using three different fuel-dissolution models, are evaluated by comparing the expected groundwater dose from each of the models with the basecase expected groundwater doses. The expected groundwater dose from the basecase, and from the three fuel-dissolution alternative conceptual models, is shown in Figure 3-36.

3.5.1.1 Fuel-Dissolution Model 1

The expected groundwater dose in Figure 3-36 (labeled as Model 1) shows an earlier release and higher dose than the basecase after 5,500 years. The small increase in dose between 5,500 and 10,000 years in Figure 3-36(a) for Model 1 is attributable to the delayed release and ingrowth of Np-237 in the saturated zone from initially defective failures. From 50,000 to 100,000 years, the Model 1 dose maintains a dose output approximately 3 to 7 times the basecase model. Compared with Model 2, dissolution Model 1 is characterized by a higher release rate resulting from faster dissolution.

3.5.1.2 Fuel-Dissolution Model 3 (Natural Analog)

The groundwater expected dose in Figure 3-36 (labeled as Natural Analog), which displays similar dose results from the schoepite dissolution model for the first 7,000 years, shows laterrelease with lower doses throughout the 100,000-year simulation period, than the basecase dose, indicating a slower dissolution rate. After 40,000 years, this model exhibits slight fluctuations that dissipate after 80,000 years. As stated in Section 2.3.2.1.2, this model uses a fixed dissolution rate of 24 kg/yr [53 lb/yr] and is limited by the fraction of wetted waste packages and the fuel wetting factors.

3.5.1.3 Fuel-Dissolution Model 4 (Schoepite Dissolution)

The groundwater expected dose in Figure 3-36 (labeled as Schoepite) displays the lowest dose of all the fuel-dissolution models for the 10,000- and 100,000-year simulation periods. The variations in dose after 40,000 years for this dissolution model are similar to Model 3. The variations display larger displacement but at a reduced dose than that of Model 3.

3.5.2 Fuel-Wetting Assumptions

The amount of water contacting a waste package affects the engineered barrier subsystem release rate and the time of the release. This section presents results that investigate the assumptions for fuel wetting with five alternative conceptual models. The groundwater expected doses computed using these models and the basecase results are provided in Figure 3-37.

3.5.2.1 Flow-Through Model with Fuel-Dissolution Model 2

The groundwater expected dose in Figure 3-37 (labeled as Flwthru-2) has an earlier release and higher dose than the basecase expected dose for the first 10,000 years. An earlier dose is expected because in the flow-through model, release from the waste package occurs instantaneously (i.e., no time to fill waste package). Beyond 10,000 years, the basecase dose is higher than the flow-through model dose because rapid release in the flow-through Model 2 depletes the inventory.

3.5.2.2 Flow-Through Model with Fuel-Dissolution Model 1

Groundwater expected dose in Figure 3-37 (labeled as Flwthru-1) indicates an earlier release and higher dose than the basecase expected dose at the beginning of the simulation and following the onset of waste package corrosion. At other times during the 100,000-year simulation period (13,000 to 44,000 years), the basecase dose exceeds the flow-through Model 1 dose, a behavior consistent with the faster dissolution rate and source depletion associated with Model 1.

3.5.2.3 Focused Flow

As presented in Figure 3-37, the groundwater expected dose (labeled as Focflow), computed using a focused flow of water onto the waste package, is greater than the basecase dose, before approximately 5,000 years. The basecase groundwater expected dose is approximately 2 to 4 times more than the expected dose from the focused flow model for the remainder of the 100,000-year simulation period. These results are consistent with solubility-limited releases associated with higher flows at earlier times and lower doses thereafter, which is the net result of fewer waste packages receiving more water.

3.5.2.4 Cladding Credit with Model 1

The groundwater expected dose in Figure 3-37 (labeled as Clad-M1), calculated for this conceptual model, is less than the groundwater expected dose for the basecase after approximately 4,000 years. Before 4,000 years, the dose with cladding protection is slightly greater than the basecase dose because of the much faster dissolution rate associated with Model 1. The groundwater expected dose for this alternative conceptual model is approximately 2 orders of magnitude less than the basecase dose after 5,000 years as expected, because the cladding protects the spent nuclear fuel.

3.5.2.5 Grain-Size Model with Fuel-Dissolution Model 1

The groundwater expected dose in Figure 3-37 (labeled as Grain1) produces higher doses than the basecase after 5,500 years. The higher release for this model is caused by water contacting a larger surface area of spent nuclear fuel.

3.5.3 Transport Alternatives

The three alternative conceptual models that test assumptions about transport in the engineered barrier subsystem, the unsaturated and the saturated zones are assessed in this section. Figure 3-38 presents the groundwater expected doses for these conceptual models and the basecase dose.

3.5.3.1 No Retardation of Plutonium, Americium, and Thorium

As presented in Figure 3-38, the groundwater expected dose (labeled as NoRet), calculated assuming no retardation for plutonium, americium, and thorium in the unsaturated and saturated zones, is greater than the basecase expected dose for the entire 100,000-year simulation period. Moreover, the general characteristics of the groundwater expected dose are consistent with the dose with no retardation and are approximately one to three orders of magnitude greater than the basecase dose throughout the 100,000-year simulation period.

3.5.3.2 No-Solubility Limit Model

The groundwater expected dose presented in Figure 3-38 [labeled No Sol Limit(Bathtub)] has earlier release and higher dose than the basecase prior to 4,700 years. After 4,700 years it has similar dose levels to the basecase expected dose. During the remaining 10,000-year simulation period, the two dose curves cross at least three times, and the levels are never more than approximately one order of magnitude apart. The three main contributors to early dose (I-129, Tc-99, and Cl-36) have relatively high solubilities {129 kg/m^3 [8.05 lb/ft^3], 99.3 kg/m^3 [6.20 lb/ft^3], and 36.0 kg/m^3 [2.25 lb/ft^3]} for the basecase, so additional increases had little effect on the expected dose. Other contributors such as Np-237 have low solubilities {0.00024 kg/m^3 [1.50 × 10^{-5}]}, and increases in their solubility did have an effect on the expected dose. If the water contact models are changed from bathtub to flow-through [labeled No Sol Limit(Flowthru)], the expected dose curve displays earlier release and is increased by one to two orders of magnitude for early times (2,700 to 7,000 years).

3.5.3.3 No Matrix Diffusion

The groundwater expected dose presented in Figure 3-38 [labeled No Matdif] has earlier release and higher does than the basecase. The peak expected dose for the no matrix diffusion case {3.1 × 10^{-4} mSv/yr [0.031 mrem/yr]} occurs approximately 450 years earlier and is 50 percent greater than the basecase peak expected dose {2.1 × 10^{-4} mSv [0.021 mrem/yr]}.

The increase in the peak expected dose resulting from the no matrix diffusion case is a direct result of the early arrival time of the radionuclides at the pumping well. For example, Np-237 breaks through 3,600 years earlier for the no-matrix diffusion case compared with the basecase in which the matrix diffusion coefficient is specified as 10^{-3} per year. In the basecase, matrix diffusion not only contributes to increased travel time but also exposes matrix surface for radionuclide sorption. In this regard, the sorbing radionuclides (e.g., Np-237) are delayed longer than the nonsorbing radionuclides (e.g., Tc-99).

3.6 Disruptive Events

The TPA Version 4.1 code results from faulting and igneous activity are presented in this section for single and multiple realizations. The disruptive events and the ground surface doses from igneous activity are compared with doses computed using the basecase data set.

3.6.1 Single-Realization Analysis of Disruptive Events

To determine the number of waste packages ruptured by seismically induced rockfall, which is part of the basecase, the time evolution of seismicity that includes the number, time, and magnitude of seismic events is obtained using the seismic hazard curve presented in Figure 3-39. The vertical extent of rockfall associated with different categories of seismic events (Figure 3-40), and the joint spacing information (Figure 3-41) for computing the rockfall area, are used in determining the rockfall volume. The rockfall volume is then used to compute impact stress which, if it induces a plastic strain on the waste package at the contact of impact exceeding 2 percent, will fail the waste package. Other associated information is presented in Table 3-14 and Figure 3-42.

To determine the number of waste packages failed by a faulting disruptive event, the TPA Version 4.1 code uses the time of the faulting event and the fault length and width information summarized in Table 3-15. Faults modeled in the TPA Version 4.1 code are hidden faults (i.e., either unknown and unmapped faults or underestimated faults), and thus the total-system performance assessment calculations recognize that the waste packages will be emplaced with an appropriate setback distance from known faults. The recurrence rate for a faulting event is 5×10^{-5} per year (Mohanty, et al., 2002). Igneous activity contributes to waste package failures for both extrusive and intrusive events. As modeled, extrusive events result in the direct release of radionuclides to the ground surface, whereas intrusive events contribute to groundwater releases. The igneous event occurs between 100- and 10,000-years postclosure, with a recurrence rate of 1×10^{-7} per year. The parameters corresponding to the determination of the timing of future igneous events, the subsurface area affected by a volcanic event, and the number of waste packages affected by intrusions extending laterally from the volcanic conduit are presented in Table 3-16.

After the volcanic event penetrates the repository and exhumes spent nuclear fuel, the areal density of deposited ash and radionuclides is computed at the compliance point. Input parameters, such as eruption height, wind velocity, and parameters that determine the transport and deposition of radionuclides in ash are presented in Table 3-16. The radionuclides modeled for extrusive releases, in addition to those evaluated for groundwater transport, are listed in Table 3-17 with corresponding initial inventories and half-lives. Parameters associated with surface erosion of radionuclides from the ash blanket deposited after an extrusive igneous event are presented in Table 3-18. For the ground surface pathway, the areal densities calculated for each radionuclide, computed with the ASHPLUME (Jarzemba, et al., 1997) ash transport model, are used in determining the total effective dose equivalents. Dose conversion factors are computed internally in the TPA Version 4.1 code by using GENTPA, a modification of the GENII computer code (Napier, et al., 1988). Table 3-19 presents only the mean of the values used in the TPA Version 4.1 code.

3.6.2 Multiple-Realization Analysis of Disruptive Events

The variability in the average dose arising from faulting events and igneous activity for the multiple-realization simulations is presented in this section. The dose history for faulting events for the 100,000-year simulation period without probability weighting is presented in

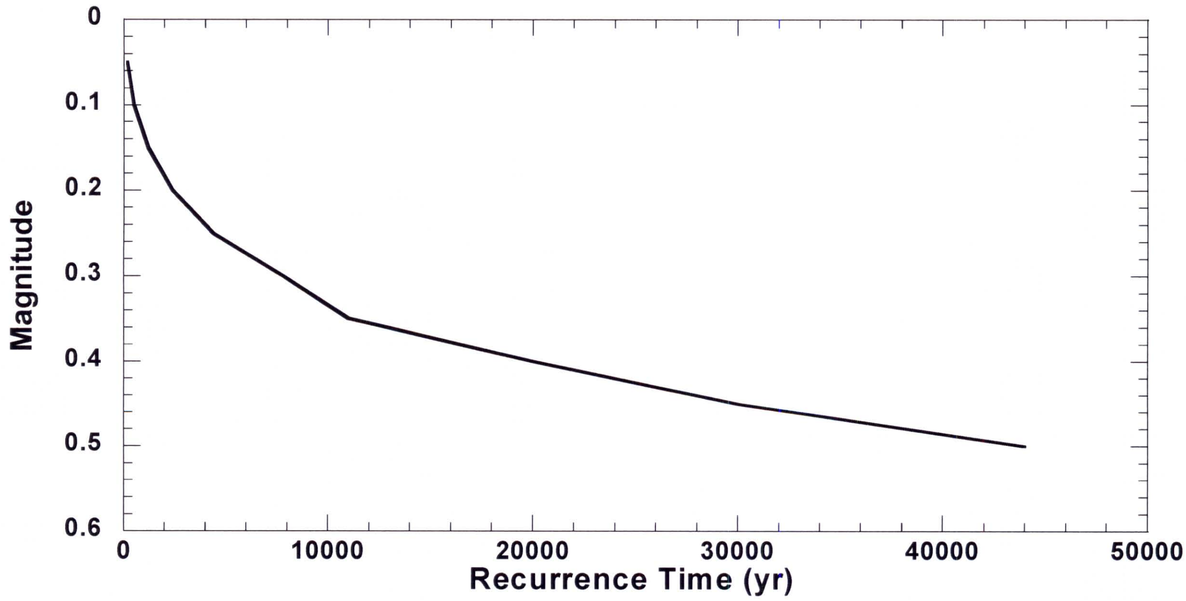

Figure 3-39. Seismic Hazard Curve Comprises Ground Accelerations and Recurrence Times Used to Determine the Time of Seismic Events

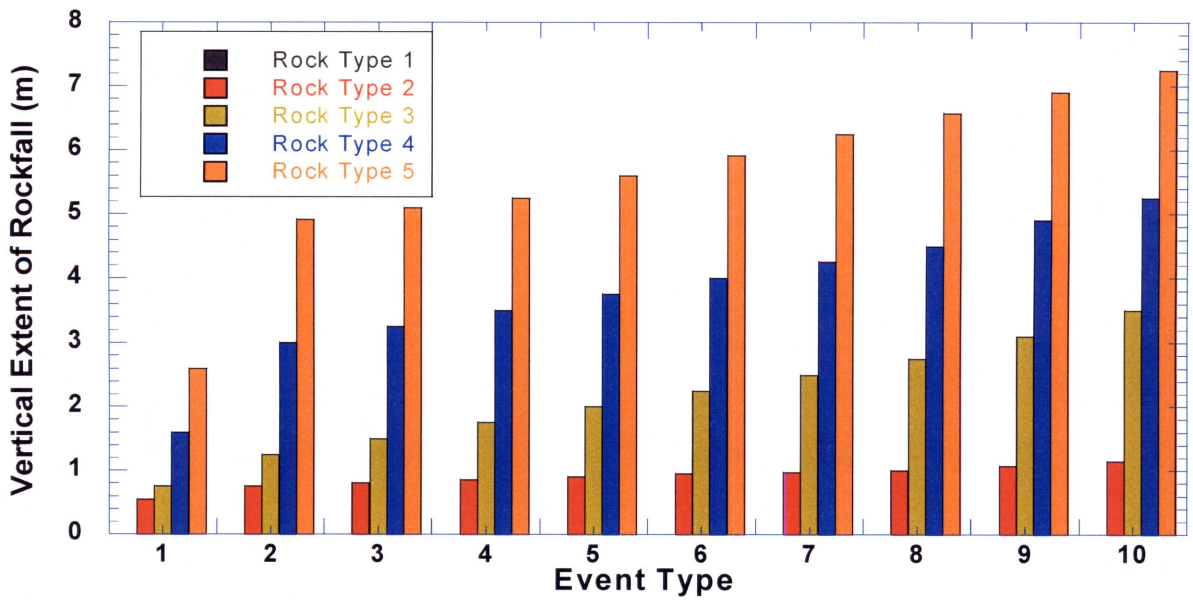

Figure 3-40. Vertical Extent of Rockfall Associated with the 5 Rock Types and 10 Seismic Events Defined by the Seismic Hazard Curve

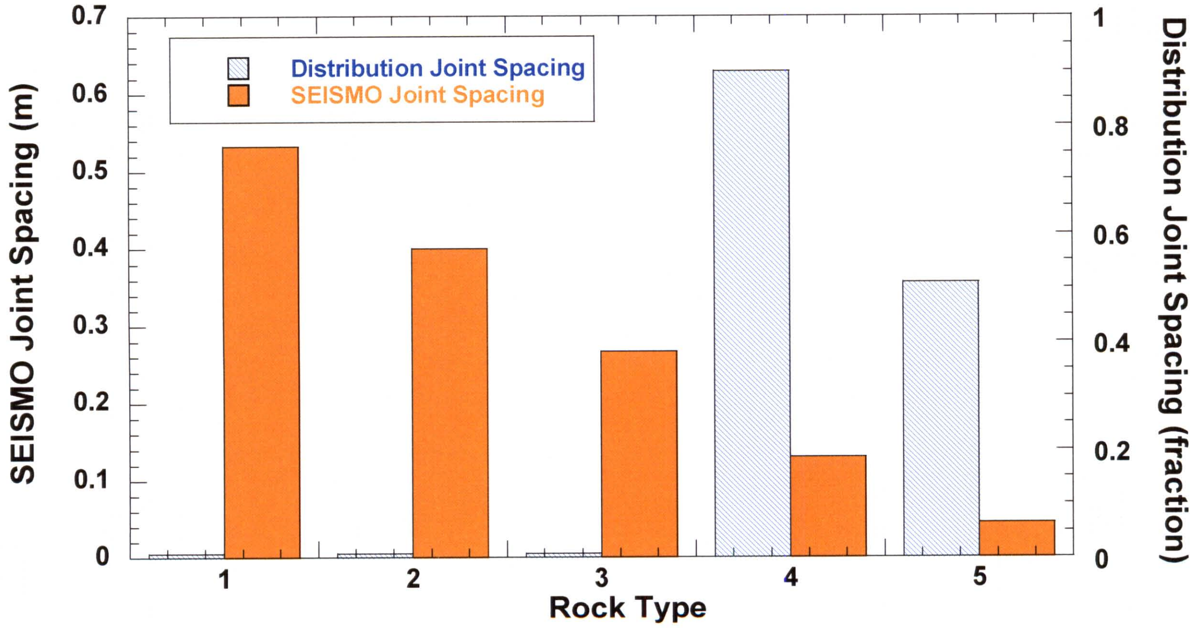

Figure 3-41. Joint Spacing of the 5 Rock Types and 10 Seismic Events

Table 3-14. Parameters Used in Determining Seismic Failure of Waste Packages

Parameter	Mean Value	Distribution
Waste package stiffness for SEISMO	1.21×10^{10} Pa m	—
Waste package modulus of elasticity for SEISMO	1.76×10^{11}	—
Rock modulus of elasticity for SEISMO	3.45×10^{10} Pa	Normal; 2.76×10^{10}, 4.14×10^{10}
Waste package Poisson ratio for SEISMO	2.00×10^{-1}	—
Rock Poisson ratio for SEISMO	2.00×10^{-1}	Normal; 0.15, 0.25
Rock falling distance for SEISMO	2.00 m	—
Waste package falling distance for SEISMO	3.00×10^{-1} m	—
Waste package number of support pair for SEISMO	2.00	—
Waste package support stiffness for SEISMO	5.50×10^{9} Pa m	—
Waste package ultimate strength	6.20×10^{8} Pa	—
Grain density for Topopah Spring-welded for SEISMO	2.55 g/cm^{3}	—
Waste package yield point	2.00×10^{-3}	—
Waste package plastic elongation	0.05	—

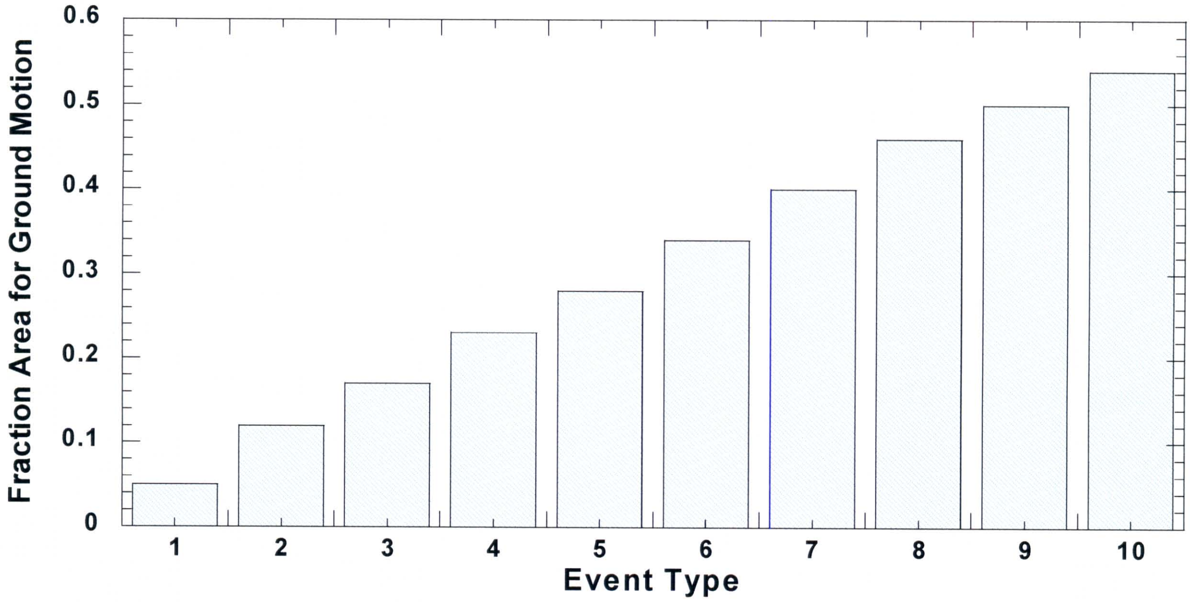

Figure 3-42. Fraction of the Area with Ground Motion for each of the 10 Seismic Events Defined by the Seismic Hazard Curve

Table 3-15. Faulting Disruptive Event Parameters		
Parameter	**Mean Value**	**Distribution**
Time of next faulting event in region of interest	4.89×10^3 years	Finite exponential; 100.0, 10,000.0, 2.0×10^{-5}
Threshold displacement for fault disruption of waste package	2.00×10^{-1} m	User distribution; 4 values: 0.1, 0.2, 0.3, 0.4
X coordinate of faulting event in region of interest	5.48×10^5 m	Uniform; 547,400.0, 548,600.0
Y coordinate of faulting event in region of interest	4.08×10^6 m	Uniform; 4,076,000.0, 4,079,600.0
Probability for NW orientation of faults	5.00×10^{-2}	—
Random number to determine fault orientation	5.00×10^{-1}	Uniform; 0.0, 1.0
NW fault strike orientation measured from north—clockwise	−32.5°	—
NE fault strike orientation measured from north—clockwise	10°	—
NW fault trace length	4.00×10^3 m	—
NE fault trace length	4.00×10^3 m	—
NW fault zone width	2.16×10^1 m	Beta; 0.5, 275.0, 1.25, 15.0
NE fault zone width	2.85×10^1 m	Beta; 0.5, 365.0, 1.25, 15.0
NW amount of largest credible displacement	1.34×10^{-1} m	Lognormal; 5.41×10^{-2}, 3.30×10^{-1}

Table 3-15. Faulting Disruptive Event Parameters (continued)		
Parameter	Mean Value	Distribution
NW cumulative displacement rate	5.00×10^{-5} mm/yr	—
NE cumulative displacement rate	5.00×10^{-5} mm/yr	—

Figure 3-43(a). The average groundwater dose from the faulting events is approximately 50 to 100 percent greater than the dose without a faulting event from 5,000 to 50,000 years. After 70,000 years, the groundwater dose with faulting and the basecase in the 100,000-year simulation period are not distinguishable.

The probability-weighted expected dose from igneous activity is presented in Figure 3-42(b) together with the groundwater dose computed using the basecase data set. In the 10,000-year simulation period, the probability-weighted dose from igneous activity is approximately one to five orders of magnitude greater than the basecase groundwater dose. The next section presents the methodology used to determine the risk arising from faulting and igneous disruptive events.

3.7 Calculation of Risk

Risk is defined in this report as the probability-weighted dose. Doses are calculated from three scenario classes: (i) basecase with seismicity, (ii) faulting, and (iii) igneous activity. The probability of the three scenario classes sums to unity; this implies these scenario classes are assumed exhaustive.

The average risk to a receptor can be computed by summing contributions to dose from each Monte Carlo simulation, weighted by the scenario probability and the conditional probability of each realization within the scenario. The methodology for computing conditional risk (i.e., assuming the scenario has a probability of one) from scenarios other than extrusive igneous activity is presented in Section 3.7.1. The methodology used to determine the conditional risk from scenarios with extrusive igneous activity is described in Section 3.7.2. The methodology for combining the conditional risks to an overall risk is presented in Section 3.7.3.

3.7.1 Scenarios Other Than Extrusive Igneous Activity

The risk or expected effective dose equivalent is the product of the consequence (i.e., dose) and the probability that the dose has occurred. Estimates of dose are uncertain because the models and their input parameters are uncertain, as are the times of occurrence of the disruptive events such as faulting and intrusive igneous activity. Monte Carlo analysis is used to account for the uncertainty in parameters and events. Monte Carlo analysis propagates the uncertainty in model inputs through the conceptual models by evaluating a model repeatedly, using input values randomly selected. The output of the Monte Carlo analysis is a set of results, such as dose versus time, for each randomly chosen input set of values. Generally, each Monte Carlo output result has equal probability. Thus, each dose curve from the Monte Carlo analysis has a probability of occurrence equal to $1/N$, where N is the number of Monte Carlo samples. The analysis in this section does not explicitly include conceptual model uncertainty other than that captured by changes in the input parameters.

Table 3-16. Igneous Activity Parameters		
Parameter	**Mean Value**	**Distribution**
Volcano model (1 = geometric, 2 = distribution)	1	—
Time of next volcanic event in region of interest	5.05×10^3 years	Finite exponential; 100.0, 10,000.0, 1.0×10^{-7}
X location in region of interest	5.48×10^5 m	—
Y location in region of interest	4.08×10^6 m	—
Random number to determine if extrusive or intrusive volcanic event	5.00×10^{-1}	Uniform; 0.0, 1.0
Fraction of time volcanic event is extrusive	9.99×10^{-1}	—
Angle of volcanic dike measured from north—clockwise	7.50°	Uniform; 0.0, 15.0
Length of volcanic dike	6.50×10^3 m	Uniform; 2,000.0, 11,000.0
Width of volcanic dike	5.50 m	Uniform; 1.0, 10.0
Diameter of volcanic conduit	5.13×10^1 m	Uniform; 24.6, 77.9
Density of air at standard pressure	1.29×10^{-3} g/cm^3	—
Viscosity of air at standard pressure	1.80×10^{-4} g/cm-s	—
Constant relating fall time to eddy diffusivity	4.00×10^2 cm^2/sec$^{5/2}$	—
Maximum particle diameter for particle transport	1.00×10^1 cm	—
Minimum fuel particulate size	1.00×10^{-4} cm	—
Mode fuel particulate size	1.00×10^{-3} cm	—
Maximum fuel particulate size	1.00×10^{-2} cm	—
Minimum ash density for variation with size	0.8 g/cm^3	—
Maximum ash density for variation with size	1.60 g/cm^3	—
Minimum ash log diameter for density variation	−2.00	—
Maximum ash log diameter for density variation	−1.00	—
Particle shape parameter	5.00×10^{-1}	—
Incorporation ratio	3.00×10^{-1}	—
Wind direction	−90°	—
Wind speed	1.20×10^3 cm/sec	Exponential; 8.3×10^{-4}
Volcanic event duration	4.85×10^5 sec	Log-uniform; 1.80×10^5, 1.30×10^6
Volcanic event power	4.31×10^{10} W	Log-uniform; 3.59×10^9, 5.30×10^{11}
Volcanic column constant beta	1.00×10^1	—
Ash mean particle log diameter	1.00×10^{-1} cm	Log triangular; 0.01, 0.1, 1.0
Ash particle size distribution standard deviation	1.00	—
Relative rate of blanket removal	0.0007	—

Table 3-16. Igneous Activity Parameters (continued)		
Parameter	**Mean Value**	**Distribution**
Fraction of precipitation lost to evapotranspiration	6.80×10^{-1}	—
Fraction of irrigation lost to evapotranspiration	5.00×10^{-1}	—
Fraction of year soil is saturated from precipitation	5.40×10^{-3}	—
Fraction of year soil is saturated from irrigation	2.00×10^{-1}	—
Ash bulk density	1.40 g/cm^3	—
Ash volumetric moisture fraction at saturation	4.00×10^{-1}	—
Depth of the rooting zone	1.50×10^{-1} m	—
Subarea of volcanic event (Model 2)	2.00	—
Number of waste packages contained by ejecta (Model 2)	50.677	Beta 1.0, 150, 1.0, 2.0
Number of magma induced mechanical failures remaining in drift (Model 2)	37.40	Log uniform; 1.0, 1402.0

Table 3-17. Initial Inventory and Half-Life of Additional Radionuclides Considered for Ground Surface Release, But Not for Groundwater Release		
Radionuclide	**Inventory at 10 Years from Reactor (Ci/WP)**	**Half-Life (Years)**
Ac-227	5.93×10^{-5}	2.18×10^{1}
Ag-108m	1.00×10^{1}	4.18×10^{2}
Am-241	1.64×10^{4}	4.32×10^{2}
Am-242m	196×10^{2}	1.52×10^{2}
Am-243	2.08×10^{2}	7.38×10^{3}
C-14	1.14×10^{1}	5.73×10^{3}
Cl-36	9.00×10^{2}	3.01×10^{5}
Cm-243	2.01×10^{2}	2.85×10^{1}
Cm-244	2.11×10^{4}	1.81×10^{1}
Cm-245	2.89×10^{0}	8.50×10^{3}
Cm-246	6.00×10^{1}	4.73×10^{3}
Cs-135	4.23×10^{0}	2.30×10^{6}
Cs-137	7.22×10^{5}	3.00×10^{1}
I-129	2.80×10^{1}	1.57×10^{7}
Mo-93	1.20×10^{1}	3.50×10^{3}
Nb-94	6.69×10^{0}	2.03×10^{4}
Ni-59	1.93×10^{1}	8.00×10^{4}
Ni-63	2.94×10^{3}	9.20×10^{1}
Np-237	3.42×10^{1}	2.14×10^{6}
Pa-231	2.12×10^{-4}	3.28×10^{4}
Pb-210	4.47×10^{-7}	2.23×10^{1}
Pd-107	1.03×10^{0}	6.50×10^{6}
Pu-238	2.97×10^{4}	8.77×10^{1}
Pu-239	2.91×10^{3}	2.41×10^{4}

Table 3-17. Initial Inventory and Half-Life of Additional Radionuclides Considered for Ground Surface Release, But Not for Groundwater Release (continued)		
Radionuclide	**Inventory at 10 Years from Reactor (Ci/WP)**	**Half-Life (Years)**
Pu-240	4.29×10^{3}	6.54×10^{3}
Pu-241	7.27×10^{5}	1.44×10^{1}
Pu-242	1.66×10^{1}	3.87×10^{5}
Ra-226	3.24×10^{-6}	1.60×10^{3}
Se-79	2.10×10^{1}	1.10×10^{6}
Sm-151	3.38×10^{3}	9.00×10^{1}
Sn-121m	8.21×10^{0}	5.00×10^{1}
Sn-126	6.98×10^{0}	1.00×10^{5}
Sr-90	4.93×10^{5}	2.91×10^{1}
Tc-99	1.14×10^{2}	2.13×10^{5}
Th-229	2.17×10^{-6}	7.34×10^{3}
Th-230	1.08×10^{-3}	7.70×10^{4}
U-232	3.10×10^{1}	7.20×10^{1}
U-233	2.71×10^{4}	1.59×10^{5}
U-234	9.31×10^{0}	2.45×10^{5}
U-235	1.30×10^{1}	7.04×10^{8}
U-236	2.22×10^{0}	2.34×10^{7}
U-238	2.49×10^{0}	4.47×10^{9}
Zr-93	1.95×10^{1}	1.53×10^{6}

Table 3-18. Parameters Used in Computing Ash and Radionuclide Removal from the Ground Surface		
Element	**K_d in Volcanic Ash (cm^3/g)**	**Solubility in Volcanic Ash (mol/L)**
Ac	4.50×10^{2}	1.00×10^{6}
Am	1.90×10^{3}	1.00×10^{6}
C	5.00	1.00
Cs	2.80×10^{2}	1.00
Cl	0.25	1.00
Cm	4.00×10^{3}	1.00×10^{6}
I	1.00	1.00
Pb	2.70×10^{2}	3.20×10^{7}
Mo	1.00×10^{1}	1.00
Np	5.00	1.00×10^{4}
Ni	4.00×10^{2}	2.00×10^{3}
Nb	1.60×10^{2}	1.00×10^{8}
Pd	5.50×10^{1}	9.50×10^{4}
Pu	5.50×10^{2}	5.00×10^{6}
Pa	5.50×10^{2}	3.20×10^{8}
Ra	5.00×10^{2}	1.00×10^{7}
Sm	2.45×10^{2}	5.00×10^{6}
Se	1.50×10^{2}	1.00
Au	5.50×10^{1}	1.00
Sr	1.50×10^{1}	1.30×10^{4}
Tc	1.00×10^{-1}	1.00
Th	3.20×10^{3}	3.20×10^{9}
Sb	1.30×10^{2}	5.00×10^{8}
U	3.50×10^{1}	4.50×10^{5}
Zr	6.00×10^{2}	3.20×10^{10}
Sn	1.30×10^{2}	5.00×10^{8}

Table 3-18. Parameters Used in Computing Ash and Radionuclide Removal from the Ground Surface (continued)		
Element	**K_d in Volcanic Ash (cm^3/g)**	**Solubility in Volcanic Ash (mol/L)**
Ag	5.50 × 10^{1}	1.00 × 10^{0}

Other Parameters		
Parameter	**Mean Value**	**Distribution**
Distance cutoff for dose conversion duality in DCAGS module	19.99	—
Airborne mass load for igneous activity dose calculation	1.00 × 10 ^{3} g/m^{3}	Log-uniform; 1.2 × 10 ^{3}, 1.6 × 10 ^{2}
Occupancy factor for igneous activity dose calculation	0.605	—
Depth of resuspendable layer	3.00 × 10 ^{1} cm	—
Airborne mass load above fresh ash blanket	4.30 × 10 ^{3}	Log-uniform; 1.2 × 10 ^{3}, 1.6 × 10 ^{2}
Airborne mass load above soil	1.20 × 10 ^{4}	Log-uniform; 5.0 × 10 ^{5}, 3.0 × 10 ^{4}
Rate of reduction of mass loading factor	0.70	—

Table 3-19. Biosphere Dose Conversion Factors of All 43 Nuclides for Ground Surface at the 20-km [12.4-mi] Receptor Location				
Nonpluvial and Pluvial Dose Conversion Factors				
Radionuclide	**Direct Exposure (rem/yr)/(Ci/m^2)**	**Inhalation (rem/yr)/(Ci/m^3)**	**Ingestion of Animal Products (rem/yr)/(Ci/m^2)**	**Ingestion of Crops (rem/yr)/(Ci/m^2)**
Ac-237	7.60	1.40 × 10^{14}	4.46 × 10^{2}	6.44 × 10^{4}
Ag-108m	1.24 × 10^{5}	5.94 × 10^{9}	5.40	5.00 × 10^{1}
Am-241	1.34 × 10^{3}	9.32 × 10^{12}	3.00 × 10^{1}	1.58 × 10^{4}
Am-242m	1.46 × 10^{2}	8.92 × 10^{12}	2.82 × 10^{1}	1.52 × 10^{4}
Am-243	2.60 × 10^{3}	9.24 × 10^{12}	3.00 × 10^{1}	1.58 × 10^{4}
C-14	7.80 × 10 ^{1}	4.38 × 10^{7}	0.00	3.40 × 10 ^{1}
Cl-36	3.40 × 10^{1}	4.60 × 10^{8}	4.20 × 10^{3}	1.52 × 10^{4}
Cm-243	6.20 × 10^{3}	6.44 × 10^{12}	5.60 × 10^{1}	1.10 × 10^{4}
Cm-244	4.40 × 10^{1}	5.20 × 10^{12}	4.60 × 10^{1}	8.80 × 10^{3}
Cm-245	4.20 × 10^{3}	9.54 × 10^{12}	8.40 × 10^{1}	1.62 × 10^{4}
Cm-246	3.80 × 10^{1}	9.46 × 10^{12}	8.40 × 10^{1}	1.62 × 10^{4}
Cs-135	1.66	9.54 × 10^{7}	1.40 × 10^{1}	7.00 × 10^{1}
Cs-137	2.60 × 10^{4}	6.70 × 10^{8}	9.60 × 10^{1}	4.80 × 10^{2}
I-129	1.24 × 10^{3}	3.64 × 10^{9}	4.00 × 10^{2}	1.32 × 10^{3}
Mo-93	2.60 × 10^{2}	5.98 × 10^{8}	6.20	7.40 × 10^{1}
Nb-94	7.40 × 10^{4}	8.70 × 10^{9}	1.36 × 10 ^{3}	4.60 × 10^{1}
Ni-59	0.00	5.66 × 10^{7}	3.80 × 10 ^{1}	2.20
Ni-63	0.00	1.32 × 10^{8}	1.06	6.00
Np-237	1.46 × 10^{3}	1.13 × 10^{13}	1.30 × 10^{3}	3.80 × 10^{4}
Pa-231	1.96 × 10^{3}	2.70 × 10^{13}	7.60 × 10^{1}	4.80 × 10^{4}
Pb-210	1.24 × 10^{2}	2.84 × 10^{11}	5.58 × 10^{2}	2.66 × 10^{4}
Pd-107	0.00	2.68 × 10^{8}	1.58 × 10 ^{1}	2.40
Pu-236	1.66 × 10^{1}	8.22 × 10^{12}	9.00 × 10	1.38 × 10^{4}
Pu-239	1.76 ×10^{1}	9.00 × 10^{12}	1.00 × 10^{1}	1.52 × 10^{4}
Pu-240	4.00 × 10^{1}	9.00 × 10^{12}	1.00 × 10^{1}	1.52 × 10^{4}
Pu-241	2.60 × 10 ^{1}	1.73 × 10^{11}	1.90 × 10 ^{1}	3.00 × 10^{2}

Table 3-19. Biosphere Dose Conversion Factors of All 43 Nuclides for Ground Surface at the 20-km [12.4-mi] Receptor Location (continued)				
Nonpluvial and Pluvial Dose Conversion Factors				
Radionuclide	**Direct Exposure (rem/yr)/(Ci/m^2)**	**Inhalation (rem/yr)/(Ci/m^3)**	**Ingestion of Animal Products (rem/yr)/(Ci/m^2)**	**Ingestion of Crops (rem/yr)/(Ci/m^2)**
Pu-242	3.40×10^{1}	8.62×10^{12}	9.40×10	1.46×10^{4}
Ra-226	3.20×10^{2}	1.80×10^{11}	1.06×10^{2}	6.60×10^{3}
Se-79	1.02	2.06×10^{8}	1.98×10^{1}	5.00×10^{1}
Sm-151	$2.40 \times 10^{\ 1}$	6.28×10^{8}	$3.40 \times 10^{\ 2}$	1.94
Sn-121m	2.40×10^{2}	2.42×10^{8}	3.86	1.42×10^{1}
Sn-126	2.60×10^{3}	2.10×10^{9}	3.38×10^{2}	1.31×10^{2}
Sr-90	1.34×10^{1}	2.72×10^{10}	2.94×10^{2}	6.72×10^{3}
Tc-99	3.80	1.75×10^{8}	3.80×10^{1}	5.60×10^{3}
Th-229	4.20×10^{3}	4.50×10^{13}	1.71×10^{2}	1.66×10^{4}
Th-230	3.60×10^{1}	6.84×10^{12}	$2.60 \times 10^{\ 1}$	2.40×10^{3}
U-232	5.00×10^{1}	1.38×10^{13}	1.18×10^{2}	7.24×10^{3}
U-233	3.60×10^{1}	2.84×10^{12}	1.80×10^{2}	1.58×10^{3}
U-234	3.60×10^{1}	2.78×10^{12}	1.76×10^{2}	1.54×10^{3}
U-235	7.20×10^{3}	2.58×10^{12}	1.64×10^{2}	1.45×10^{3}
U-236	3.20×10^{1}	2.64×10^{12}	1.66×10^{2}	1.46×10^{3}
U-238	2.60×10^{1}	2.48×10^{12}	1.61×10^{2}	1.41×10^{3}
Zr-93	0.00	6.76×10^{9}	$5.68 \times 10^{\ 4}$	7.24

The expected dose-versus-time relationship for scenario *j* (e.g., intrusive volcanic scenario) can be developed by summing, for all realizations, the probability-weighted contributions from the family of dose relationships produced by the *N* Monte Carlo samples. The mathematical representation of this calculation is

$$\overline{D}_j(t) = \sum_{i=1}^{N} p_i C_{i,j}(t) \tag{3-1}$$

where

$\overline{D}_j(t)$ — average annual dose to the receptor individual as a function of time for the *j*th scenario

$C_{i,j}$ — dose as a function of time for the *i*th realization of the *j*th scenario

p_i — probability assigned to the dose curve for the *j*th realization; for Monte Carlo sampling, $p_j = (1/N)$

N — number of model simulations that compose the family of dose curves (i.e., *N* Monte Carlo samples of the model inputs are used to generate *N* model outputs in the form of dose curves)

The index indicates the event can occur at any time between [0,*t*].

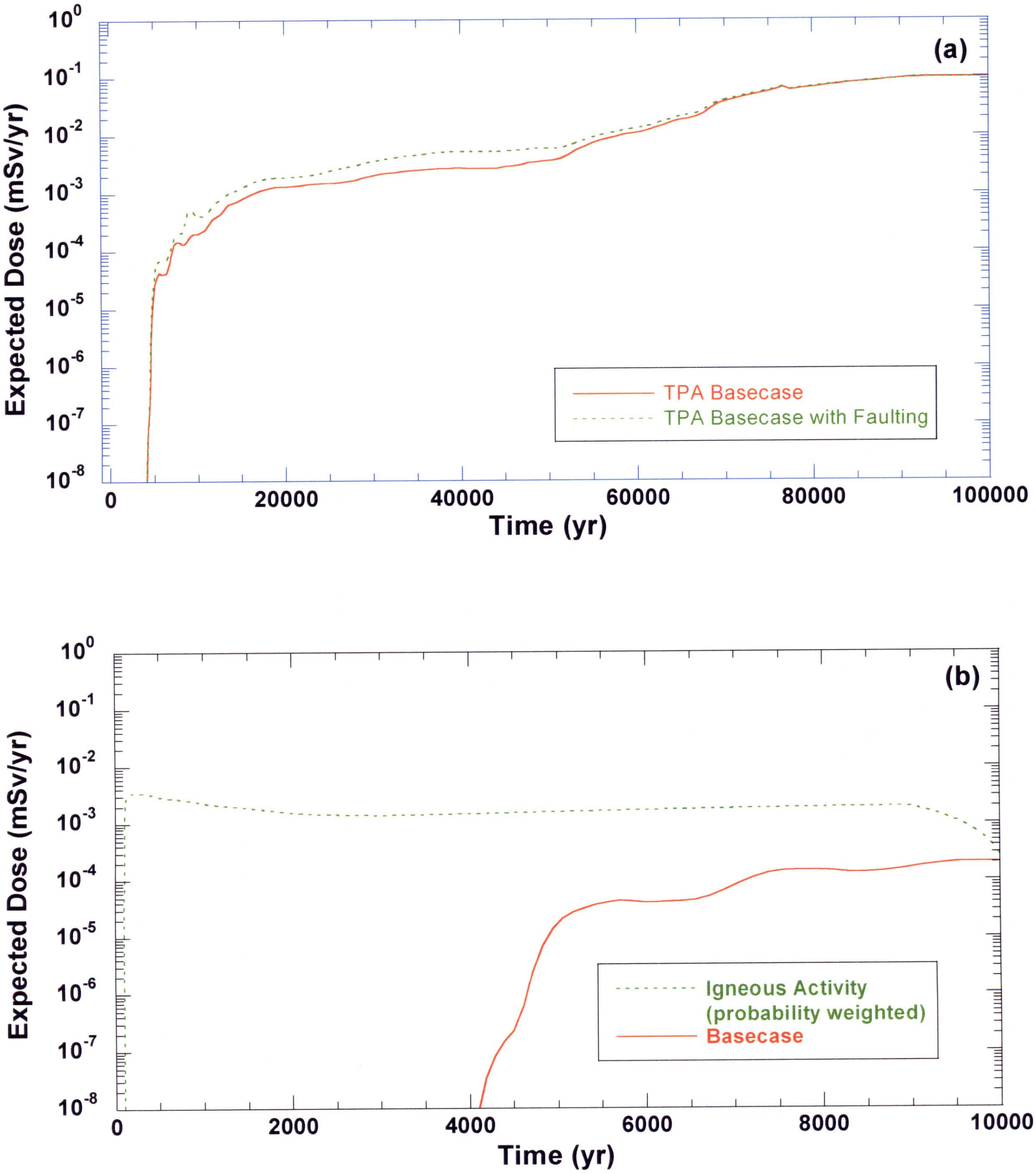

Figure 3-43. Groundwater Dose for (a) Faulting (Shown for 100,000 Year) and (b) Igneous Activity (Shown for 10,000 Years), for 350 Realizations. (Only the Ground-Surface Dose for Releases Caused by Extrusive Igneous Activity in (b) Is Probability-Weighted. Faulting Dose Is Not Probability Weighted.)

3.7.2 Extrusive-Igneous Activity Scenario

Disruptive events, such as a volcanic eruption through the repository block, are generally of short duration (several years) compared to the nominal case (tens of thousands of years). Although the standard Monte Carlo approach is suitable for the nominal case that has long-term, gradually evolving consequences, and relatively high probability of occurrence, the method is not well suited to the incorporation of the effects of low-probability, high-consequence disruptive events such as volcanism.

For a typical nominal case evaluation of the proposed Yucca Mountain repository performance, the number of Monte Carlo samples, which must be greater than the number of sampled variables, is generally 350 or more to generate a stable mean dose curve. On the other hand, a standard Monte Carlo simulation involving low-probability volcanism of short duration would require an unreasonably large number of realizations to generate a stable risk curve. For example, if the probability of extrusive volcanism through the repository is 10^{-7} per year, there would have to be approximately 1,000 realizations per simulated volcanic event in 10,000 years. Also, there would have to be many hundreds or thousands of events to produce a tolerably stable mean dose curve, given that the duration of the volcanic release is relatively short. A Monte Carlo simulation with such a large number of realizations would be prohibitively expensive because each realization could take several minutes to compute.

The current NRC staff approach to generate the risk curve for low-probability events is to convolute the conditional mean dose curves generated assuming the event has taken place at a time after repository closure, t_e. A person living at time t' will be at risk from all events taking place prior to or at t'. For the volcanism scenario, the average annual dose, D, to a person living at time t' who is exposed to a volcano occurring at time t_e would be

$$D = af\left(t_e, t'-t_e\right) \tag{3-2}$$

where a is the peak amplitude of the dose if the event happened at time = 0, $f(t_e, t'-t_e)$ is a function expressing the relative dose occurring at time t' from an event at time t_e. The relative dose, f, is a function both of the time of the event after site closure and the time between the event and the evaluation time. Considering the volcanic event has a fixed probability of occurring in any year, the risk to a person living at t' is the convolution of all possible prior volcanic events multiplied by the annual probability, p

$$\overline{D}(t') = \int_{t_{min}}^{t'} apf\left(\tau, t'-\tau\right)d\tau \tag{3-3}$$

where t_{min} is the earliest time that volcanism is considered to occur (e.g., 100 years after closure in this analysis, which reflects an effective control period that would limit radiological exposures).

For the igneous-activity scenario, dose consequences are largest for events that occur soon after repository closure, while the relatively short-lived, but high-activity, radionuclides, such as Am-241, are still present in significant quantities. Radionuclides can reach the affected population in short times (hours to days) but persist in the environment and also can cause lower levels of exposure long after the event (hundreds to thousands of years). The procedure for developing the expected dose curve for the igneous-activity scenario involves the following steps:

- Conduct probabilistic analyses at specific event times.

  Dose consequences of igneous activity are calculated at specific event times rather than randomly selecting occurrence times in a Monte Carlo approach. In the present model, the event times t_e are 100 years; 500 years; and 1,000–10,000 years, in 1,000-year steps (Figure 3-44).

- Generate conditional expected dose curves for specific event times.

  Each of the separate probabilistic analyses described previously is used to develop a separate conditional expected dose versus time curve as in Eq. (3-2) for the specific event time t_e.

- Generate an overall expected dose curve.

  The expected dose at any given time t′ is determined by cumulating the mean dose curves at the 12 specified event times. Equation (3-3) describes how the expected annual dose to the receptor individual is convoluted from the conditional dose curves. In practice, the function f within the integrand of Eq. (3-3) is generated from the 12 mean dose curves at fixed values of t_e using linear interpolation to generalize to any value of t_e.

The probability-weighted dose curve calculated with this more efficient approach is presented in Figure 3-45. As expected, the consequences of an igneous event are highest at early times. The probability-weighted dose curve goes through a maximum at approximately 250 years, which results from the accumulation of risk from earlier events.

3.7.3 Combining Conditional Risks into an Overall Risk

The overall risk, $\overline{D}(t)$, is calculated by summing the scenario mean doses weighted by the scenario probability, P_j. The mathematical representation of this calculation is

$$\overline{D}_j(t) = \sum_{j=1}^{M} \overline{D}_j(t) P_j \qquad (3\text{-}4)$$

where

$\overline{D}_j(t)$	—	dose rate from scenario j, averaged for the Monte Carlo realizations
M	—	number of scenario classes
P_j	—	annual probability of scenario j

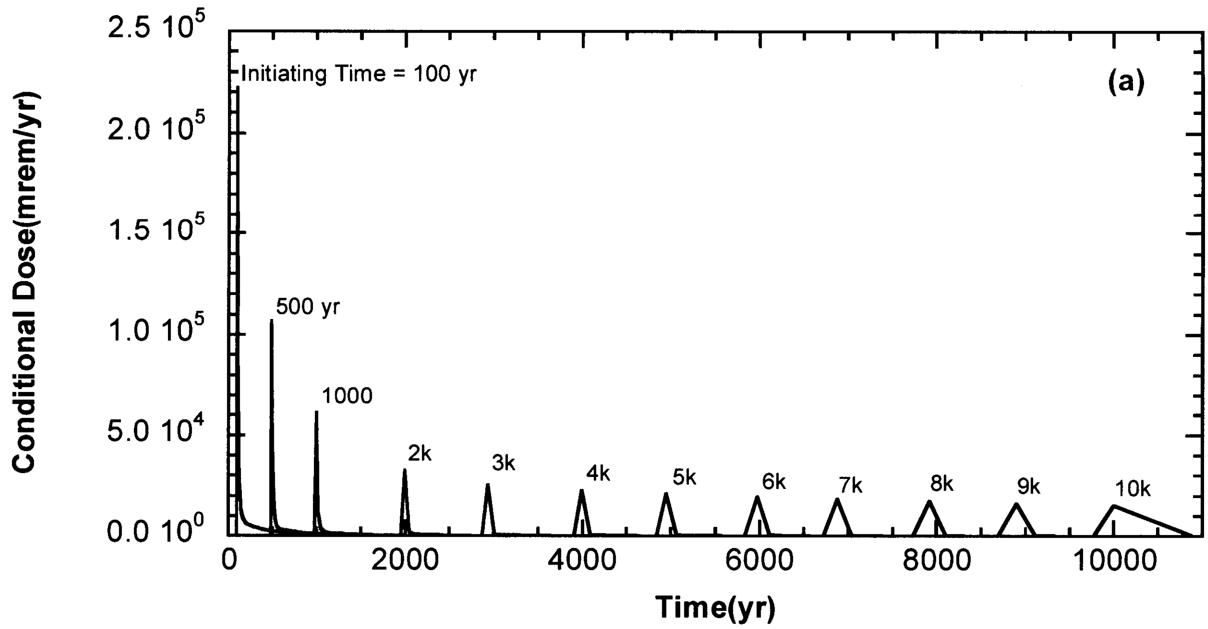

Figure 3-44. Mean Dose Arising from Extrusive Igneous Activity Shown with Various Times for the Volcanic Event in 400 Realizations

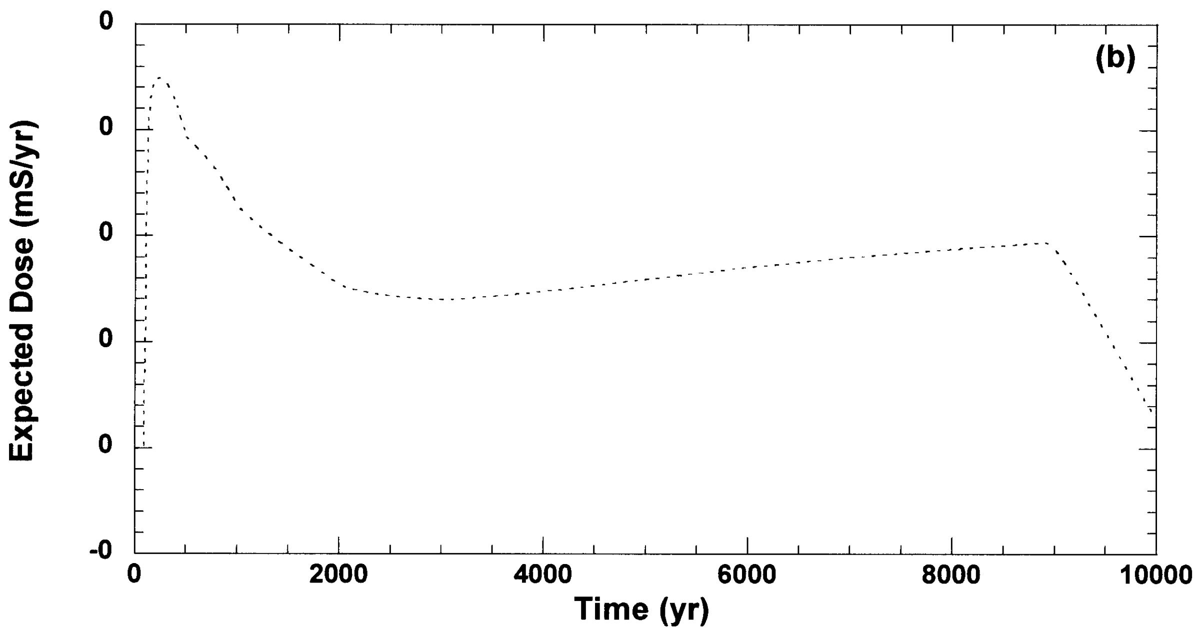

Figure 3-45. Contribution of Extrusive Igneous Activity to the Total Dose, Weighted by an Annual Probability for the Volcanic Event of 10^{-7}